Article

Cell Reports

Accumulation of Basic Amino Acids at Mitochondria Dictates the Cytotoxicity of Aberrant Ubiquitin

Graphical Abstract

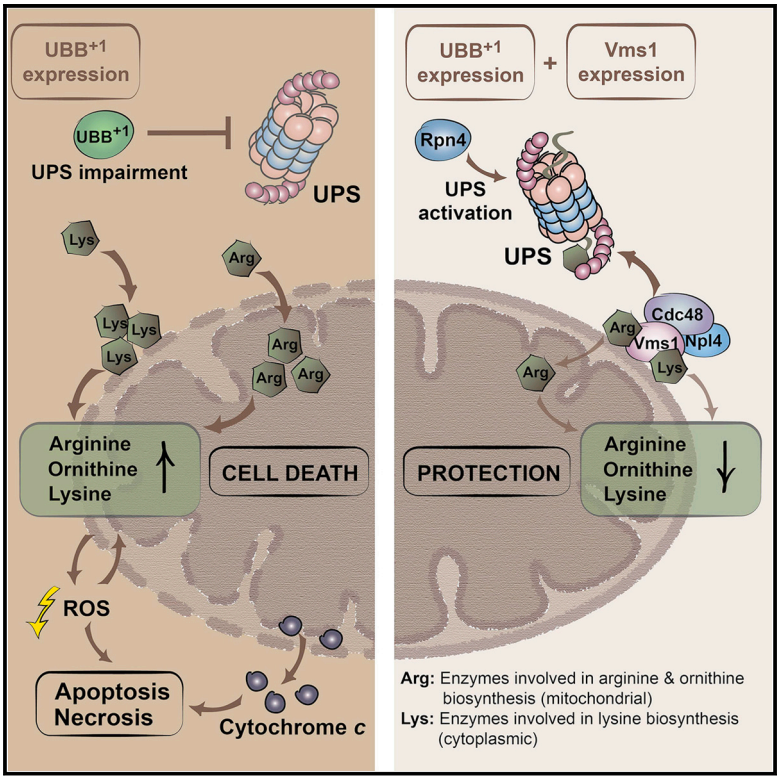

Highlights

- UBB^{+1} co-exists with the UPS component VMS1 in neurofibrillary tangles
- UBB^{+1} accumulation impairs the UPS and mitochondria, triggering cell death
- UBB^{+1} causes accumulation of basic amino acids at mitochondria
- Vms1 reverts UBB^{+1}-triggered basic amino acid accumulation and cell death

Authors

Ralf J. Braun, Cornelia Sommer, ..., Guido Kroemer, Frank Madeo

Correspondence

ralf.braun@uni-bayreuth.de (R.J.B.), frank.madeo@uni-graz.at (F.M.)

In Brief

Braun et al. demonstrate that basic amino acid accumulation at mitochondria is a decisive toxic event upon cellular accumulation of UBB^{+1}, an Alzheimer's-disease-associated ubiquitin variant. Triggering the mitochondrion-specific branch of the ubiquitin-proteasome system is sufficient to prevent UBB^{+1}-triggered cytotoxicity, which has potentially far-reaching pathophysiological implications.

Braun et al., 2015, Cell Reports *10*, 1557–1571
March 10, 2015
http://dx.doi.org/10.1016/j.celrep.2015.02.009

Cell Reports
Article

Accumulation of Basic Amino Acids at Mitochondria Dictates the Cytotoxicity of Aberrant Ubiquitin

Ralf J. Braun,[1,12,*] Cornelia Sommer,[2,3,12] Christine Leibiger,[1,12] Romina J.G. Gentier,[4,12] Verónica I. Dumit,[5] Katrin Paduch,[1] Tobias Eisenberg,[2] Lukas Habernig,[2] Gert Trausinger,[6] Christoph Magnes,[6] Thomas Pieber,[6,7] Frank Sinner,[6,7] Jörn Dengjel,[5] Fred W. van Leeuwen,[4] Guido Kroemer,[8,9,10,11] and Frank Madeo[2,3,*]

[1]Institute of Cell Biology, University of Bayreuth, 95440 Bayreuth, Germany
[2]Institute of Molecular Biosciences, NAWI Graz, University of Graz, 8010 Graz, Austria
[3]BioTechMed-Graz, 8010 Graz, Austria
[4]Department of Neuroscience, Faculty of Health, Medicine and Life Sciences, Maastricht University, 6229 ER Maastricht, the Netherlands
[5]FRIAS Freiburg Institute for Advanced Studies, Department of Dermatology, Medical Center, ZBSA Center for Biological Systems Analysis, BIOSS Centre for Biological Signalling Studies, University of Freiburg, 79104 Freiburg, Germany
[6]HEALTH Institute for Biomedicine and Health Sciences, Joanneum Research, 8010 Graz, Austria
[7]Division of Endocrinology and Metabolism, Medical University of Graz, 8036 Graz, Austria
[8]Apoptosis, Cancer and Immunity Laboratory, Team 11, Equipe labellisée Ligue contre le Cancer, INSERM Cordeliers Research Cancer, 75006 Paris, France
[9]Cell Biology and Metabolomics Platforms, Gustave Roussy Comprehensive Cancer Center, 94805 Villejuif, France
[10]Pôle de Biologie, Hôpital Européen Georges Pompidou, AP-HP, 75015 Paris, France
[11]Université Paris Descartes, Sorbonne Paris Cité, 75005 Paris, France
[12]Co-first author
*Correspondence: ralf.braun@uni-bayreuth.de (R.J.B.), frank.madeo@uni-graz.at (F.M.)
http://dx.doi.org/10.1016/j.celrep.2015.02.009

SUMMARY

Neuronal accumulation of UBB^{+1}, a frameshift variant of ubiquitin B, is a hallmark of Alzheimer's disease (AD). How UBB^{+1} contributes to neuronal dysfunction remains elusive. Here, we show that in brain regions of AD patients with neurofibrillary tangles UBB^{+1} co-exists with VMS1, the mitochondrion-specific component of the ubiquitin-proteasome system (UPS). Expression of UBB^{+1} in yeast disturbs the UPS, leading to mitochondrial stress and apoptosis. Inhibiting UPS activity exacerbates while stimulating UPS by the transcription activator Rpn4 reduces UBB^{+1}-triggered cytotoxicity. High levels of the Rpn4 target protein Cdc48 and its cofactor Vms1 are sufficient to relieve programmed cell death. We identified the UBB^{+1}-induced enhancement of the basic amino acids arginine, ornithine, and lysine at mitochondria as a decisive toxic event, which can be reversed by Cdc48/Vms1-mediated proteolysis. The fact that AD-induced cellular dysfunctions can be avoided by UPS activity at mitochondria has potentially far-reaching pathophysiological implications.

INTRODUCTION

UBB^{+1}, a loss-of-function variant of ubiquitin B (UBB), accumulates in neurofibrillary tangles, a pathological hallmark in Alzheimer's disease (AD) (van Leeuwen et al., 1998). UBB^{+1} is translated from an aberrant mRNA encoding a +1 frameshift protein in which the C-terminal glycine residue required for ubiquitylation is replaced by an extension of 20 amino acids (Dennissen et al., 2010). The detrimental impact of UBB^{+1} has been studied in neuronal cell cultures, transgenic mice, and yeast (De Vrij et al., 2001; Fischer et al., 2009; Tank and True, 2009). UBB^{+1} is a substrate for truncation, ubiquitylation, and proteasomal degradation (Dennissen et al., 2011; Lindsten et al., 2002; van Tijn et al., 2007, 2010). Whereas the ubiquitin-proteasome system (UPS) can assure the degradation of low levels of UBB^{+1}, higher levels impair the UPS and subvert the homeostatic mechanisms allowing for its elimination (Fischer et al., 2009; Lindsten et al., 2002; van Tijn et al., 2007, 2010). At high levels, UBB^{+1} affects mitochondrial dynamics and triggers neuronal cell death (De Vrij et al., 2001; Tan et al., 2007) through as-yet elusive mechanisms.

Yeast is an established model for studying programmed cell death mechanisms that are often shared with animal cells, including the contribution of caspases and mitochondrion-associated cell death proteins, such as cytochrome *c* (Carmona-Gutierrez et al., 2010). Yeast models have been used to explore cell killing by neurotoxic proteins, such as Parkinson-disease-associated α-synuclein, and the outcome could be successfully translated to fly, worm, and murine disease models, as well as to human disease (Braun et al., 2010; Büttner et al., 2013).

Driven by these premises, we established a yeast cell death model for UBB^{+1}-triggered neurotoxicity. Our findings revealed that UBB^{+1} interfered with the UPS and triggered the perturbation of the mitochondrion-associated basic amino acid synthesis executing cell death. The mitochondrion-associated UPS subroutine, depending on the AAA-ATPase Cdc48 and its co-factor Vms1, strongly antagonized UBB^{+1} cytotoxicity. Since VMS1,

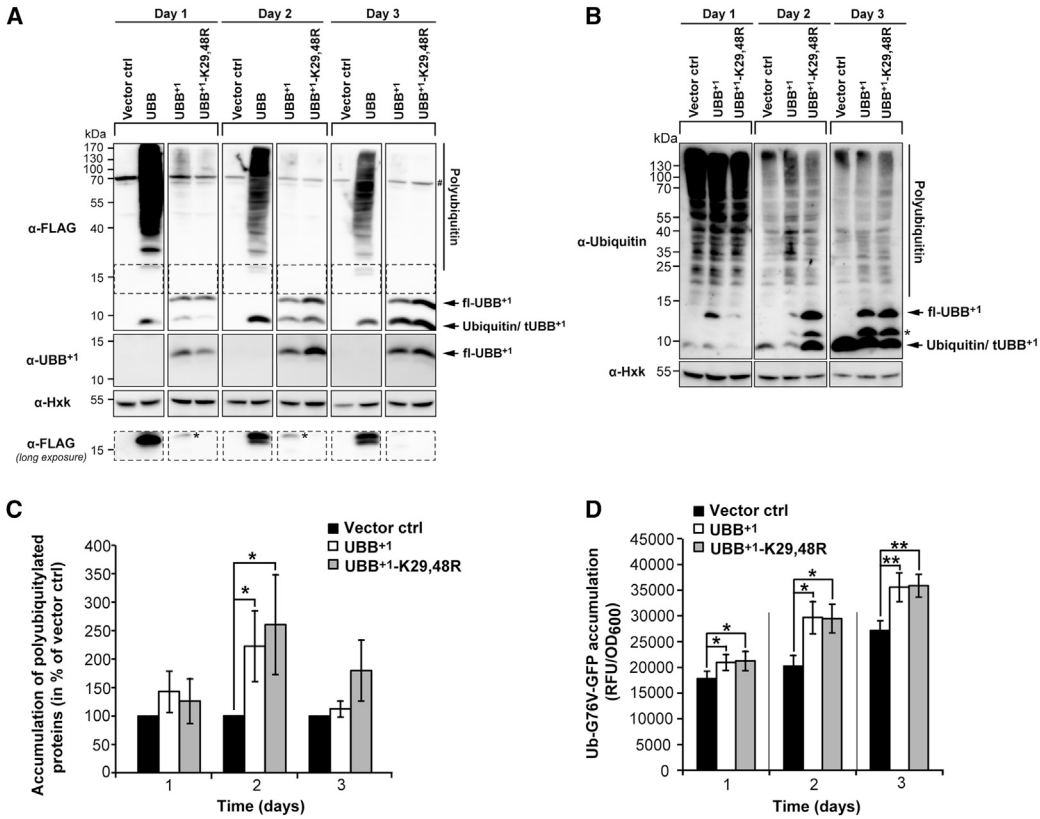

Figure 1. Expression of UBB^{+1} in Yeast and Its Effect on UPS Activity

(A) Proteins were expressed for 1, 2, or 3 days and determined by immunoblotting of cell extracts using antibodies directed against the N-terminal FLAG-tag, or the specific C terminus of UBB^{+1}. Hexokinase (Hxk) was used as loading control. #, unspecific protein band; fl-UBB^{+1}, full-length UBB^{+1}; tUBB^{+1}, truncated UBB^{+1}.

(B) The level of polyubiquitylated proteins and of UBB^{+1} in cell extracts was determined by immunoblotting using an antibody directed against ubiquitin. *Uncharacterized ubiquitin variant.

(C) Quantification of (B). The levels of polyubiquitylated proteins of cells transformed with vector controls were set to 100% in every experiment.

(D) Cellular level of ubiquitin-G76V-GFP upon UBB^{+1} expression. GFP fluorescence (relative fluorescence units, RFUs) was normalized to optical densities (OD_{600}).

Data: percentage change values (C) and mean values (D), respectively. Error bars: SE. p values: *p < 0.05, **p < 0.01. See Table S1 and Figure S1.

the human homolog of yeast Vms1, co-exists with UBB^{+1} in neurofibrillary tangles, these data imply a potential pivotal role of the UPS at mitochondria in AD.

RESULTS

Expression of Human UBB^{+1} in Yeast Recapitulates Hallmarks of UBB^{+1} in Neurons

To investigate whether the introduction of UBB^{+1} into yeast recapitulates hallmarks of UBB^{+1} accumulation in neurons, we expressed monomeric ubiquitin B (UBB), UBB^{+1}, as well as an UBB^{+1} variant lacking two lysine residues (K29,48R) that are important for its ubiquitylation. When expressing UBB, we detected a discrete immunoreactive band at the size of monomeric ubiquitin (9 kDa), and an immunoreactive smear across a wide range of the immunoblot that corresponds to ubiquitylated proteins (Figure 1A). This smear was not detectable upon transformation with UBB^{+1} or UBB^{+1}-K29,48R, reflecting their loss of function. Instead, UBB^{+1} or UBB^{+1}-K29,48R were detectable as 12 and 9 kDa protein species (full-length and truncated UBB^{+1}; fl-UBB^{+1} and tUBB^{+1}) that accumulated over time (Figures 1A, S1A, and S1B). In cells expressing UBB^{+1}, a faint higher molecular weight species corresponding to the size of monoubiquitylated fl-UBB^{+1} (21 kDa) appeared (Figure 1A, FLAG long exposure, asterisks). Consistent with a role of lysines 29 and/or 48 in the ubiquitylation of UBB^{+1}, this band was absent in cells expressing UBB^{+1}-K29,48R. These results suggest that in yeast human UBB (but not UBB^{+1}) can serve as a substrate for ubiquitin ligases and that, like in neurons, UBB^{+1} is ubiquitylated and truncated.

Next, we investigated whether UBB^{+1} expression results in UPS impairment by means of three complementary assays: (1) the measurement of polyubiquitylated endogenous proteins by immunoblot; (2) the assessment of the abundance of transgenic ubiquitin-G76V-GFP, which is a substrate of the ubiquitin-fusion degradation pathway; and (3) an enzymatic assay designed to quantify the chymotrypsin-like proteasomal activity. Cells expressing UBB^{+1} or UBB^{+1}-K29,48R contained a higher level of

polyubiquitylated proteins than cells transformed with vector controls (Figures 1B and 1C), suggesting decreased UPS-dependent protein turnover. The steady-state levels of ubiquitin-G76V-GFP were significantly increased upon expression of UBB^{+1} or UBB^{+1}-K29,48R (Figure 1D). In contrast, UBB^{+1} or UBB^{+1}-K29,48R expression did not reduce chymotrypsin-like proteasomal activities (Figure S1C). These data suggest that, in yeast like in neurons, UBB^{+1} expression impairs the UPS. However, in yeast UBB^{+1} does neither directly affect the enzymatic activity of proteasomes, nor is its ubiquitylation essential for UPS dysfunction.

UBB^{+1} Triggers Oxidative Stress and Programmed Cell Death upon Protracted Expression

To assess its effects on the fitness of proliferating cells, we performed growth assays on agar plates and in liquid cultures. As a positive control of cytotoxicity, TDP-43, a causal factor for motor neuron degeneration, was expressed. In sharp contrast with TDP-43, UBB^{+1} and UBB^{+1}-K29,48R failed to compromise the growth of cells on agar plates (Figure 2A), and in liquid cultures (Figure 2B), suggesting that UBB^{+1} is unable to kill proliferating cells.

Next, we studied the effects of UBB^{+1} or UBB^{+1}-K29,48R on chronologically aged cultures. For this, the proportion of viable cells capable of forming a colony (clonogenicity) on nutrient-containing solid medium was studied at different time points following UBB^{+1} or UBB^{+1}-K29,48R expression. Consistent with the growth assays, 16 hr (day 1) after UBB^{+1} or UBB^{+1}-K29,48R expression cells exhibited a similar clonogenic potential as did cells expressing vector controls (Figure 2C). In contrast, we observed a 10% and 25% decrease in clonogenic cell survival when expressing UBB^{+1} for 2 and 3 days, respectively. Exogenously applied stressors, including acetate and hydrogen peroxide, further enhanced the cytotoxicity of prolonged UBB^{+1} expression (Figures S2A and S2B, left). Upon both chronological aging and stress experiments, UBB^{+1}-K29,48R turned out to be slightly less cytotoxic as compared to UBB^{+1} (Figures 2C, S2A, and S2B, left), suggesting that ubiquitylated UBB^{+1} is slightly more cytotoxic than UBB^{+1}.

We next examined whether the UBB^{+1}-induced loss of clonogenicity correlated with the manifestation of oxidative stress, which can be detected by the intracellular conversion of the reactive oxygen species (ROS)-sensitive stain dihydroethidium (DHE) to fluorescent ethidium. We observed indistinguishable low levels of oxidative stress after expressing UBB^{+1} or UBB^{+1}-K29,48R for 16 hr (day 1) (Figure 2D). At later time points, the levels of oxidative stress progressively increased in all cultures with chronological aging, and UBB^{+1}-expressing cells exhibited a mild but significant increase in oxidative stress as compared to vector controls. Thus, upon UBB^{+1} expression increased markers of oxidative stress coincided with decreased clonogenic cell survival (cf. Figures 2C, 2D, and S2C). When combined with protracted UBB^{+1} expression, acetate or hydrogen peroxide exacerbated the signs of oxidative stress (Figures S2A and S2B, right). As shown for clonogenic survival, UBB^{+1}-K29,48R demonstrated slightly decreased levels of oxidative stress upon chronological aging or exogenously applied stress as compared to UBB^{+1} (Figures 2D, S2A, and S2B).

To determine the mode of cell death triggered by the expression of UBB^{+1} or UBB^{+1}-K29,48R, we performed double staining with Annexin V-FITC and propidium iodide (PI). Annexin V-FITC labels externalized phosphatidylserine that appears on the surface of apoptotic cells, whereas PI is a vital dye that stains cells that have lost plasma membrane integrity during necrosis. Two days after UBB^{+1} expression the frequencies of early apoptotic (Annexin V-$FITC^{+}$ PI^{-}), late apoptotic or secondary necrotic (Annexin V-$FITC^{+}$ PI^{+}), and necrotic cells (Annexin V-$FITC^{-}$ PI^{+}) were increased, as compared with vector controls (Figures 2E and S2D). Apoptosis induction by UBB^{+1} could be confirmed by the terminal deoxynucleotidyl transferase dUTP nick-end labeling (TUNEL) that detects fragmentation of nuclear DNA (Figures 2F and S2E). Consistent with the results obtained from the clonogenic survival and oxidative stress experiments, UBB^{+1}-K29,48R triggered cell death in a lower number of cells as compared to UBB^{+1} (Figures 2E and 2F). Altogether, these results indicate that the protracted expression of UBB^{+1} can induce apoptotic and necrotic killing of yeast cells, and that ubiquitylated UBB^{+1} is a slightly better killer than UBB^{+1}.

The UPS Capacity and the Ratio of Mutant to Wild-Type Ubiquitin Determine UBB^{+1}-Triggered Cytotoxicity

To investigate the putative contribution of dysfunctional UPS to UBB^{+1}-triggered cytotoxicity, we measured the cytotoxic potential of UBB^{+1} in the context of enhanced or suppressed UPS. Since full knockout of genes coding for proteasomal subunits is lethal, yeast strains bearing point mutations in one or two proteasomal genes were employed (Heinemeyer et al., 1993). The chymotrypsin-like proteasomal activity was reduced in strains carrying mutant alleles in the proteasomal subunits Pre1 and Pre2 by >88% (Figure 3A). In these conditions of close-to-complete proteasomal inactivation, significantly reduced clonogenic cell survival was only observed in the *pre1-1* and the *pre1-1/pre2-2* strains upon UBB^{+1} expression for day 1, and in the *pre1-1/pre2-2* strain upon UBB^{+1} expression for day 2 (Figures 3B and S3A), as compared to wild-type strain. One explanation for the increased UBB^{+1}-triggered cytotoxicity would be that UBB^{+1} accumulates in these strains due to impaired UBB^{+1} degradation. However, we could not observe increased steady-state levels of UBB^{+1} in these strains (neither fl-UBB^{+1}, nor tUBB^{+1}, nor ubiquitylated fl-UBB^{+1}) (Figures S3D–S3F; data not shown). Thus, although severe proteasomal inactivation can increase UBB^{+1}-triggered cell death, there is no strict correlation between the loss of proteasomal capacity on the one hand, and the increase in UBB^{+1}-triggered cytotoxicity or the increase in the steady-state levels of UBB^{+1} on the other hand.

Next, we measured UBB^{+1}-induced cytotoxicity in knockout strains lacking selective UPS genes, including (1) *UBI4* encoding ubiquitin (Finley et al., 1987), (2) *RPN4* encoding a major transcriptional UPS activator (Mannhaupt et al., 1999), (3) *UBR2* encoding the E3 ligase responsible for Rpn4 degradation (Kruegel et al., 2011), (4) *YUH1* encoding the ubiquitin protease that cleaves fl-UBB^{+1} into tUBB^{+1} (Dennissen et al., 2011), and (5) *UBP6* encoding a deubiquitinase, which can be inhibited by extended ubiquitin proteins (Krutauz et al., 2014). Only *RPN4*

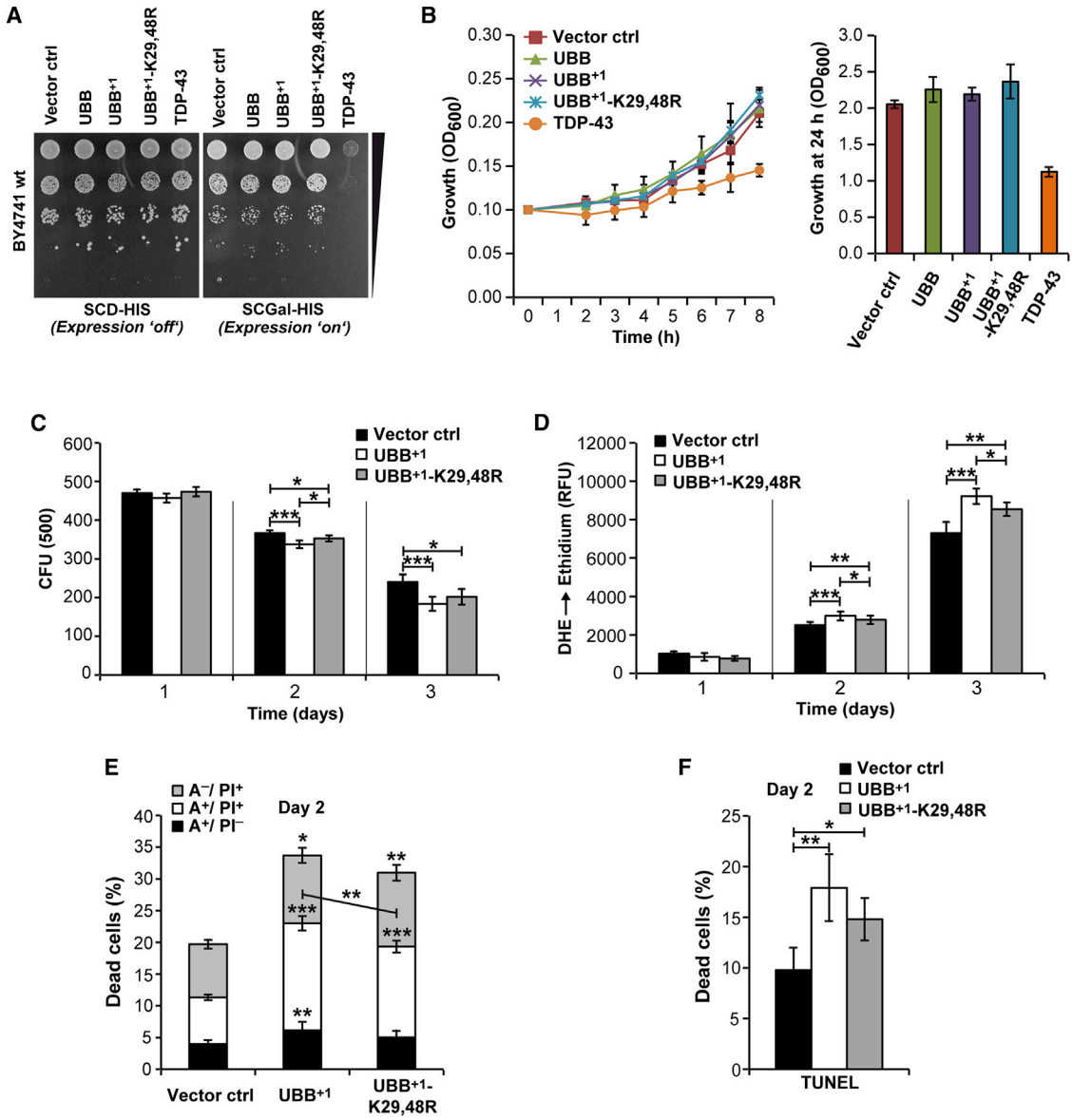

Figure 2. Cytotoxicity and Cell Death upon UBB^{+1} Expression

(A) Growth on solid media. Cultures were spotted in serial dilutions onto solid media inducing or repressing expression.

(B) Growth in liquid media. Left, growth curves. Right, cell densities during stationary phase.

(C) Yeast cells were evaluated for clonogenicity (colony forming units [CFUs]) at the indicated time points after inducing expression.

(D) Oxidative stress levels (DHE staining) were measured using a fluorescence plate reader at the indicated time points after inducing expression.

(E and F) Apoptosis and necrosis. (E) 2 days after inducing expression, yeast cells were measured for (early) apoptosis (Annexin V$^+$/PI$^-$), necrosis (Annexin V$^-$/PI$^+$), and (late) apoptosis/secondary necrosis (Annexin V$^+$/PI$^+$). (F) TUNEL-positive cells are referred to be apoptotic.

Data: mean values (B–F). Error bars: SD (B), and SE (C–F), respectively. p values: *p < 0.05, **p < 0.01, ***p < 0.001. See Table S1 and Figure S2.

deletion significantly impaired the chymotrypsin-like proteasomal capacity of the cells (Figure 3C). Notably, upon comparable fl-UBB^{+1} steady-state levels (Figures S3G and S3I), UBB^{+1}-triggered cytotoxicity was significantly increased in Δ*ubi4* as compared to Δ*rpn4* upon both stressed und unstressed conditions (Figures 3D and S3B), although the proteasomal capacity was lower in Δ*rpn4* as compared to Δ*ubi4* (Figure 3C). These data propose that the ratio of mutant ubiquitin (UBB^{+1}) to wild-type ubiquitin (encoded by *UBI4*) is more relevant for determining UBB^{+1}-triggered cytotoxicity than the proteasomal capacity.

Upon stressed conditions, UBB^{+1}-triggered cytotoxicity was markedly increased in Δ*yuh1* as compared to wild-type cells upon comparable fl-UBB^{+1} steady-state levels (Figures 3D, S3B, S3H, and S3I). These data suggest that UBB^{+1} truncation is a putative protective event, for instance, as part of a

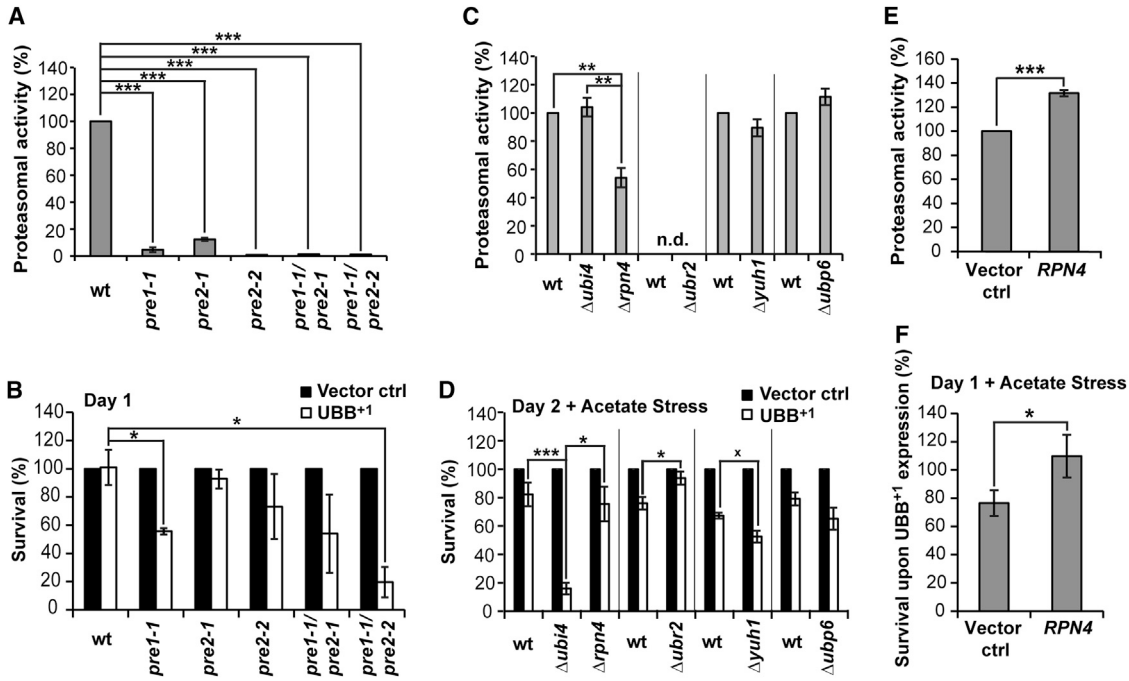

Figure 3. UBB^{+1}-Triggered Cytotoxicity in Yeast Strains with Various UPS Capacities

(A) Cultures were grown in logarithmic phase in YPD at 30°C and chymotrypsin-like activities were determined in proteasomal mutant strains. The relative luminescence units (RLUs) obtained using wild-type cells were set to 100% in every experiment.

(B) Clonogenicity in proteasomal mutant strains 1 day after inducing expression. The CFUs obtained using cells expressing vector controls were set to 100% in every experiment.

(C) Cultures were grown in logarithmic phase in YPD at 30°C and chymotrypsin-like activities were determined in UPS knockout strains. The RLUs obtained using wild-type cells were set to 100% in every experiment.

(D) Clonogenicity in UPS knockout strains 2 days after inducing expression following acetate treatment. The CFUs obtained using cells expressing vector controls were set to 100% in every experiment.

(E) Cultures were grown in logarithmic phase in defined medium inducing expression of the transcription activator *RPN4*, and chymotrypsin-like proteasomal activities were determined. The RLUs obtained using cells carrying vector controls were set to 100% in every experiment.

(F) Clonogenicity of UBB^{+1}-expressing cultures in strains with endogenous (vector control) and elevated levels of Rpn4 (Rpn4), respectively. Clonogenicity was determined 1 day after inducing expression followed by acetate treatment. The CFUs obtained using cells with endogenous and elevated levels of Rpn4, respectively, but lacking UBB^{+1}, were set to 100% in every experiment (not shown).

Data: percentage change values. Error bars: SE. p values: $^{x}p < 0.1$, $^{*}p < 0.05$, $^{**}p < 0.01$, $^{***}p < 0.001$. See Table S1 and Figure S3.

mechanism to degrade excessive UBB^{+1}. In Δ*ubp6* as compared to wild-type cells UBB^{+1}-triggered cytotoxicity was unaltered upon comparable fl-UBB^{+1} steady-state levels (Figures 3D, S3B, S3G, and S3I), suggesting that Ubp6 activity is not protective against the accumulation of the extended ubiquitin UBB^{+1}.

UBB^{+1}-triggered cytotoxicity was significantly relieved in Δ*ubr2* cells upon stressed conditions (Figures 3D and S3B), in which Rpn4 is stabilized and consequently the UPS activity is increased (Kruegel et al., 2011). Consistently, Rpn4 expression, which also leads to increased UPS activities (Figure 3E), was protective for UBB^{+1}-expressing wild-type cells (Figures 3F and S3C) but not for cells lacking *UBI4* (Figure S3C). In both cases, the protective effect cannot be explained by decreased steady-state levels of UBB^{+1} (Figures S3G and S3I–S3K). These data show that increasing UPS capacity is protective for UBB^{+1}-expressing cells, but not by affecting the turnover of UBB^{+1} itself but rather by interrupting the lethal signaling cascade triggered by UBB^{+1}.

UBB^{+1} Causes Lethal Mitochondrial Dysfunction

Oxidative stress and mitochondrial impairment are hallmarks of neurotoxin-elicited death in yeast and neurons (Braun, 2012; Debattisti and Scorrano, 2013). Therefore, we analyzed whether oxidative stress, which occurred starting by day 2 of UBB^{+1} expression (Figure 4A), correlated with mitochondrial impairment. Two days after inducing UBB^{+1} expression, the mitochondrial network was fragmented in both UBB^{+1}-expressing cells, as well as in cells carrying vector controls (data not shown), which is typical for stationary phase cultures. However, after shifting these cultures to fresh growth medium (which represses UBB^{+1} expression) the recovery of the mitochondrial network was significantly compromised in cultures transformed with UBB^{+1}-encoding constructs as compared with vector controls (Figures 4B and S4A). These data suggest that mitochondrial and oxidative stresses coincide in cells expressing UBB^{+1}.

We further tested for mitochondrial impairment by measuring the cellular oxygen consumption, the mitochondrial membrane potential, and the ATP levels in cells expressing UBB^{+1} for

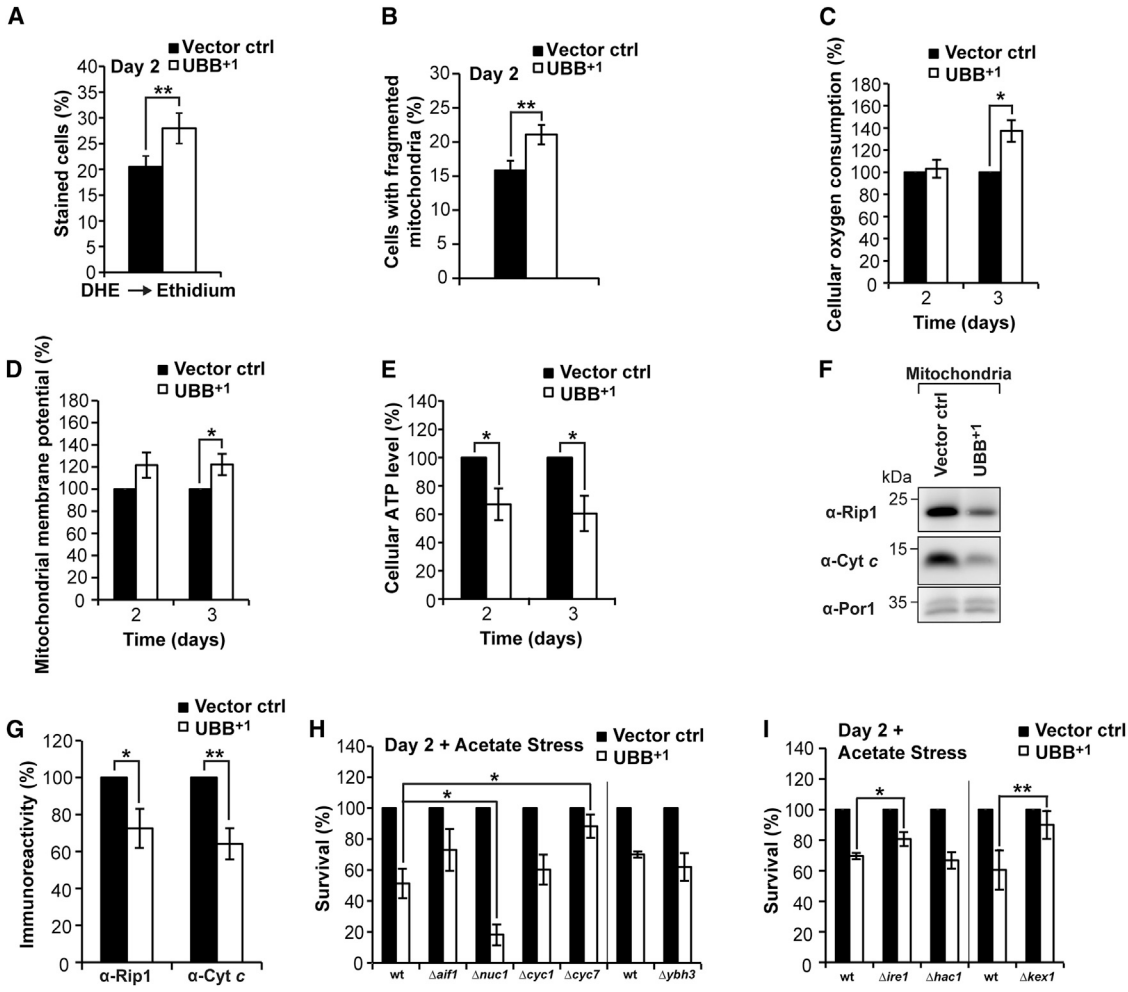

Figure 4. Pivotal Mitochondrial Impairment upon UBB^{+1} Expression

(A) Oxidative stress levels were measured by flow cytometry 2 days after inducing expression.

(B) Mitochondrial fragmentation. UBB^{+1} and RFP fused with a mitochondrial targeting sequence were expressed. 2 days after induction, cultures were shifted to fresh media repressing expression, and after 3 hr the proportion of cells with fragmented mitochondria was quantified.

(C–E) Cellular oxygen consumption (C), mitochondrial membrane potential (D), and cellular ATP levels (E) were determined 2 and 3 days after inducing UBB^{+1} expression. The oxygen consumption (C), mitochondrial membrane potential (D), and ATP levels (E) measured using cells carrying vector controls were set to 100% in every experiment.

(F and G) Protein alterations in crude mitochondria. UBB^{+1} was expressed for 24 hr and crude mitochondria were isolated by differential centrifugation. (F) Immunoblot demonstrating the steady-state levels of Rip1, cytochrome *c* (Cyt. *c*), and the mitochondrial outer membrane protein Por1 as loading control. (G) Quantification of (F). The immunoreactive signals obtained using cells carrying vector controls were set to 100% in every strain and experiment.

(H and I) UBB^{+1}-triggered cytotoxicity in strains deleted from genes encoding mitochondrial cell death (H), and ER-associated proteins (I), respectively. Clonogenicity was determined 2 days after inducing expression followed by acetate treatment. The CFUs obtained using cells carrying vector controls were set to 100% in every experiment.

Data: mean values (A and B), and percentage change values (C–E, G–I), respectively. Error bars: SE. p values: *p $\leq$ 0.05, **p < 0.01. See Table S1 and Figure S4.

days 2 and 3. Whereas the cellular oxygen consumption and mitochondrial membrane potential were significantly increased by day 3 in (surviving) cells expressing UBB^{+1} (Figures 4C and 4D), the cellular ATP levels were significantly decreased by days 2 and 3 (Figure 4E). These data hint at hyperactive mitochondria, which are incapable to prevent a metabolic crisis in UBB^{+1}-expressing cells.

In yeast, alterations in the cytochrome bc_1 complex of the mitochondrial respiratory chain may contribute to the loss of respiratory capacity and the production of lethal ROS (Diaz et al., 2012; Eisenberg et al., 2007). For instance, loss of the Rieske iron-sulfur protein Rip1, a key component of the cytochrome bc_1 complex, results in increased ROS generation and mitochondrial dysfunction (Diaz et al., 2012). Indeed, the cellular level of Rip1 was markedly decreased by days 2 and 3 upon UBB^{+1} expression as compared with vector controls (Figures S4B and S4C). Consistently, Rip1 and cytochrome *c* were depleted in the mitochondrial fraction of

UBB^{+1}-expressing cells (Figures 4F and 4G). These data further hint at a major UBB^{+1}-induced mitochondrial dysfunction, in which the respiratory chain is impaired (depletion of Rip1 and cytochrome *c*), leading to the production of ROS (for which cellular oxygen is needed), and the decline of cellular ATP levels.

Hyperpolarization of mitochondria may precede mitochondrion-dependent yeast death (Eisenberg et al., 2007); therefore, we expressed UBB^{+1} in strains deleted for genes encoding a range of mitochondrial cell death proteins, including the yeast BH3-only protein (Ybh3) that translocates to mitochondria to mediate their permeabilization, and several potentially cytotoxic proteins that can be released from mitochondria such as apoptosis-inducing factor 1 (Aif1), endonuclease G (Nuc1), and the two cytochrome *c* isoforms (Cyc1, Cyc7). Deletion of *NUC1* resulted in a paradoxical increase in UBB^{+1}-triggered cytotoxicity, and loss of Ybh3 did not have any effect upon both stressed and unstressed conditions (Figures 4H and S4D). In contrast, UBB^{+1}-mediated cytotoxicity was significantly decreased in strains depleted from isoform 2 of cytochrome *c* (Δ*cyc7*) upon stressed conditions (Figures 4H and S4D). The steady-state levels of UBB^{+1} were not decreased in the Δ*cyc7* as compared to wild-type strain (Figure S4F), and this strain maintained a normal state of respiratory competence (presumably due to the presence of the cytochrome *c* isoform 1 Cyc1) (Figure S4I), excluding trivial explanations for the cytoprotective action of Δ*cyc7*. Thus, our data suggest the implication of mitochondria in UBB^{+1}-triggered cell death.

Next, we tested for a possible role of the unfolded protein response (UPR) and the ER in UBB^{+1}-triggered cytotoxicity and expressed UBB^{+1} for 2 days in cells lacking the UPR kinase Ire1 and its downstream target Hac1, as well as in cells lacking the ER cell death protease Kex1 (which executes cell death in which mitochondria play a pivotal role [Hauptmann and Lehle, 2008]). Upon stress, UBB^{+1}-triggered cytotoxicity was relieved in Δ*ire1* and Δ*kex1* but not in Δ*hac1* cells (Figures 4I and S4E), under conditions where the steady-state levels of UBB^{+1} were comparable (Figures S4G and S4H). These data suggest for an implication of the ER in UBB^{+1}-triggered cytotoxicity, but, due to the lack of rescue in the Δ*hac1* cells, a critical involvement of the UPR is unlikely.

Perturbation of Basic Amino Acid Synthesis at Mitochondria Is a Decisive Toxic Event upon UBB^{+1} Accumulation

Next, we performed quantitative proteomic analyses of crude mitochondria after "stable isotope labeling by amino acids in cell culture" (SILAC). This approach led to the identification of 16 proteins whose abundance was significantly altered (increased for ten or decreased for six proteins) upon UBB^{+1} expression (Figure 5A; Table S2). Among the proteins with established mitochondrial localization, three were enzymes participating in amino acid metabolism, namely, Put1 (involved in proline degradation), Arg5,6, and Arg8 (involved in arginine and ornithine biosynthesis). In addition, UBB^{+1} induced the accumulation of the cytosolic enzyme Lys1 (involved in lysine biosynthesis), an increase in the motor protein Myo3 and the (putative) peroxisomal proteins Gpd1 and Str3, in crude mitochondria. Upon acetate stress, deletion of the *ARG5,6*, *ARG8*, and the *LYS1* genes restored the clonogenic potential of UBB^{+1}-expressing cells, whereas the deletion of all other genes had no effect (Figures 5B and S5A). These data point to a hitherto unexpected involvement of the biosynthesis of basic amino acids (arginine, ornithine, and lysine) in UBB^{+1}-triggered cytotoxicity.

To challenge this hypothesis, we measured the cellular steady-state levels of arginine, ornithine, and lysine in cultures expressing UBB^{+1} (Figure 5C). Indeed, we observed a marked increase in the cellular levels of all three basic amino acids, in particular, ornithine, upon UBB^{+1} accumulation. To weigh the contribution of arginine and ornithine (as opposed to their metabolic intermediates) to UBB^{+1} cytotoxicity, we measured ROS production upon UBB^{+1} expression in strains depleted from the arginine and ornithine biosynthetic enzymes (Figure 5D). Depletion of all enzymes operating upstream of cytosolic ornithine (Arg2, Arg5,6, Arg7, and Ort1) significantly relieved UBB^{+1}-triggered cytotoxicity both in unstressed and acetate-stressed conditions (Figures 5E and S5B). In contrast, none of the enzymes downstream of cytosolic ornithine (Arg3, Arg1, and Arg4, which are needed for the conversion of ornithine into arginine) were required for the cytotoxic action of UBB^{+1}. Notably, all tested enzymes operating upstream of cytosolic ornithine are mitochondrion-associated (Ljungdahl and Daignan-Fornier, 2012). Therefore, we concluded that UBB^{+1} triggers the mitochondrion-associated biosynthesis of ornithine, leading to increased cytosolic levels of ornithine (and its product arginine). This plays a decisive role in executing UBB^{+1}-triggered cell death.

If this model is true, increasing cytosolic levels of either ornithine or arginine (which can easily be interconverted into each other) should recover the cytotoxic effect of UBB^{+1} in strains with interrupted mitochondrion-associated biosynthesis of ornithine. Therefore, we measured UBB^{+1}-triggered cell death in the strain depleted for the mitochondrial protein Ort1 in growth media with increasing concentrations of arginine and ornithine, respectively. It turned out that Δ*ort1* cells were not able to efficiently uptake ornithine from the growth media, because the severe growth deficit of the Δ*ort1* strain in growth media lacking arginine could not be relieved by increasing concentrations of ornithine in the growth media (data not shown). In contrast, Δ*ort1* cells grew well in the presence of arginine in growth media lacking ornithine (data not shown), demonstrating the efficient cellular uptake of arginine. As expected, yeast cells lacking Ort1 were protected from UBB^{+1}-triggered cell death upon moderate concentrations of arginine (30 and 50 mg/l) in the growth media (Figure 5F). In contrast, elevated concentrations of arginine in the growth media (150 and 300 mg/l) recovered the cytotoxic effect of UBB^{+1} (Figure 5F), substantiating the decisive role of increased cellular levels of arginine (and cytosolic ornithine) in executing UBB^{+1}-triggered cell death.

In order to address the role of cellular levels of lysine, we measured UBB^{+1}-triggered cell death in the strain depleted from Lys1 in growth media with increasing concentrations of lysine. Whereas deletion of *LYS1* relieved UBB^{+1}-triggered cytotoxicity as compared to wild-type strain (Figure 5B), increasing the lysine concentrations did not promote cytotoxicity in the

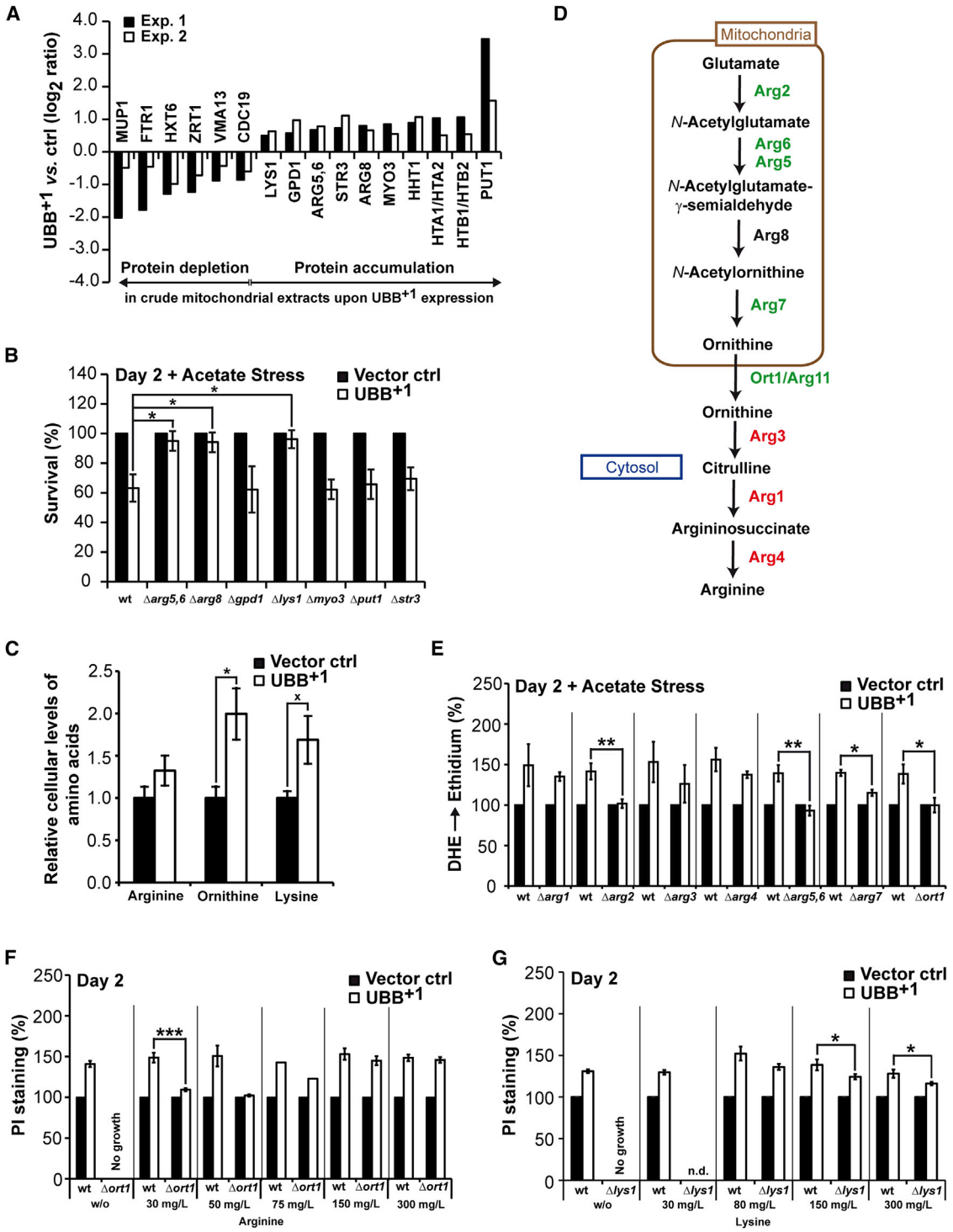

Figure 5. Perturbation of Basic Amino Acid Synthesis upon UBB^{+1} Expression

(A) Protein alterations in crude mitochondria were quantified by SILAC in two independent experiments. Changes are shown that were significant in both experiments.

(B) UBB^{+1}-triggered cytotoxicity in strains deleted from genes encoding proteins accumulating in crude mitochondria upon UBB^{+1} expression. Clonogenicity was determined 2 days after inducing expression followed by acetate treatment. The CFUs obtained using cells carrying vector controls were set to 100% in every experiment.

(C) Basic amino acids were isolated from cultures expressing UBB^{+1} or vector controls, respectively. The mean values of amino acids from cells carrying vector controls were set to 1.0 for every amino acid.

(legend continued on next page)

Δ*lys1* strain (Figure 5G). Thus, in contrast to arginine/ornithine the cellular lysine level appears to be negligible in accelerating UBB^{+1}-triggered cell death.

Cdc48/Vms1-Stimulated Mitochondrial UPS Protects from UBB^{+1}-Triggered Cytotoxicity

The aforementioned data incriminate mitochondria and the UPS in the execution of UBB^{+1}-triggered cytotoxicity, notably because of the protective impact of the removal of mitochondrial enzymes involved in basic amino acid synthesis and the overexpression of the transcriptional UPS activator Rpn4. Among the known Rpn4 targets are the conserved AAA-ATPase Cdc48 and its cofactor Npl4 (Bosis et al., 2010). Cdc48 and Npl4 are involved in the UPS, and determined by their cofactor Vms1, regulate mitochondrion-associated protein degradation (Heo et al., 2010). Driven by these premises, we evaluated the involvement of the Cdc48/Vms1/Npl4-dependent UPS pathway to UBB^{+1}-triggered cytotoxicity. For this, we measured UBB^{+1}-triggered cytotoxicity in normal and acetate-stressed conditions in strains expressing increased levels of wild-type Cdc48 or the pro-apoptotic Cdc48-S565G variant (Madeo et al., 1997), which is characterized by decreased Vms1 binding and mitochondrion-associated degradation (Heo et al., 2010). We also determined the cytotoxicity of UBB^{+1} in strains depleted from the Cdc48 cofactors Npl4 and Vms1, or overexpressing Vms1. UBB^{+1}-triggered cytotoxicity was markedly attenuated in cultures expressing increased levels of wild-type Cdc48, as compared to cells expressing Cdc48-S565G or controls with endogenous Cdc48 only (Figures 6A and S6A). UBB^{+1}-triggered cytotoxicity was significantly increased in cultures depleted from Npl4 under non-stressed conditions (Figures 6B and S6B). Depletion of Vms1 resulted in a marked elevation in cytotoxicity upon stress (Figures 6C and S6C), while overexpression of Vms1 significantly protected against UBB^{+1} upon acetate stress, as measured by the clonogenic approach (Figures 6D and S6D). High levels of Vms1 also protected from cell death and oxidative stress induced by UBB^{+1} expression (Figures 6E and 6F). Notably, high amounts of Cdc48 and Cdc48-S565G resulted in markedly decreased steady-state levels of UBB^{+1} (Figures S6E and S6F), whereas neither the deletion of *VMS1*, nor its overexpression had an effect on the cellular UBB^{+1} amounts (Figures S6G–S6J). These data point to a protective role of Vms1, which is independent from UBB^{+1} degradation, potentially by improving the quality control at mitochondria. In contrast, the beneficial role of high amounts of Cdc48 could be due to both increased Vms1-independent UBB^{+1} degradation and improved Vms1-dependent mitochondrial quality control.

In order to address whether elevated Vms1 levels prevent from UBB^{+1}-triggered mitochondrial impairment, we measured the cellular oxygen consumption, the mitochondrial membrane potential, and the cellular ATP levels in cells expressing UBB^{+1} upon endogenous or elevated amounts of Vms1 (Figures 6G–6I). Whereas the cellular oxygen consumption and the mitochondrial membrane potential were significantly decreased by day 3 and days 2 and 3, respectively, cellular ATP levels were significantly increased by day 2 upon high amounts of Vms1. In other words, high amounts of Vms1 reverted the mitochondrial damage induced by high levels of UBB^{+1} (see Figures 4C–4E).

In a next step, we used SILAC technology to comparatively assess alterations of the mitochondrial proteome between UBB^{+1}-expressing cells with endogenous and high levels of Vms1 (Figure 6J; Table S3). We observed that among the 16 proteins whose abundance levels were altered by UBB^{+1} as compared with the vector control (Figure 5A; Table S2), ten were no more altered upon expression of both UBB^{+1} and Vms1 (Figure 6J, blue-labeled proteins). Among these ten proteins, which were particularly stringently associated with the cytopathic activity of UBB^{+1}, the basic amino acid synthesis enzymes Arg5,6, Arg8, and Lys1 were significantly decreased in UBB^{+1}-expressing cells upon high levels of Vms1, as compared to endogenous Vms1 levels. Consistently, Vms1 overexpression blunted the UBB^{+1}-mediated increase in the steady-state levels of arginine, ornithine, and lysine (Figure 6K, see Figure 5C). These data point to a pivotal role of the Vms1-dependent mitochondrial UPS activity in avoiding the UBB^{+1}-triggered lethal overproduction of basic amino acids.

VMS1 Co-exists with tau and UBB^{+1} in Hippocampal Neurons from AD Patients

The hippocampus is severely affected during AD progression. Pathological hallmarks include intracellular neurofibrillary tangles comprising aberrant forms of the microtubule-associated protein tau, UBB^{+1}, and the mitochondrial outer membrane voltage-dependent anion channel 1 (VDAC1) (Reddy, 2013; van Leeuwen et al., 1998). Immunohistochemistry revealed expression of VMS1, the human homolog of yeast Vms1, in pyramidal cells within the hippocampi from AD patients and aged non-demented controls (Figure 7A, all arrows; Tables S5 and S6). VMS1 stained structures reminiscent of tau pathology, including tangle-like (yellow arrows) and neuropil thread-like structures (blue arrows), as well as other cellular staining patterns (green arrows), were observed in samples from AD patients, and aged non-demented controls with tau pathology. We also observed these tangle-like and thread-like staining patterns when analyzing the sections for aberrant tau, UBB^{+1}, and

(D) Arginine and ornithine biosynthetic pathway in *S. cerevisiae*. Green: deletion of genes encoding these enzymes does significantly prevent (green) and does not prevent (red) from UBB^{+1}-triggered oxidative stress, respectively (see E and Figure S5B); Black: no data.
(E) Oxidative stress in strains with disrupted arginine/ornithine biosynthesis was measured 2 days after inducing UBB^{+1} expression followed by acetate treatment. The oxidative stress levels obtained using cells carrying vector controls were set to 100% in every experiment.
(F) Cell death in strains with disrupted arginine/ornithine biosynthesis and increased levels of arginine in the growth media was measured 2 days after inducing UBB^{+1} expression. The proportion of dead cells carrying vector controls was set to 100% in every experiment.
(G) Cell death in strains with disrupted lysine biosynthesis and increased levels of lysine in the growth media was measured 2 days after inducing UBB^{+1} expression. The proportion of dead cells carrying vector controls was set to 100% in every experiment.
Data: percentage change values (B and E–G) and mean values (C), respectively. Error bars: SE. p values: $^{x}p < 0.1$, $^{*}p < 0.05$, $^{**}p < 0.01$, $^{***}p < 0.001$. See Tables S1, S2, and S4 and Figure S5.

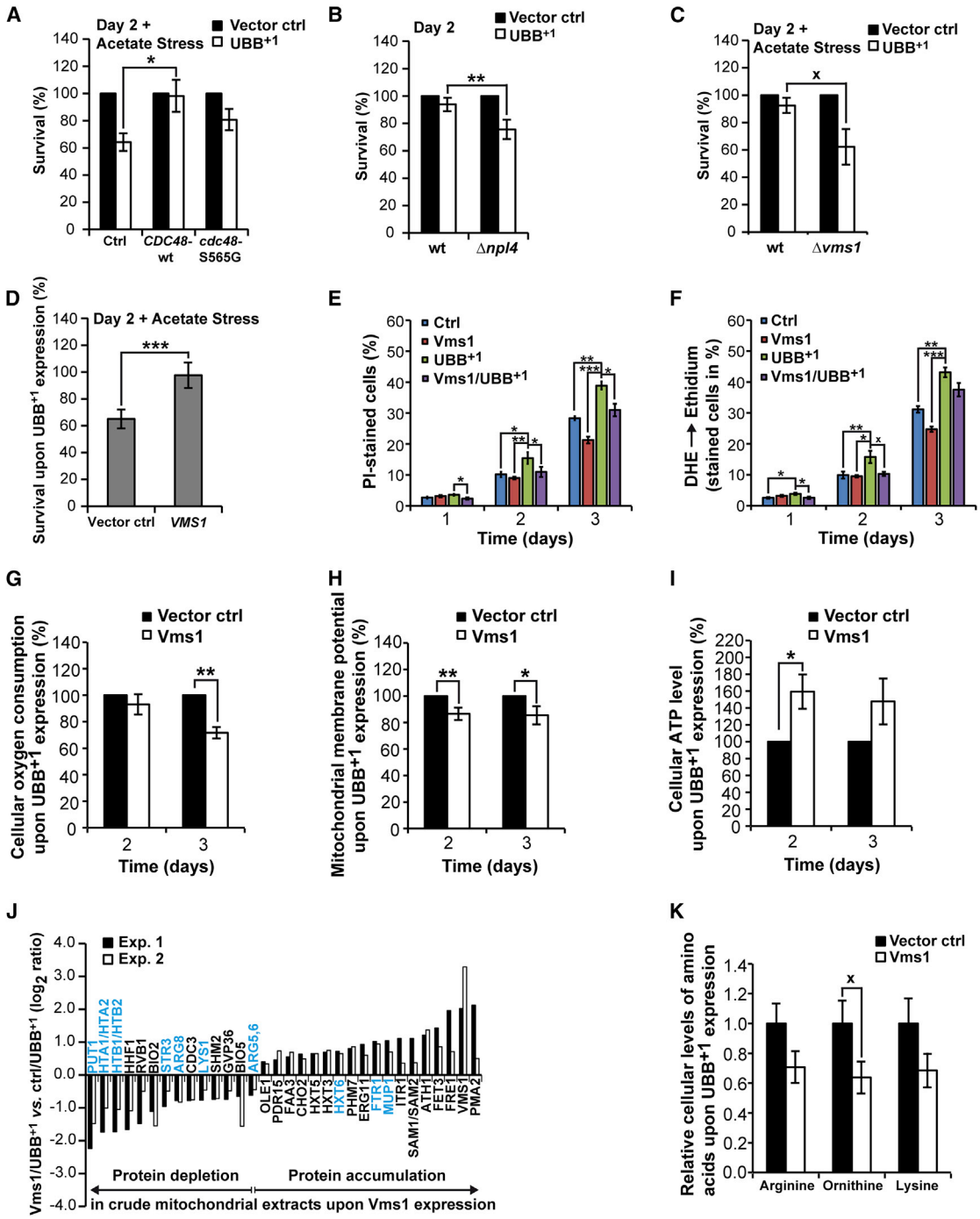

Figure 6. Role of Cdc48/Npl4/Vms1 Complex in UBB^{+1}-Triggered Cytotoxicity

(A–C) UBB^{+1} was expressed in strains with elevated levels of Cdc48 or Cdc48-S565G (A) and strains deleted for *NPL4* (B) and *VMS1* (C). Clonogenicity was determined 2 days after inducing expression before (B) and after acetate stress (A and C). The CFUs obtained using cells carrying vector controls were set to 100% in every experiment.

(D) Clonogenicity of UBB^{+1}-expressing cultures in strains with endogenous (vector control) and elevated levels of Vms1 (Vms1), respectively. Clonogenicity was determined 2 days after inducing expression followed by acetate treatment. The CFUs obtained using cells with endogenous and elevated levels of Vms1, respectively, but lacking UBB^{+1}, were set to 100% in every experiment (not shown).

(E and F) Cell death and oxidative stress was measured 1, 2, and 3 days after inducing expression of UBB^{+1} and/or Vms1.

(legend continued on next page)

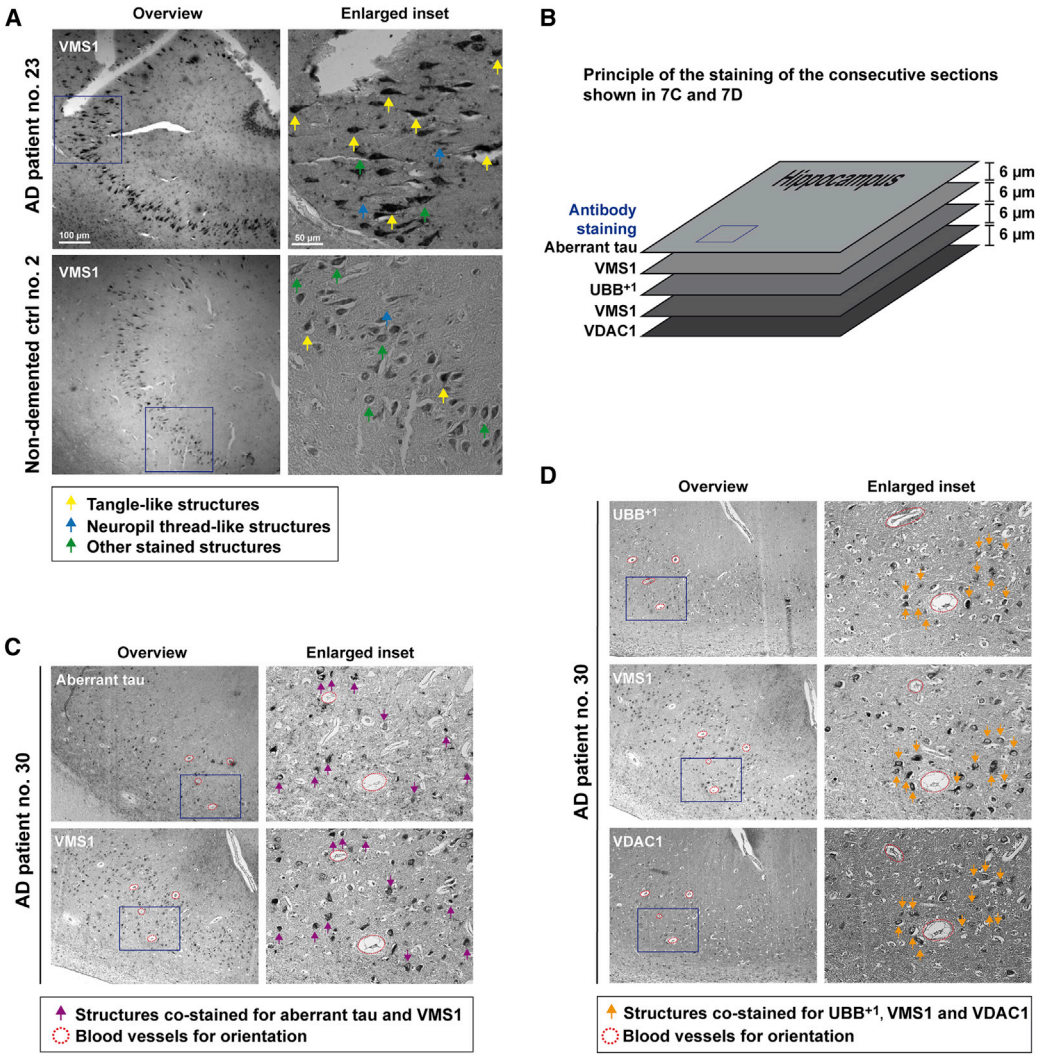

Figure 7. VMS1 Co-existence with Aberrant tau, UBB^{+1}, or VDAC1 in Hippocampi of AD Patients

(A) VMS1 staining in AD patient and non-demented control.

(B) Principle of the staining of consecutive sections from the hippocampus of an AD patient shown in (C) and (D).

(C) Co-existence of aberrant tau (MC1) and VMS1.

(D) Co-existence of UBB^{+1} (Ubi2a), VMS1, and VDAC1.

See Figure S7 and Tables S5 and S6.

VDAC1 (Figure S7). Immunohistochemistry of consecutive paraffin sections from the hippocampi of AD patients (Figure 7B) confirmed the identification of pyramidal cells with intracellular tangle-like structures, which co-stained for aberrant tau and VMS1 (Figure 7C, violet arrows), and for UBB^{+1}, VMS1, and VDAC1 (Figure 7D, orange arrows). These data suggest that

(G–I) UBB^{+1} was expressed in wild-type strain with endogenous (vector ctrl) and increased levels of Vms1 (Vms1). Cellular oxygen consumption (G), mitochondrial membrane potential (H), and cellular ATP levels (I) were determined 2 and 3 days after inducing expression. The oxygen consumption (G), mitochondrial membrane potential (H), and ATP levels (I) measured using cells with endogenous Vms1 were set to 100% in every experiment.

(J) Protein alterations in crude mitochondria upon Vms1 expression. Mitochondria were isolated from cultures expressing UBB^{+1} in cells with increased or endogenous levels of Vms1, respectively. Protein alterations were quantified by SILAC in two independent experiments. Changes were shown that were significant in both experiments. Blue-labeled proteins are inversely regulated as compared to Figure 5A.

(K) Cellular levels of basic amino acids upon Vms1 expression. Basic amino acids were isolated from cultures expressing UBB^{+1} in cells with endogenous (vector control) or increased levels of Vms1 (Vms1), respectively. The mean values of amino acids from cells with endogenous Vms1 levels were set to 1.0 for every amino acid.

Data: percentage change values (A–D, G–I) and mean values (E, F, K), respectively. Error bars: SE. p values: $^{x}p < 0.1$, $^{*}p < 0.05$, $^{**}p < 0.01$, $^{***}p < 0.001$. See Tables S1, S3, and S4 and Figure S6.

VMS1 is a component of neurofibrillary tangles comprising aberrant tau, UBB^{+1}, and VDAC1, underscoring a potential role of the Cdc48/VMS1 complex in UBB^{+1}-mediated AD progression.

DISCUSSION

We established a yeast model for dissecting cell death mechanisms triggered by UBB^{+1}, in which mitochondria play a pivotal role in the execution of cell death (see the Supplemental Discussion). UBB^{+1} triggers neuronal apoptosis accompanied by reduced mitochondrial movement (Tan et al., 2007), and mitochondrial impairment likely contributes to AD (Rodolfo et al., 2010). Thus, our yeast model corroborates features of cell-death-relevant mitochondrion dysfunctions found in AD neurons.

Yeast strains expressing UBB^{+1} accumulated the basic amino acids arginine, ornithine, and lysine. Deletion of mitochondrion-associated enzymes involved in their synthesis abolished UBB^{+1}-triggered cell killing, which could be recovered by increasing concentrations of arginine in the growth media. The accumulation of basic amino acids may trigger mitochondrial damage and cell death in mammalian cells and in yeast (Almeida et al., 2007; Biczó et al., 2011). For instance, increased production of nitric oxide from arginine executes yeast apoptosis (Almeida et al., 2007) and increased levels of polyamines, which are produced from ornithine, may impair neuronal ion channel activities (Inoue et al., 2013). The levels of arginine, ornithine, and/or their polyamine products were altered in aged human brains and in brains from AD patients (Inoue et al., 2013; Liu et al., 2014; Rushaidhi et al., 2012). The results of these studies are controversial, and it remains not yet clear whether the observed alterations are cause or consequence of AD. Despite that, our data suggest that perturbed basic amino acid synthesis is a decisive event triggering mitochondrion-dependent cell death upon UBB^{+1} accumulation in yeast. Further studies aiming at analyzing the role of arginine/ornithine metabolism during aging or AD progression should consider a potential pivotal contribution of UPS and mitochondrial dysfunctions.

We observed that UBB^{+1} accumulation impaired the UPS, and that the UPS activity, in turn, determined UBB^{+1} cytotoxicity. Yeast cultures that were depleted from ubiquitin (Δ*ubi4*) were highly vulnerable to UBB^{+1}. In contrast, yeast cultures in which the UPS was stimulated by the transcriptional activator Rpn4 were insensitive to UBB^{+1}, but not in cells lacking the ubiquitin gene *UBI4*. Extended ubiquitin variants have been proposed to be specific inhibitors of the deubiquitinase Ubp6 in yeast (Krutauz et al., 2014). Since the UBB^{+1}-triggered cytotoxicity was unaltered in a strain deleted for *UBP6* as compared to wild-type strain, our data suggest that the lethal effect of the extended ubiquitin UBB^{+1} does not essentially depend on Ubp6. It is tempting to speculate that the ratio of mutant (UBB^{+1}) to wild-type ubiquitin determines UBB^{+1}-triggered cytotoxicity with UBB^{+1} as a competitive inhibitor of wild-type ubiquitin, affecting numerous ubiquitin-regulated cellular processes.

We established that elevated amounts of Cdc48 or its cofactor Vms1 conferred tolerance against UBB^{+1} expression. More specifically, Vms1 overexpression relieved the UBB^{+1}-triggered mitochondrial damage and accumulation of the basic amino acids arginine, ornithine, and lysine. The Cdc48/Vms1 complex enables the degradation of mitochondrion-associated proteins (Heo et al., 2010). Whereas under normal conditions, this complex is predominantly cytosolic, Vms1 recruits Cdc48 to the mitochondrial outer membrane upon stress, presumably with the scope of improving the local quality of proteins. Our data suggest that Cdc48/Vms1-mediated processes can prevent the UBB^{+1}-triggered lethal derangement of mitochondria. In one possible scenario, Cdc48/Vms1 might remove protein junk from the mitochondrial outer membrane. Alternatively, Cdc48/Vms1 might specifically prevent the accumulation of arginine, ornithine, and lysine, through regulation of the turnover of the enzymes Arg5,6, Arg8, and Lys1, which are pivotal for their synthesis. Whereas the activity of the cytoplasmic enzyme Lys1 could be regulated by its degradation, the activities of the mitochondrion-associated Arg5,6 and Arg8 could be controlled by preventing their import into mitochondria via ubiquitylation and proteasomal degradation. Lys1, Arg5,6, and Arg8 are known targets for ubiquitylation (Xu et al., 2009), and the UPS regulates the import of mitochondrial intermembrane space proteins (Bragoszewski et al., 2013; Harbauer et al., 2014). It is tempting to speculate for a UPS-dependent regulation of the import of the mitochondrial matrix proteins Arg5,6 and Arg8. Further studies are needed to address the influence of UPS (dys)function on the turnover of these and other mitochondrial proteins. This is important because recent studies demonstrated that UPS dysfunction can lead to mitochondrial dysfunction and vice versa (Livnat-Levanon et al., 2014; Maharjan et al., 2014; Segref et al., 2014), and our data revealed the unexpected link between UBB^{+1}-triggered UPS dysfunction and the accumulation of functional enzymes in the mitochondrial matrix leading to potentially cytotoxic accumulation of basic amino acids.

Human VMS1 and mitochondrial VDAC1 co-existed with UBB^{+1} in neurofibrillary tangles of AD patients and aged non-demented controls with tau pathology. UBB^{+1} accumulates and the number of neurofibrillary tangles and damaged mitochondria markedly increase during AD progression (Dennissen et al., 2010; Rodolfo et al., 2010). We propose that VMS1-dependent mitochondrial quality control might retard the AD-associated neuronal dysfunction, which is elicited by the accumulation of both aberrant tau and UBB^{+1}.

EXPERIMENTAL PROCEDURES

Yeast Strains and Growth Conditions

Yeast expression constructs, strains, and growth conditions were described in the Supplemental Experimental Procedures. Gene expression was under the control of galactose-regulated promoters. For stressing cells, cultures were treated for 4 hr with acetate. For stable isotope labeling (SILAC), cells expressing vector controls, UBB^{+1}, or UBB^{+1} and Vms1 were grown in media supplemented either with Lys0 and Arg0 (normal isotopes), or with Lys4 and Arg6, or with Lys8 and Arg10 (heavy isotopes, Silantes).

Measuring Cytotoxicity Based on Growth and Clonogenicity

Assays were performed as described in the Supplemental Experimental Procedures. Briefly, growth deficits upon expression of proteins of interest on solid or liquid media, as compared to vector controls, suggest for cytotoxic effects of these proteins on (growing) yeast cells. For clonogenic assays, 500 cells from liquid yeast cultures expressing proteins of interest or vector controls, respectively, were plated on agar plates, on which

expression is repressed. The number of colonies (colony forming units [CFUs]) formed after 2 days of incubation correlates with the fitness of the culture.

Measurement of Oxidative Stress, Cell Death, Apoptosis, and Necrosis

Oxidative stress was determined by measuring the conversion of dihydroethidium (DHE, Sigma-Aldrich) to the red fluorescent ethidium applying a fluorescence plate reader or a flow cytometer. Cell death was measured by the incorporation of the "vital dye" propidium iodide (PI, Sigma-Aldrich) in cells that have lost their plasma membrane integrity using a flow cytometer. Annexin V/PI co-staining (Annexin V-FLUOS Staining Kit, Roche Applied Science) for discriminating early and late apoptosis, as well as necrosis, and terminal deoxynucleotidyl transferase dUTP nick end labeling (TUNEL) for measuring apoptosis (In Situ Cell Death Detection Kit, Roche Applied Science) were performed by flow cytometry. See the Supplemental Experimental Procedures for details.

Measurement of Cellular Oxygen Consumption, Mitochondrial Membrane Potential, and Cellular ATP Levels

Oxygen consumption of stationary yeast cultures was analyzed using the FireSting optical oxygen sensor system (Pyro Science). The decrease of the oxygen concentration over time in yeast cultures was determined. Mitochondrial membrane potential was assessed with flow cytometry after staining cells with tetramethylrhodamine methyl ester (TMRM, Molecular Probes, Life Technologies), a fluorescent dye that accumulates within mitochondria dependent on their membrane potential. To determine the ATP level of yeast cultures, intracellular metabolites were obtained using hot ethanol extraction. ATP was measured using the ATP Determination Kit (Molecular Probes, Life Technologies). This assay is based on an ATP-dependent reaction of recombinant firefly luciferase, which induces bioluminescence of its substrate D-luciferin and is directly correlated with the ATP content. All data were normalized to the number of living cells within the samples. See the Supplemental Experimental Procedures for details.

Measurement of UPS Activities

For determining the level of polyubiquitylated proteins in cellular extracts, immunoblots of cellular extracts were incubated with an ubiquitin-specific antibody and immunosignals were quantified with ImageJ 1.47 m. For measuring the turnover of UPS substrates, the ubiquitin-fusion protein ubiquitin-G76V-GFP was co-expressed with UBB^{+1} or vector controls. GFP fluorescence (relative fluorescence units [RFUs]) and optical densities (OD_{600}) were determined using the FLUOstar Omega plate reader. RFU was normalized to OD_{600}, in order to determine the level of ubiquitin-GFP fusion proteins per culture. Measurement of chymotrypsin-like proteasomal activities were performed using the FLUOstar Omega plate reader, applying the luminescence-based Proteasome-Glo Cell-Based Assay (Promega). See the Supplemental Experimental Procedures for details.

Generation of Cell Extracts, SDS-PAGE, and Immunoblot Analyses

Yeast cultures were incubated in expression media (SCGal) for the indicated time points. Cell extracts were generated by pre-treating yeast pellets in NaOH followed by heating in SDS lysis buffer. Protein extracts were separated on Tricine-SDS polyacrylamide gels, transferred on PVDF membranes, and incubated with primary and secondary antibodies coupled to horseradish peroxidase. Immunodetection was done using luminol. Membranes were digitized in an ImageQuant LAS 4000 (GE Healthcare). Images were processed with Adobe Photoshop CS6. Immunoblot quantification was done with the gel analysis method in ImageJ 1.47 m. See the Supplemental Experimental Procedures for details.

Mass Spectrometry

Crude mitochondrial extracts were taken up in SDS lysis buffer, thawed, reduced with DTT, and alkylated using iodoacetamide (Sigma-Aldrich). Protein mixtures were separated by SDS-PAGE using Bis-Tris gels (NuPAGE, Invitrogen). The gel lanes were cut into slices, which were in-gel digested with trypsin (Promega), and the resulting peptide mixtures were processed on STAGE tips. Mass spectrometry was performed on a LTQ Orbitrap XL mass spectrometer (Thermo Fisher Scientific) coupled to an Eksigent NanoLC-ultra. See the Supplemental Experimental Procedures for details.

Metabolomics

For extraction of metabolites cultures were harvested by filtration, washed with ddH_2O, and quenched in liquid nitrogen. Metabolites were extracted by acid extraction using trichloroacetic acid and by hot ethanol extraction. Extracts obtained from uniformly ^{13}C-labeled yeast cells served as internal standard. Metabolites were determined using ion pair reversed-phase liquid chromatography coupled to negative electro spray high-resolution mass spectrometry (IP-RP-LC/HRMS). LC/MS measurements were normalized to the total number of cells of each sample. See the Supplemental Experimental Procedures for details.

Immunohistochemistry

Experiments with human materials were in accordance with the local ethical committees at the Universities of Bayreuth (Germany) and Maastricht (the Netherlands). Postmortem tissues of hippocampi from AD patients and non-demented controls were obtained from the Netherlands Brain Bank (Table S6) as paraffin sections. For immunohistochemistry, sections were deparaffinated, incubated with primary antibodies against the indicated proteins, and with biotin-coupled secondary antibodies followed by the avidin-biotin-peroxidase complex. Immunodetection was performed by the colorimetric reaction of 3,3′-diaminobenzidine. Sections were dehydrated and coverslipped. See the Supplemental Experimental Procedures for details.

SUPPLEMENTAL INFORMATION

Supplemental Information includes Supplemental Discussion, Supplemental Experimental Procedures, seven figures, and six tables and can be found with this article online at http://dx.doi.org/10.1016/j.celrep.2015.02.009.

AUTHOR CONTRIBUTIONS

R.J.B. and F.M. initiated the project; R.J.B., C.S., F.M., T.E., C.M., J.D., and F.W.v.L. designed the experiments; R.J.B., C.S., C.L., R.J.G.G., V.I.D., K.P., T.E., L.H., and G.T. performed the experiments; R.J.B., C.S., C.L., V.I.D., T.E., R.J.G.G., F.W.v.L., K.P., and G.T. analyzed the data; R.J.B., C.S., F.M., and F.W.v.L. prepared figures and tables; R.J.B., F.M., and G.K. wrote the manuscript. See detailed author contributions in the Supplemental Information.

ACKNOWLEDGMENTS

We would like to thank Benedikt Westermann for critical reading of the manuscript and Jasmin Großer, Adil Günal, and Daniel Lux for technical support. We are grateful to the Deutsche Forschungsgemeinschaft (DFG) for grant BR 3706/3-1 to R.J.B., to the Federation of European Biochemistry Societies (FEBS) for short-term fellowship to R.J.B., to the Fonds zur Förderung der wissenschaftlichen Forschung (FWF) for grant DKplus Metabolic and Cardiovascular Disease to C.S., L.H., and F.M., for grants LIPOTOX, I1000, P23490-B12, and P24381-B20 to F.M., and to the Internationale Stichting Alzheimer Onderzoek (ISAO) for project 09-514 to F.W.v.L. T.E. is a recipient of an APART fellowship of the Austrian Academy of Sciences at the Institute of Molecular Biosciences, University of Graz. V.I.D. and J.D. are supported by the Excellence Initiative of the German Federal and State Governments through FRIAS and the excellence cluster BIOSS. G.T., C.M., F.S., and T.P. are grateful to the Austrian Federal Ministry for Transport, Innovation and Technology (bmvit) for project Met2Net. G.K. is financed by the Ligue contre le Cancer (équipe labelisée); Agence National de la Recherche (ANR); Association pour la recherche sur le cancer (ARC); Cancéropôle Ile-de-France; Institut National du Cancer (INCa); Fondation Bettencourt-Schueller; Fondation de France; Fondation pour la Recherche Médicale (FRM); the European Commission (ArtForce); the European Research Council (ERC); the LabEx Immuno-Oncology; the SIRIC Stratified Oncology Cell DNA Repair and Tumor Immune Elimination

(SOCRATE); the SIRIC Cancer Research and Personalized Medicine (CARPEM); and the Paris Alliance of Cancer Research Institutes (PACRI). This publication was funded by the University of Bayreuth in the funding program Open Access Publishing.

Received: June 26, 2014
Revised: December 23, 2014
Accepted: January 31, 2015
Published: March 5, 2015

REFERENCES

Almeida, B., Büttner, S., Ohlmeier, S., Silva, A., Mesquita, A., Sampaio-Marques, B., Osório, N.S., Kollau, A., Mayer, B., Leão, C., et al. (2007). NO-mediated apoptosis in yeast. J. Cell Sci. *120*, 3279–3288.

Biczó, G., Hegyi, P., Dósa, S., Shalbuyeva, N., Berczi, S., Sinervirta, R., Hracskó, Z., Siska, A., Kukor, Z., Jármay, K., et al. (2011). The crucial role of early mitochondrial injury in L-lysine-induced acute pancreatitis. Antioxid. Redox Signal. *15*, 2669–2681.

Bosis, E., Salomon, D., Ohayon, O., Sivan, G., Bar-Nun, S., and Rabinovich, E. (2010). Ssz1 restores endoplasmic reticulum-associated protein degradation in cells expressing defective cdc48-ufd1-npl4 complex by upregulating cdc48. Genetics *184*, 695–706.

Bragoszewski, P., Gornicka, A., Sztolsztener, M.E., and Chacinska, A. (2013). The ubiquitin-proteasome system regulates mitochondrial intermembrane space proteins. Mol. Cell. Biol. *33*, 2136–2148.

Braun, R.J. (2012). Mitochondrion-mediated cell death: dissecting yeast apoptosis for a better understanding of neurodegeneration. Front. Oncol. *2*, 182.

Braun, R.J., Büttner, S., Ring, J., Kroemer, G., and Madeo, F. (2010). Nervous yeast: modeling neurotoxic cell death. Trends Biochem. Sci. *35*, 135–144.

Büttner, S., Habernig, L., Broeskamp, F., Ruli, D., Vögtle, F.N., Vlachos, M., Macchi, F., Küttner, V., Carmona-Gutierrez, D., Eisenberg, T., et al. (2013). Endonuclease G mediates α-synuclein cytotoxicity during Parkinson's disease. EMBO J. *32*, 3041–3054.

Carmona-Gutierrez, D., Ruckenstuhl, C., Bauer, M.A., Eisenberg, T., Büttner, S., and Madeo, F. (2010). Cell death in yeast: growing applications of a dying buddy. Cell Death Differ. *17*, 733–734.

De Vrij, F.M., Sluijs, J.A., Gregori, L., Fischer, D.F., Hermens, W.T., Goldgaber, D., Verhaagen, J., Van Leeuwen, F.W., and Hol, E.M. (2001). Mutant ubiquitin expressed in Alzheimer's disease causes neuronal death. FASEB J. *15*, 2680–2688.

Debattisti, V., and Scorrano, L. (2013). *D. melanogaster*, mitochondria and neurodegeneration: small model organism, big discoveries. Mol. Cell. Neurosci. *55*, 77–86.

Dennissen, F.J., Kholod, N., Steinbusch, H.W., and Van Leeuwen, F.W. (2010). Misframed proteins and neurodegeneration: a novel view on Alzheimer's and Parkinson's diseases. Neurodegener. Dis. *7*, 76–79.

Dennissen, F.J., Kholod, N., Hermes, D.J., Kemmerling, N., Steinbusch, H.W., Dantuma, N.P., and van Leeuwen, F.W. (2011). Mutant ubiquitin (UBB+1) associated with neurodegenerative disorders is hydrolyzed by ubiquitin C-terminal hydrolase L3 (UCH-L3). FEBS Lett. *585*, 2568–2574.

Diaz, F., Enríquez, J.A., and Moraes, C.T. (2012). Cells lacking Rieske iron-sulfur protein have a reactive oxygen species-associated decrease in respiratory complexes I and IV. Mol. Cell. Biol. *32*, 415–429.

Eisenberg, T., Büttner, S., Kroemer, G., and Madeo, F. (2007). The mitochondrial pathway in yeast apoptosis. Apoptosis *12*, 1011–1023.

Finley, D., Ozkaynak, E., and Varshavsky, A. (1987). The yeast polyubiquitin gene is essential for resistance to high temperatures, starvation, and other stresses. Cell *48*, 1035–1046.

Fischer, D.F., van Dijk, R., van Tijn, P., Hobo, B., Verhage, M.C., van der Schors, R.C., Li, K.W., van Minnen, J., Hol, E.M., and van Leeuwen, F.W. (2009). Long-term proteasome dysfunction in the mouse brain by expression of aberrant ubiquitin. Neurobiol. Aging *30*, 847–863.

Harbauer, A.B., Zahedi, R.P., Sickmann, A., Pfanner, N., and Meisinger, C. (2014). The protein import machinery of mitochondria-a regulatory hub in metabolism, stress, and disease. Cell Metab. *19*, 357–372.

Hauptmann, P., and Lehle, L. (2008). Kex1 protease is involved in yeast cell death induced by defective N-glycosylation, acetic acid, and chronological aging. J. Biol. Chem. *283*, 19151–19163.

Heinemeyer, W., Gruhler, A., Möhrle, V., Mahé, Y., and Wolf, D.H. (1993). PRE2, highly homologous to the human major histocompatibility complex-linked RING10 gene, codes for a yeast proteasome subunit necessary for chrymotryptic activity and degradation of ubiquitinated proteins. J. Biol. Chem. *268*, 5115–5120.

Heo, J.M., Livnat-Levanon, N., Taylor, E.B., Jones, K.T., Dephoure, N., Ring, J., Xie, J., Brodsky, J.L., Madeo, F., Gygi, S.P., et al. (2010). A stress-responsive system for mitochondrial protein degradation. Mol. Cell *40*, 465–480.

Inoue, K., Tsutsui, H., Akatsu, H., Hashizume, Y., Matsukawa, N., Yamamoto, T., and Toyo'oka, T. (2013). Metabolic profiling of Alzheimer's disease brains. Sci. Rep. *3*, 2364.

Kruegel, U., Robison, B., Dange, T., Kahlert, G., Delaney, J.R., Kotireddy, S., Tsuchiya, M., Tsuchiyama, S., Murakami, C.J., Schleit, J., et al. (2011). Elevated proteasome capacity extends replicative lifespan in *Saccharomyces cerevisiae*. PLoS Genet. *7*, e1002253.

Krutauz, D., Reis, N., Nakasone, M.A., Siman, P., Zhang, D., Kirkpatrick, D.S., Gygi, S.P., Brik, A., Fushman, D., and Glickman, M.H. (2014). Extended ubiquitin species are protein-based DUB inhibitors. Nat. Chem. Biol. *10*, 664–670.

Lindsten, K., de Vrij, F.M., Verhoef, L.G., Fischer, D.F., van Leeuwen, F.W., Hol, E.M., Masucci, M.G., and Dantuma, N.P. (2002). Mutant ubiquitin found in neurodegenerative disorders is a ubiquitin fusion degradation substrate that blocks proteasomal degradation. J. Cell Biol. *157*, 417–427.

Liu, P., Fleete, M.S., Jing, Y., Collie, N.D., Curtis, M.A., Waldvogel, H.J., Faull, R.L., Abraham, W.C., and Zhang, H. (2014). Altered arginine metabolism in Alzheimer's disease brains. Neurobiol. Aging *35*, 1992–2003.

Livnat-Levanon, N., Kevei, É., Kleifeld, O., Krutauz, D., Segref, A., Rinaldi, T., Erpapazoglou, Z., Cohen, M., Reis, N., Hoppe, T., and Glickman, M.H. (2014). Reversible 26S proteasome disassembly upon mitochondrial stress. Cell Rep. *7*, 1371–1380.

Ljungdahl, P.O., and Daignan-Fornier, B. (2012). Regulation of amino acid, nucleotide, and phosphate metabolism in *Saccharomyces cerevisiae*. Genetics *190*, 885–929.

Madeo, F., Fröhlich, E., and Fröhlich, K.U. (1997). A yeast mutant showing diagnostic markers of early and late apoptosis. J. Cell Biol. *139*, 729–734.

Maharjan, S., Oku, M., Tsuda, M., Hoseki, J., and Sakai, Y. (2014). Mitochondrial impairment triggers cytosolic oxidative stress and cell death following proteasome inhibition. Sci. Rep. *4*, 5896.

Mannhaupt, G., Schnall, R., Karpov, V., Vetter, I., and Feldmann, H. (1999). Rpn4p acts as a transcription factor by binding to PACE, a nonamer box found upstream of 26S proteasomal and other genes in yeast. FEBS Lett. *450*, 27–34.

Reddy, P.H. (2013). Is the mitochondrial outermembrane protein VDAC1 therapeutic target for Alzheimer's disease? Biochim. Biophys. Acta *1832*, 67–75.

Rodolfo, C., Ciccosanti, F., Giacomo, G.D., Piacentini, M., and Fimia, G.M. (2010). Proteomic analysis of mitochondrial dysfunction in neurodegenerative diseases. Expert Rev. Proteomics *7*, 519–542.

Rushaidhi, M., Jing, Y., Kennard, J.T., Collie, N.D., Williams, J.M., Zhang, H., and Liu, P. (2012). Aging affects L-arginine and its metabolites in memory-associated brain structures at the tissue and synaptoneurosome levels. Neuroscience *209*, 21–31.

Segref, A., Kevei, É., Pokrzywa, W., Schmeisser, K., Mansfeld, J., Livnat-Levanon, N., Ensenauer, R., Glickman, M.H., Ristow, M., and Hoppe, T. (2014). Pathogenesis of human mitochondrial diseases is modulated by reduced activity of the ubiquitin/proteasome system. Cell Metab. *19*, 642–652.

Tan, Z., Sun, X., Hou, F.S., Oh, H.W., Hilgenberg, L.G., Hol, E.M., van Leeuwen, F.W., Smith, M.A., O'Dowd, D.K., and Schreiber, S.S. (2007). Mutant ubiquitin found in Alzheimer's disease causes neuritic beading of mitochondria in association with neuronal degeneration. Cell Death Differ. *14*, 1721–1732.

Tank, E.M., and True, H.L. (2009). Disease-associated mutant ubiquitin causes proteasomal impairment and enhances the toxicity of protein aggregates. PLoS Genet. *5*, e1000382.

van Leeuwen, F.W., de Kleijn, D.P., van den Hurk, H.H., Neubauer, A., Sonnemans, M.A., Sluijs, J.A., Köycü, S., Ramdjielal, R.D., Salehi, A., Martens, G.J., et al. (1998). Frameshift mutants of beta amyloid precursor protein and ubiquitin-B in Alzheimer's and Down patients. Science *279*, 242–247.

van Tijn, P., de Vrij, F.M., Schuurman, K.G., Dantuma, N.P., Fischer, D.F., van Leeuwen, F.W., and Hol, E.M. (2007). Dose-dependent inhibition of proteasome activity by a mutant ubiquitin associated with neurodegenerative disease. J. Cell Sci. *120*, 1615–1623.

van Tijn, P., Verhage, M.C., Hobo, B., van Leeuwen, F.W., and Fischer, D.F. (2010). Low levels of mutant ubiquitin are degraded by the proteasome in vivo. J. Neurosci. Res. *88*, 2325–2337.

Xu, P., Duong, D.M., Seyfried, N.T., Cheng, D., Xie, Y., Robert, J., Rush, J., Hochstrasser, M., Finley, D., and Peng, J. (2009). Quantitative proteomics reveals the function of unconventional ubiquitin chains in proteasomal degradation. Cell *137*, 133–145.

Cell Reports

Supplemental Information

Accumulation of Basic Amino Acids at Mitochondria Dictates the Cytotoxicity of Aberrant Ubiquitin

Ralf J. Braun, Cornelia Sommer, Christine Leibiger, Romina J.G. Gentier, Verónica I. Dumit, Katrin Paduch, Tobias Eisenberg, Lukas Habernig, Gert Trausinger, Christoph Magnes, Thomas Pieber, Frank Sinner, Jörn Dengjel, Fred W. van Leeuwen, Guido Kroemer, and Frank Madeo

Supplemental Information

Supplemental Items Inventory

- *Supplemental Figures and Legends*
  - Figure S1 (related to Figure 1)
    Expression of UBB^{+1} in yeast and its effect on proteasomal activities
  - Figure S2 (related to Figure 2)
    Stressors elevating UBB^{+1}-triggered cytotoxicity, and markers of oxidative stress, apoptosis and necrosis
  - Figure S3 (related to Figure 3)
    UBB^{+1}-triggered cytotoxicity in yeast strains with various UPS capacities, and expression controls
  - Figure S4 (related to Figure 4)
    Mitochondrial impairment upon UBB^{+1} expression, respiratory and expression capacities of strains deleted for cell death genes
  - Figure S5 (related to Figure 5)
    Cytotoxicity of UBB^{+1} in strains with disrupted arginine/ornithine biosynthesis
  - Figure S6 (related to Figure 6)
    Role of Cdc48/Npl4/Vms1 complex in UBB^{+1}-triggered cytotoxicity and steady-state levels of UBB^{+1}
  - Figure S7 (related Figure 7)
    Pathological hallmarks in AD patients, and in non-demented controls
- *Supplemental Tables*
  - Table S1 (related to Figures 1-6)
    Data pooling and statistics
  - Table S2 (related to Figure 5)
    Protein alterations in crude mitochondrial extracts upon expression of UBB^{+1}
  - Table S3 (related to Figure 6)
    Protein alterations in crude mitochondrial extracts upon expression of UBB^{+1} and increased levels of Vms1
  - Table S4 (related to Tables S2+S3)
    Protein identifications and quantification by SILAC analysis of crude mitochondrial extracts
  - Table S5 (related to Figure 7)
    Immunoreactivities in the human hippocampus and entorhinal cortex for VMS1
  - Table S6 (related to Figures 7+S7 and Table S5)
    Clinico-pathological information of non-demented controls and AD patients
- *Supplemental Discussion*
- *Supplemental Experimental Procedures*
- *Supplemental References*
- *Detailed Author Contributions*

Supplemental Figures and Legends

Figure S1 (related to Figure 1):

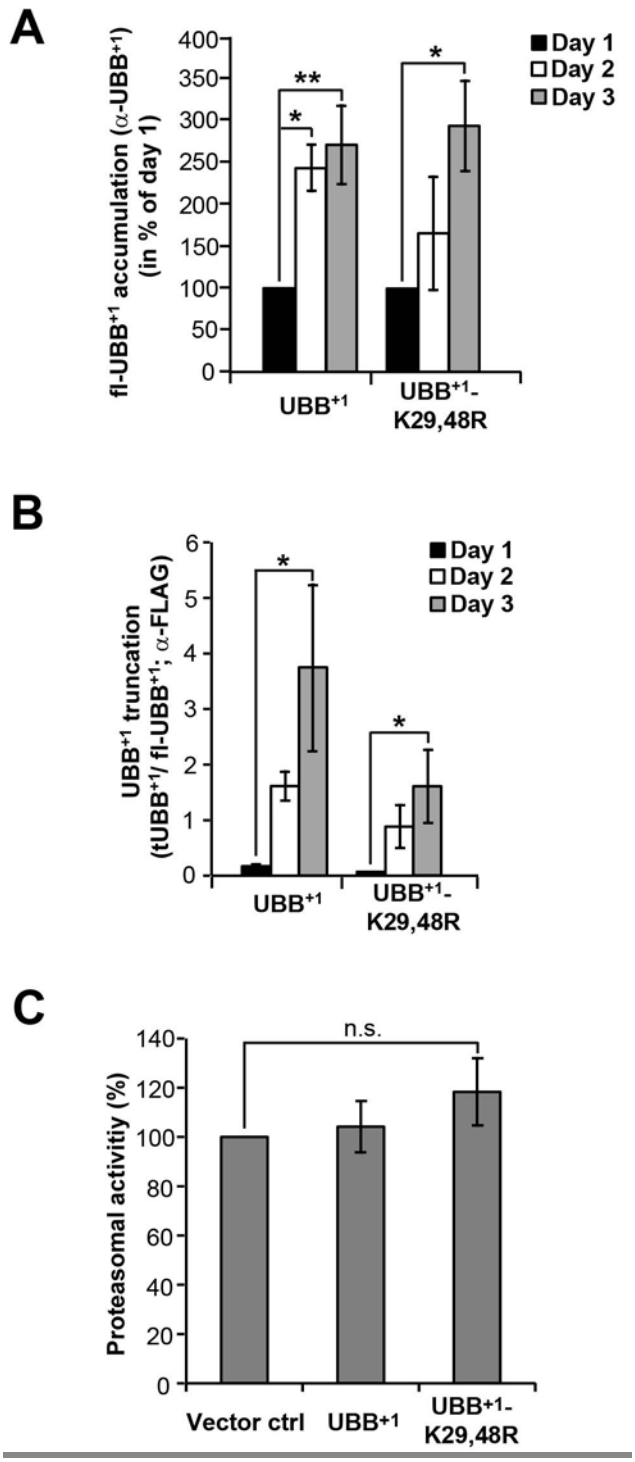

Figure S1: Expression of UBB^{+1} in yeast and its effect on proteasomal activities

(A+B) Expression of UBB^{+1} as in Figure 1A. (A) Accumulation of UBB^{+1} was determined by the quantification of immunoblots of cell extracts using antibodies directed against the specific C-terminus of UBB^{+1} and hexokinase (Hxk) as loading control. Full-length UBB^{+1} (fl-UBB^{+1}) levels at day 1 were set to 100% in every experiment. The data shown here are percent change values of five independent experiments. Error bars: standard error. *p < 0.05, **p < 0.01 (ANOVA/ Bonferroni t-test).

(B) Truncation of UBB^{+1} was determined by the quantification of immunoblots of cell extracts using an antibody directed against the N-terminal FLAG-tag of UBB^{+1}. The data shown here are mean values of five independent experiments. fl-UBB^{+1}: full-length UBB^{+1}, tUBB^{+1}: truncated UBB^{+1}. Error bars: standard error. *p < 0.05 (ANOVA on ranks/ Dunn's method).

(C) UBB^{+1} was expressed overnight. Cultures were diluted in expression medium, grown to logarithmic phase, and chymotrypsin-like proteasomal activities were determined. The proteasomal activities obtained using yeast cells expressing vector controls were set to 100% in every experiment. The data shown here are percent change values of four independent experiments. Error bars: standard error. n.s.: not significant (ANOVA).

Figure S2 (related to Figure 2):

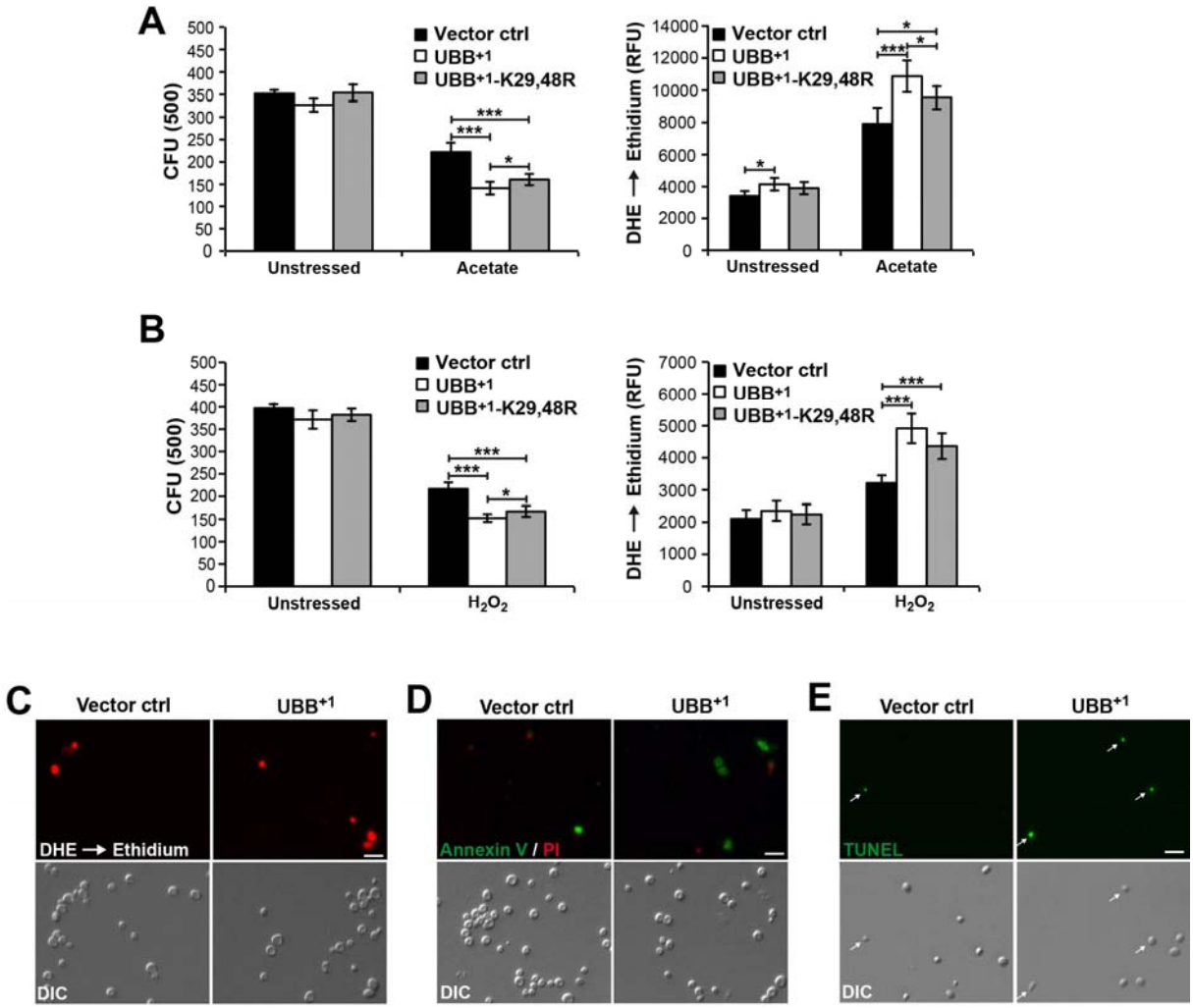

Figure S2: Stressors elevating UBB^{+1}-triggered cytotoxicity, and markers of oxidative stress, apoptosis and necrosis

(A+B) Sensitivity against mitochondrial stressors upon UBB^{+1} expression. Two days after inducing expression, yeast cultures were treated for 4 h either with 140 mM acetate (A), or 2.8 mM hydrogen peroxide (H_2O_2) (B). *Left panels:* Measurement of clonogenicity. *Right panels:* Measurement of oxidative stress (DHE staining) using a fluorescence plate reader. The data shown here are mean values of six and nine independent experiments for (A) and (B), respectively. Error bars: standard error. p-values: *p < 0.05, **p < 0.01, ***p < 0.001 (RM ANOVA/ Holm-Sidak method).

(C-E) Fluorescence microscopic analysis of DHE- (C), Annexin V/PI- (D), and TUNEL- (E) stained cells described in Figure 2D-F. Scale bar: 10 µm.

Figure S3 (related to Figure 3):

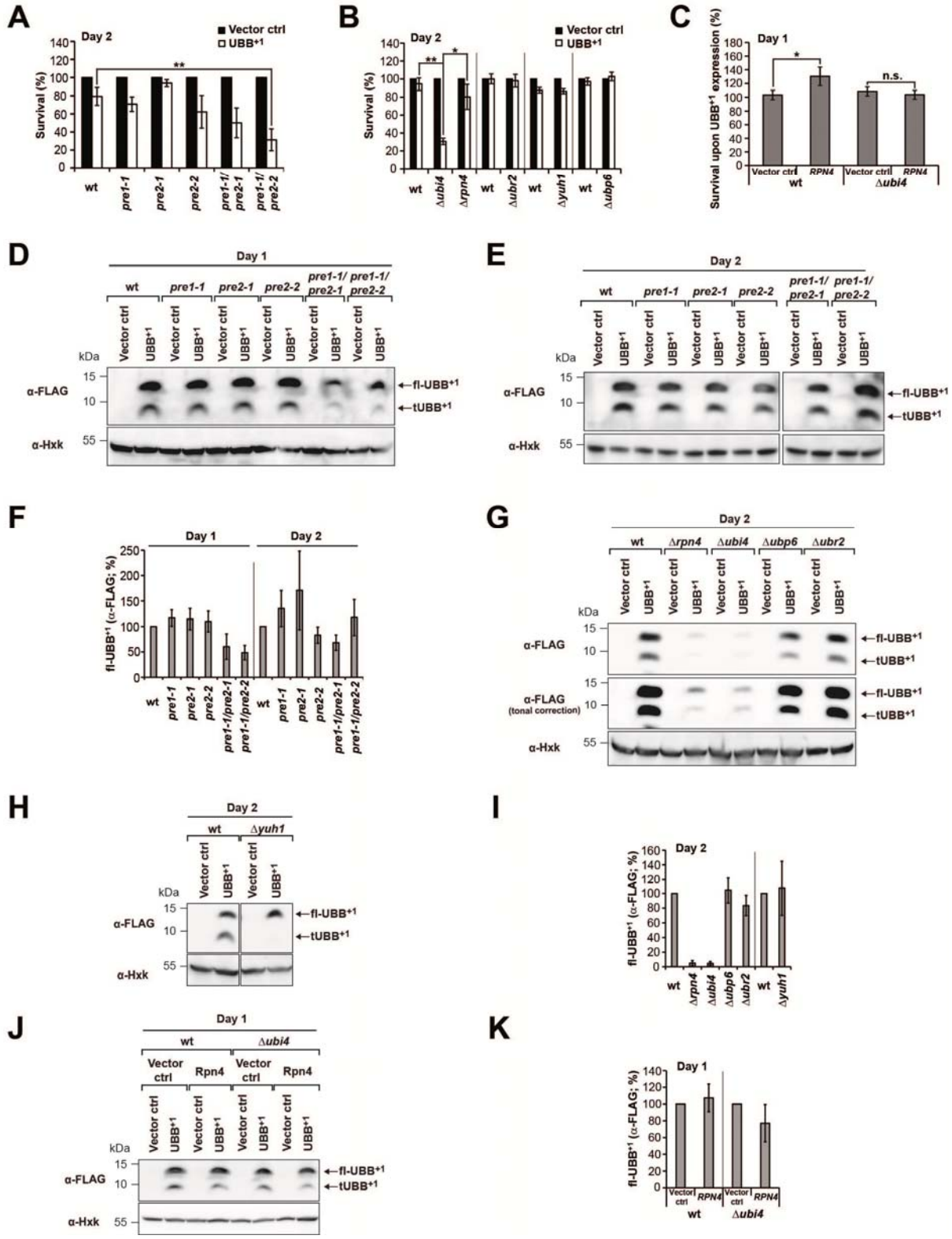

Figure S3: UBB^{+1}-triggered cytotoxicity in yeast strains with various UPS capacities, and expression controls

(A) Clonogenicity in proteasomal mutant strains. The CFUs obtained using yeast cells expressing vector controls were set to 100% in every experiment. The data shown here are

percent change values of four independent experiments for day 2 (for day 1 see Figure 3B). Error bars: standard error. **p < 0.05 (paired t-test).

(B) Clonogenicity in selected UPS knock-out strains. Unstressed controls to Figure 3D. Error bars: standard error. *p < 0.05, **p < 0.01 (paired t-test).

(C) UBB^{+1} was expressed in wild-type and Δ*ubi4* strains with endogenous (vector control) and elevated levels of Rpn4 (Rpn4). Clonogenicity was determined 1 day after inducing expression. The CFUs obtained using yeast cells with endogenous and elevated levels of Rpn4, respectively, but lacking UBB^{+1}, were set to 100% in every strain and experiment (not shown). The data shown here are percent change values of eight and six independent experiments for wt and Δ*ubi4* strains, respectively. Error bars: standard error. *p ≤ 0.05 (paired t-test).

(D-F) Steady-state levels of UBB^{+1} in proteasomal mutant strains upon expression for 1 (D) and 2 (E) days, respectively (relevant for Figures 3B and S3A). (F) Quantification of UBB^{+1} levels was done by immunoblotting of cell extracts using an antibody directed against the N-terminal FLAG-tag of UBB^{+1}. Hexokinase (Hxk) was used as loading control. The immunoreactive signals obtained using wild-type cells were set to 100% in every experiment. The data shown here are percent change values of three independent experiments. fl-UBB^{+1}: full-length UBB^{+1}. Error bar: standard error.

(G-I) Steady-state levels of UBB^{+1} in selected UPS knock-out strains upon expression for 2 days (relevant for Figures 3D and S3B). (I) Quantification of UBB^{+1} levels was done as in (F). The data shown here are percent change values of three independent experiments. fl-UBB^{+1}: full-length UBB^{+1}. Error bar: standard error.

(J+K) Steady-state levels of UBB^{+1} upon endogenous and elevated levels of Rpn4 in wild-type and Δ*ubi4* strains (relevant for Figures 3F and S3C). UBB^{+1} and Rpn4 were expressed for 1 day. Hexokinase (Hxk) was used as loading control. The immunoreactive signals obtained using wild-type yeast cells were set to 100% in every experiment. The data shown here are percent change values of three independent experiments. fl-UBB^{+1}: full-length UBB^{+1}. Error bar: standard error.

Figure S4 (related to Figure 4):

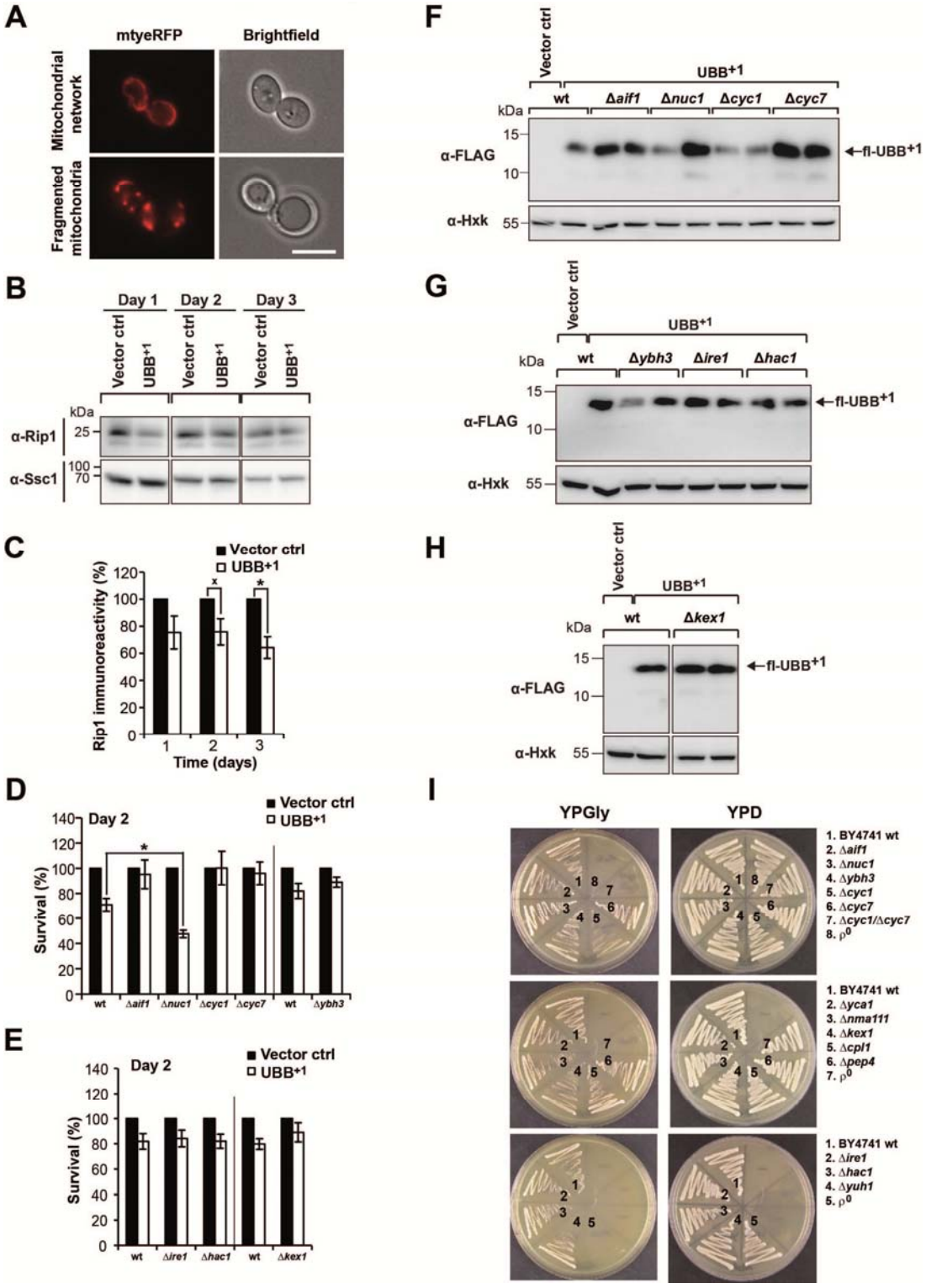

Figure S4: Mitochondrial impairment upon UBB^{+1} expression, respiratory and expression capacities of strains deleted for cell death genes

(A) Mitochondrial fragmentation. UBB^{+1} and a red fluorescent protein (yeRFP) fused with a mitochondrial targeting sequence were expressed. Representative images showing cells with

intact mitochondrial network, and with fragmented mitochondria, respectively. Size bar: 5 µm.

(B+C) Protein alterations in cell extracts. Proteins were expressed for 1 (16 h), 2, or 3 days. Steady-state levels of the mitochondrial cytochrome bc_1 complex component Rip1 and the mitochondrial chaperone Ssc1 were determined by immunoblotting of cell extracts. (B) Representative immunoblot. (C) Quantification of Rip1. Rip1 amount was normalized to Ssc1, and Rip1/Ssc1 was set to 100% in every experiment. The data shown here are percent change values of four experiments done in parallel. Error bars: standard error. p-values: $^{x}p < 0.1$, $*p < 0.05$ (paired t-test).

(D) Cytotoxicity in strains deleted from genes encoding mitochondrial cell death proteins. Unstressed controls to Figure 4H. Error bars: standard error. $*p \leq 0.05$ (paired t-test).

(E) Cytotoxicity in strains deleted from genes encoding ER-associated proteins. Unstressed controls to Figure 4I. Error bars: standard error.

(F-H) UBB^{+1} expression control in yeast strains (relevant for Figures 4H, 4I, S4D, S4E). UBB^{+1} was expressed in the indicated yeast strains for 16 h (day 1). Steady-state levels of UBB^{+1} were determined by immunoblotting. Hexokinase (Hxk) was used as loading control. Please note: Two distinct expression clones were shown per knock-out strain. fl-UBB^{+1}: full-length UBB^{+1}.

(I) Respiratory growth of yeast strains (relevant for Figures 4H, 4I, S4D, S4E). The indicated yeast strains were streaked out on YP plates with glycerol (YPGly) and glucose (YPD) as sole carbon sources, respectively, enabling obligatory respiratory and fermentative growth. ρ^0 strains and Δ*cyc1*/Δ*cyc7* double knock-out strain were used as controls for respiratory deficiency.

Figure S5 (related to Figure 5):

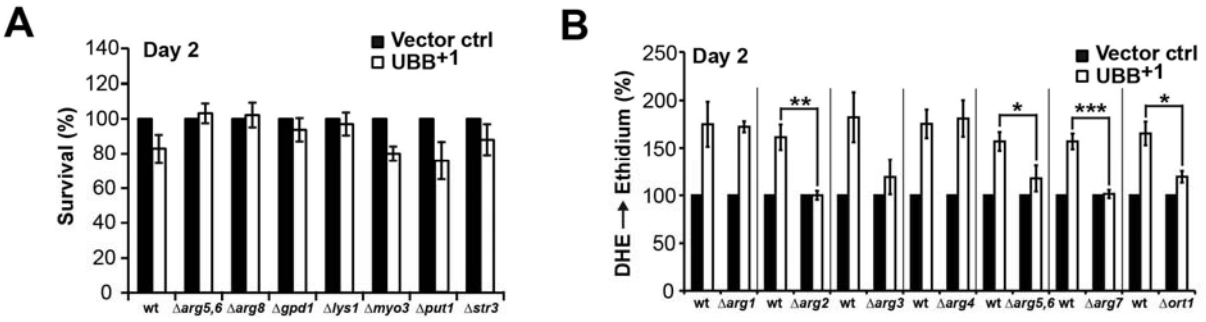

Figure S5: Cytotoxicity of UBB^{+1} in strains with disrupted arginine/ornithine biosynthesis

(A) UBB^{+1}-triggered cytotoxicity in strains deleted from genes encoding proteins accumulating in crude mitochondrial extracts upon UBB^{+1} expression. Unstressed controls to Figure 5B. Error bars: standard error.

(B) Oxidative stress upon UBB^{+1} expression in yeast strains with disrupted arginine/ornithine biosynthesis. Unstressed controls to Figure 5E. Error bars: standard error. *$p < 0.05$, **$p < 0.01$, ***$p < 0.001$ (t-test).

Figure S6 (related to Figure 6):

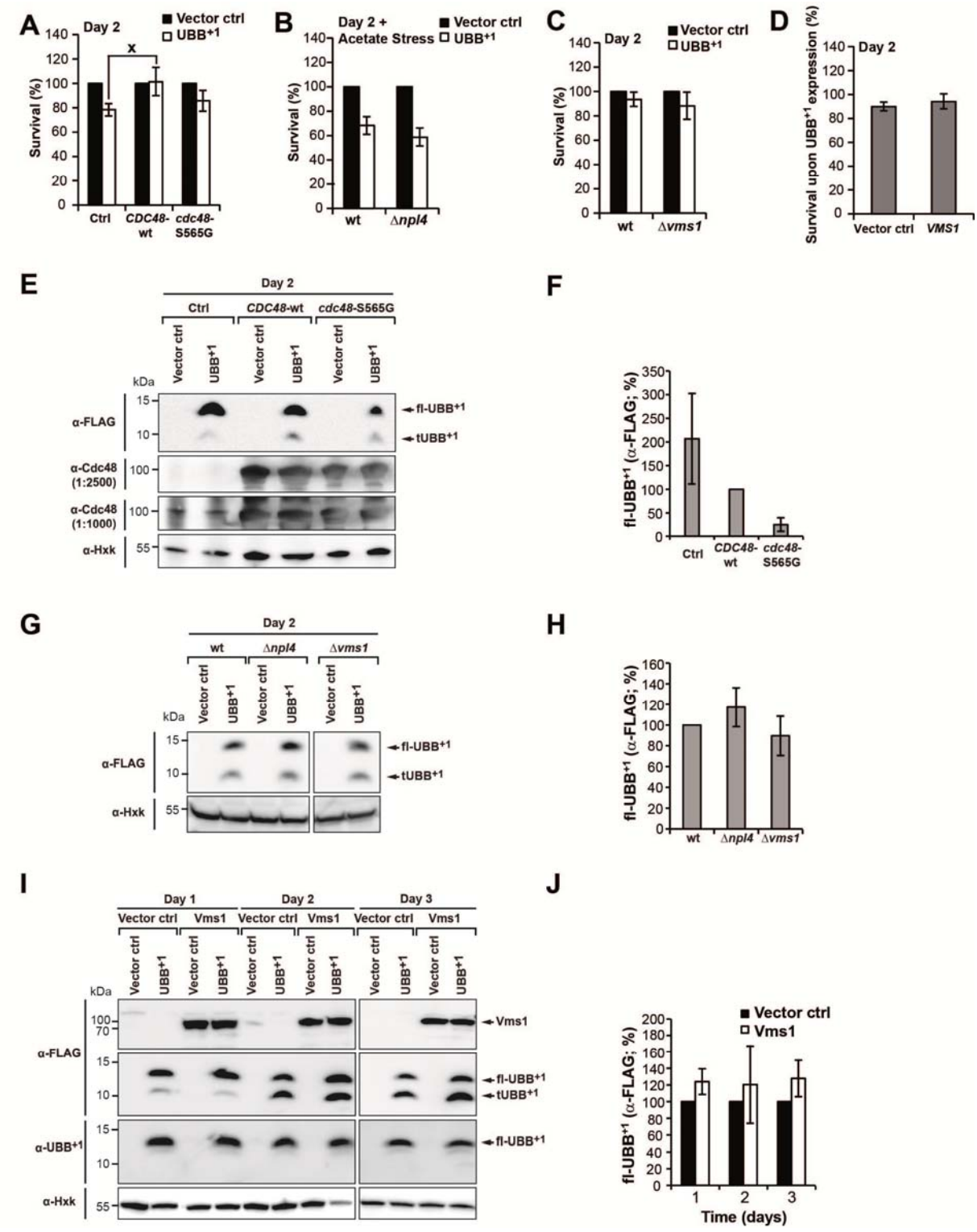

Figure S6: Role of Cdc48/Npl4/Vms1 complex in UBB^{+1}-triggered cytotoxicity and steady-state levels of UBB^{+1}

(A-C) UBB^{+1} was expressed in yeast strains with elevated levels of Cdc48 or Cdc48-S565G (A), and strains deleted for *NPL4* (B) and *VMS1* (C). Clonogenicity was determined two days after inducing expression before (A, C) and after acetate stress (B) (controls to Figure 6A-C).

The CFUs obtained using yeast cells expressing vector controls were set to 100% in every experiment. The data shown here are percent change values of six (A, B), and four (C) independent experiments. Error bars: standard error. $^{x}p < 0.1$ (paired t-test).

(D) Clonogenicity of UBB^{+1}-expressing cultures in strains with endogenous (vector control) and elevated levels of Vms1 (Vms1), respectively. Unstressed controls to Figure 6D. Error bars: standard error.

(E+F) Steady-state levels of UBB^{+1} and Cdc48 (relevant for Figures 6A, S6A). Hexokinase (Hxk) was used as loading control. (F) fl-UBB^{+1} levels in the *CDC48*-wt strain were set to 100% in every experiment. The data shown here are percent change values of three independent experiments. Error bars: standard error.

(G+H) Steady-state level of UBB^{+1} (relevant for Figures 6B+C, S6B+C). Hexokinase (Hxk) was used as loading control. (H) fl-UBB^{+1} levels in wt strain were set to 100% in every experiment. The data shown here are percent change values of three independent experiments. Error bars: standard error.

(I+J) Steady-state level of UBB^{+1} and Vms1 (relevant for Figures 6D-F, S6D). UBB^{+1} and/or Vms1 were expressed for 1 day (16 h), 2 and 3 days. Steady-state levels of Vms1 were determined by immunoblotting of cell extracts using an antibody directed against the C-terminal FLAG-tag of Vms1. Steady-state levels of UBB^{+1} were determined using an antibody directed against the N-terminal FLAG-tag of UBB^{+1} or directed against the UBB^{+1}-specific C-terminus. Hexokinase (Hxk) was used as loading control. (J) fl-UBB^{+1} levels in strains with endogenous levels of Vms1 (vector ctrl) were set to 100% in every experiment. The data shown here are percent change values of six experiments. Error bars: standard error. fl-UBB^{+1}: full-length UBB^{+1}, tUBB^{+1}: truncated UBB^{+1}.

Figure S7 (related Figure 7)

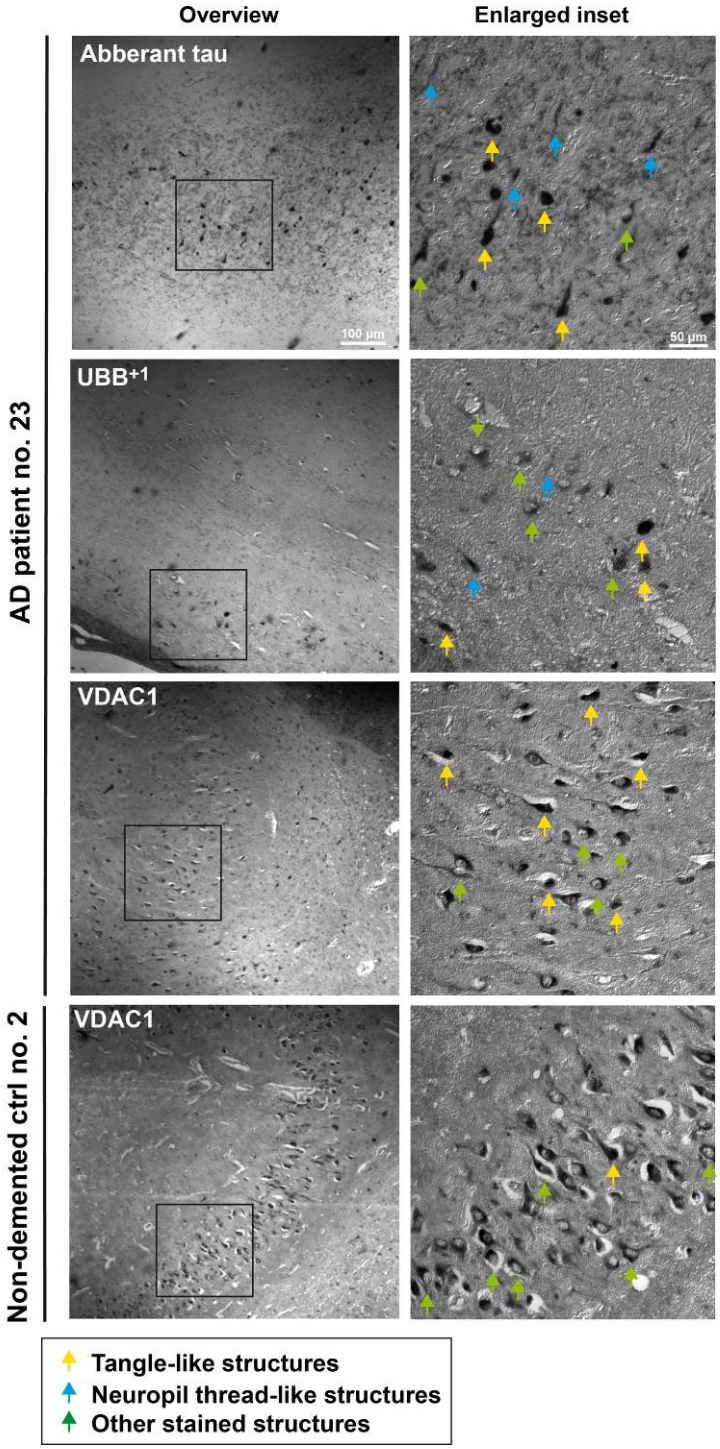

Figure S7: Pathological hallmarks in AD patients and in non-demented controls

Aberrant tau, UBB^{+1}, and VDAC1 staining in hippocampi of an AD patient.

Table S1 (related to Figures 1-6):

Data pooling and statistics

(see also Statistics in Supplemental Experimental Procedures)

Figure	Data	Error bars	Statistics
Figure 1C	Percent change values of five independent experiments	Standard error	ANOVA on ranks/ Dunn's method
Figure 1D	Mean values of nine, eight, and four independent experiments for days 1, 2, and 3, respectively	Standard error	RM ANOVA on ranks/ Dunn's method
Figure 2B	Mean values of three experiments done in parallel	Standard deviation	-
Figure 2C	Mean values of 20, 28, and 10 independent experiments for days 1, 2, and 3, respectively	Standard error	RM ANOVA/ Holm-Sidak method
Figure 2D	Mean values of 15, 25, and 5 independent experiments for days 1, 2, and 3, respectively	Standard error	RM ANOVA/ Holm-Sidak method
Figure 2E+F	Mean values of eight independent experiments	Standard error	RM ANOVA/ Holm-Sidak method
Figure 3A	Percent change values of three independent experiments	Standard error	RM ANOVA/ Holm-Sidak method
Figure 3B	Percent change values of three independent experiments	Standard error	Two-tailed paired t-test
Figure 3C	Percent change values of three, three, and four independent experiments for wt/Δ*ubi4*/Δ*rpn4*, wt/Δ*yuh1*, and wt/Δ*ubp6*, respectively	Standard error	RM ANOVA/ Holm-Sidak method
Figure 3D	Percent change values of four, four, five, and eight independent experiments for wt/Δ*ubi4*/Δ*rpn4*, wt/Δ*yuh1*, and wt/Δ*ubp6*, respectively	Standard error	Two-tailed paired t-test
Figure 3E	Percent change values of three independent experiments	Standard error	Two-tailed unpaired t-test
Figure 3F	Percent change values of four independent experiments	Standard error	Two-tailed paired t-test
Figure 4A	Mean values of nine independent experiments	Standard error	Two-tailed paired t-test
Figure 4B	Mean values of twelve independent experiments. At least 500 cells were evaluated per experiment and condition	Standard error	Two-tailed paired t-test
Figure 4C	Percent change values of four and three independent experiments for days 2 and 3, respectively	Standard error	Two-tailed unpaired t-test
Figure 4D	Percent change values of five and four independent experiments for days 2 and 3 respectively	Standard error	Rank Sum Test
Figure 4E	Percent change values of four independent experiments	Standard error	Rank Sum Test
Figure 4G	Percent change values of five independent experiments	Standard error	Two-tailed unpaired t-test
Figure 4H	Percent change values of five and seven independent experiments for wt/Δ*aif1*/Δ*nuc1*/Δ*cyc1*/Δ*cyc7* and wt/Δ*ybh3*, respectively	Standard error	Two-tailed paired t-test
Figure 4I	Percent change values of seven and four independent experiments for wt/Δ*ire1*/Δ*hac1* and wt/Δ*kex1*, respectively	Standard error	Two-tailed paired t-test
Figure 5B	Percent change values of four, and five independent experiments for Δ*gpd1*, Δ*put1*, Δ*str3*, Δ*myo3* and wild-type, Δ*arg5,6*, Δ*arg8*, Δ*lys1*, respectively	Standard error	ANOVA/ Holm-Sidak method
Figure 5C	Mean values of four experiments done in parallel (in each case two performed with the acid and two with the hot ethanol extraction methods)	Standard error	Two-tailed unpaired t-test
Figure 5E	Percent change values of three independent experiments for wt/Δ*arg1* and wt/Δ*arg3* and five independent experiments for the other comparisons	Standard error	Two-tailed unpaired t-test
Figure 5F	Percent change values of three, eight, two, one, five and five independent experiments for growth media without arginine (w/o) and with 30, 50, 75, 150, and 300 mg/L arginine, respectively	Standard error	Two-tailed unpaired t-test
Figure 5G	Percent change values of three and six independent experiments for growth media without lysine (w/o) and with 30, 80, 150, and 300 mg/L lysine	Standard error	Two-tailed unpaired t-test
Figure 6A-C	Percent change values of sic (A), eight (B), and four (C) independent experiments	Standard error	Two-tailed paired t-test
Figure 6D	Percent change values of six independent experiments	Standard error	Two-tailed paired t-test

Figure 6E+F	Mean values of 15 samples per condition analyzed in four independent experiments	Standard error	ANOVA on ranks/ Tukey test
Figure 6G	Percent change values of four and three independent experiments for days 2 and 3, respectively	Standard error	Two-tailed unpaired t-test
Figure 6H	Percent change values of five and four independent experiments for days 2 and 3, respectively	Standard error	Rank Sum Test
Figure 6I	Percent change values of four independent experiments	Standard error	Rank Sum Test
Figure 6K	Mean values of four experiments done in parallel (in each case two performed with the acid and two with the hot ethanol extraction methods)	Standard error	Two-tailed unpaired t-test

Table S2 (related to Figure 5):

Protein alterations in crude mitochondrial extracts upon expression of UBB^{+1}

Protein alterations in crude mitochondrial extracts were determined with the quantitative SILAC approach in two independent experiments (this Table, and Tables S3, S4). Protein alterations upon expression of UBB^{+1} as compared with vector controls were shown here. n.D. no Data.

Protein ID	Gene Name	ORF Name	log_2 ratio UBB^{+1} *vs.* ctrl (Exp. 1)	Significance A (Exp. 1)	log_2 ratio UBB^{+1} *vs.* ctrl (Exp. 2)	Significance A (Exp. 2)	Description	Comigration with highly purified mitochondria
P50276	MUP1	YGR055W	-2.02	0.000000	-0.49	0.016303	High-affinity methionine permease	n.D.
P40088	FTR1	YER145C	-1.78	0.000011	-0.46	0.023565	Plasma membrane iron permease	n.D.
P39003; P23585	HXT6	YDR343C	-1.29	0.001672	-0.98	0.000002	High-affinity hexose transporter HXT6	(Prokisch et al., 2004; Reinders et al., 2006; Sickmann et al., 2003)
P32804	ZRT1	YGL255W	-1.23	0.002870	-0.72	0.000401	Zinc-regulated transporter 1	n.D.
P41807	VMA13	YPR036W	-0.88	0.039215	-0.43	0.033688	V-type proton ATPase subunit H	n.D.
P00549	CDC19	YAL038W	-0.86	0.045276	-0.60	0.003465	Pyruvate kinase 1	n.D.
P38998	LYS1	YIR034C	0.50	0.040053	0.63	0.012151	Saccharopine dehydrogenase [NAD(+), L-lysine-forming]	(Ohlmeier et al., 2004)
Q00055	GPD1	YDL022W	0.57	0.021970	0.97	0.000100	Glycerol-3-phosphate dehydrogenase [NAD(+)] 1	n.D.
Q01217	ARG5,6	YER069W	0.67	0.008110	0.78	0.001660	Protein ARG5,6, mitochondrial; N-acetyl-gamma-glutamyl-phosphate reductase; Acetylglutamate kinase	(Ohlmeier et al., 2004; Prokisch et al., 2004; Reinders et al., 2006; Sickmann et al., 2003)
P53101	STR3	YGL184C	0.73	0.004291	1.11	0.000008	Cystathionine beta-lyase	n.D.
P18544	ARG8	YOL140W	0.80	0.002093	0.66	0.008115	Acetylornithine aminotransferase, mitochondrial	(Ohlmeier et al., 2004; Prokisch et al., 2004; Reinders et al., 2006; Sickmann et al., 2003)
P36006	MYO3	YKL129C	0.85	0.001161	0.55	0.027030	Myosin-3	n.D.
P61830	HHT1	YBR010W	0.89	0.000703	1.07	0.000019	Histone H3	(Prokisch et al., 2004)
P04912; P04911	HTA2; HTA1	YBL003C; YDR225W	1.03	0.000109	0.51	0.041653	Histone H2A.2; Histone H2A.1	(Prokisch et al., 2004)
P02294; P02293	HTB2; HTB1	YBL003C; YDR224C	1.06	0.000072	0.54	0.030804	Histone H2B.2; Histone H2B.1	(Prokisch et al., 2004)
P09368	PUT1	YLR142W	3.46	0.000000	1.57	0.000000	Proline dehydrogenase, mitochondrial	(Reinders et al., 2006; Sickmann et al., 2003)

Table S3 (related to Figure 6):

Protein alterations in crude mitochondrial extracts upon expression of UBB^{+1} and increased levels of Vms1

Protein alterations in crude mitochondrial extracts were determined with the quantitative SILAC approach in two independent experiments (this Table, and Tables S2, S4). Protein alterations upon co-expression of UBB^{+1} and Vms1, *i.e.* elevated Vms1 levels, as compared with the single expression of UBB^{+1}, *i.e.* endogenous Vms1 levels, were shown here. Green-labeled proteins were inversely regulated as compared with Figure 5A/Table S2. n.D.: no Data.

Protein ID	Gene Name	ORF Name	log_2 ratio UBB^{+1} + Vms1 *vs.* UBB^{+1} (Exp. 1)	Significance A (Exp. 1)	log_2 ratio UBB^{+1} + Vms1 *vs.* UBB^{+1} (Exp. 2)	Significance A (Exp. 2)	Description	Comigration with highly purified mitochondria
P09368	PUT1	YLR142W	-2.24	0.000000	-1.48	0.000000	Proline dehydrogenase, mitochondrial	(Reinders et al., 2006; Sickmann et al., 2003)
P04912; P04911	HTA2; HTA1	YBL003C; YDR225W	-1.74	0.000000	-1.01	0.000000	Histone H2A.2; Histone H2A.1	(Prokisch et al., 2004)
P02294; P02293	HTB2; HTB1	YBL003C; YDR224C	-1.73	0.000000	-1.05	0.000000	Histone H2B.2; Histone H2B.1	(Prokisch et al., 2004)
P02309	HHF1	YBR009C	-1.66	0.000000	-1.09	0.000000	Histone H4	(Prokisch et al., 2004)
Q03940	RVB1	YDR190C	-1.48	0.000002	-0.50	0.003330	RuvB-like protein 1	(Ohlmeier et al., 2004)
P32451	BIO2	YGR286C	-1.11	0.000419	-1.55	0.000000	Biotin synthase, mitochondrial	(Prokisch et al., 2004)
P53101	STR3	YGL184C	-0.96	0.002306	-0.49	0.003858	Cystathionine beta-lyase	n.D.
P18544	ARG8	YOL140W	-0.78	0.012691	-0.83	0.000001	Acetylornithine aminotransferase, mitochondrial	(Ohlmeier et al., 2004; Prokisch et al., 2004; Reinders et al., 2006; Sickmann et al., 2003)
P32457	CDC3	YLR314C	-0.78	0.013275	-0.76	0.000009	Cell division control protein 3	n.D.
P38998	LYS1	YIR034C	-0.77	0.014649	-0.46	0.006765	Saccharopine dehydrogenase [NAD(+), L-lysine-forming]	(Ohlmeier et al., 2004)
P37291	SHM2	YLR058C	-0.74	0.017978	-0.72	0.000025	Serine hydroxymethyltransferase, cytosolic	(Ohlmeier et al., 2004)
P40531	GVP36	YIL041W	-0.74	0.019444	-0.48	0.004750	Protein GVP36	(Ohlmeier et al., 2004)
P53744	BIO5	YNR056C	-0.65	0.039746	-1.56	0.000000	7-keto 8-aminopelargonic acid transporter	n.D.
Q01217	ARG5,6	YER069W	-0.62	0.049814	-0.45	0.007580	Protein ARG5,6, mitochondrial; N-acetyl-gamma-glutamyl-phosphate reductase; Acetylglutamate kinase	(Ohlmeier et al., 2004; Prokisch et al., 2004; Reinders et al., 2006; Sickmann et al., 2003)
P21147	OLE1	YGL055W	0.40	0.047961	0.34	0.034115	Acyl-CoA desaturase 1	(Prokisch et al., 2004)
Q04182	PDR15	YDR406W	0.46	0.024889	0.73	0.000006	ATP-dependent permease PDR15	(Prokisch et al., 2004)
P39002	FAA3	YIL009W	0.55	0.007085	0.69	0.000016	Long-chain-fatty-acid--CoA ligase 3	n.D.
P05374	CHO2	YGR157W	0.63	0.002186	0.49	0.002201	Phosphatidylethanolamine N-methyltransferase	(Prokisch et al., 2004)
P38695	HXT5	YHR096C	0.65	0.001401	0.65	0.000058	Probable glucose transporter HXT5	n.D.
P32466	HXT3	YDR345C	0.69	0.000719	0.75	0.000003	Low-affinity glucose transporter HXT3	(Prokisch et al., 2004)

P39003; P23585	HXT6	YDR343C	0.72	0.000418	0.65	0.000058	High-affinity hexose transporter HXT6	(Prokisch et al., 2004; Reinders et al., 2006; Sickmann et al., 2003)
Q12252	PHM7	YOL084W	0.80	0.000102	0.86	0.000000	Phosphate metabolism protein 7	n.D.
P10614	ERG11	YHR007C	0.93	0.000007	0.60	0.000176	Lanosterol 14-alpha demethylase	(Prokisch et al., 2004)
P40088	FTR1	YER145C	1.02	0.000001	0.94	0.000000	Plasma membrane iron permease	n.D.
P50276	MUP1	YGR055W	1.04	0.000000	0.70	0.000014	High-affinity methionine permease	n.D.
P30605	ITR1	YDR497C	1.11	0.000000	0.36	0.026461	Myo-inositol transporter 1	n.D.
P19358; P10659	SAM2; SAM1	YDR502C; YLR180W	1.11	0.000000	0.37	0.021859	S-adenosylmethionine synthase 2; S-adenosylmethionine synthase 1	(Ohlmeier et al., 2004)
P48016	ATH1	YPR026W	1.21	0.000000	1.37	0.000000	Vacuolar acid trehalase	(Prokisch et al., 2004)
P38993	FET3	YMR058W	1.43	0.000000	0.86	0.000000	Iron transport multicopper oxidase FET3	n.D.
P32791	FRE1	YLR214W	1.96	0.000000	0.71	0.000010	Ferric/cupric reductase transmembrane component 1	n.D.
Q04311	VMS1	YDR049W	2.02	0.000000	3.29	0.000000	Protein VMS1	(Prokisch et al., 2004; Reinders et al., 2006; Sickmann et al., 2003)
P19657	PMA2	YPL036W	2.12	0.000000	0.50	0.001871	Plasma membrane ATPase 2	(Prokisch et al., 2004; Reinders et al., 2006; Sickmann et al., 2003)

Table S4 (related to Tables S2+S3):

Protein identifications and quantification by SILAC analysis of crude mitochondrial extracts

Protein alterations in crude mitochondrial extracts were determined with the quantitative SILAC approach in two independent experiments (this table, and Tables S2, S3). PEP: posterior error probability.

Protein ID	Gene Name	ORF Name	Peptides	Sequence Coverage	PEP
Q01217	ARG5,6	YER069W	39	49.9	0
P18544	ARG8	YOL140W	16	46.1	1.55E-88
P48016	ATH1	YPR026W	2	1.9	8.72E-05
P32451	BIO2	YGR286C	17	34.4	1.19E-72
P53744	BIO5	YNR056C	4	5.9	9..93E-09
P32457	CDC3	YLR314C	4	10.4	1.83E-13
P00549	CDC19	YAL038W	17	33.6	7.78E-76
P05374	CHO2	YGR157W	19	25.8	2.27E-191
P10614	ERG11	YHR007C	6	17.7	8.05E-44
P39002	FAA3	YIL009W	5	5.5	6.59E-10
P38993	FET3	YMR058W	5	14.2	1.40E-35
P32791	FRE1	YLR214W	4	7.9	1.24E-23
P40088	FTR1	YER145C	4	11.9	1.22E-38
Q00055	GPD1	YDL022W	3	10.2	4.56E-23
P40531	GVP36	YIL041W	2	6.4	1.72E-09
P02309	HHF1	YBR009C	5	54.4	4.66E-15
P61830	HHT1	YBR010W	2	11.8	9.71E-06
P04912;	HTA2;	YBL003C;	3	34.8	2.69E-08
P04911	HTA1	YDR225W			
P02294;	HTB2;	YBL003C;	4	26.0	6.67E-13
P02293	HTB1	YDR224C			
P32466	HXT3	YDR345C	6	10.1	9.23E-57
P38695	HXT5	YHR096C	15	25.7	2.91E-122
P39003;	HXT6	YDR343C	20	32.8	0
P23585					
P30605	ITR1	YDR497C	6	7.9	2.61E-98
P38998	LYS1	YIR034C	12	50.1	1.67E-123
P50276	MUP1	YGR055W	3	3.7	4.09E-12
P36006	MYO3	YKL129C	4	4.8	1.51E-16
P21147	OLE1	YGL055W	14	33.9	9.07E-60
Q04182	PDR15	YDR406W	2	1.6	2.29E-06
Q12252	PHM7	YOL084W	6	7.7	6.00E-17
P19657	PMA2	YPL036W	42	30.0	0
P09368	PUT1	YLR142W	4	9.7	3.04E-29
Q03940	RVB1	YDR190C	6	19.7	2.90E-41
P19358;	SAM2;	YDR502C;	3	7.3	1.14E-18
P10659	SAM1	YLR180W			
P37291	SHM2	YLR058C	18	40.3	1.57E-161
P53101	STR3	YGL184C	3	7.7	1.63E-52
P41807	VMA13	YPR036W	7	15.1	6.38E-48
Q04311	VMS1	YDR049W	26	40.0	4.19E-182
P32804	ZRT1	YGL255W	6	14.4	4.93E-34

Table S5 (related to Figure 7):

Immunoreactivities in the human hippocampus and entorhinal cortex for VMS1

Tissues were obtained from non-demented controls and AD patients. The neuropathological state was confirmed by the presence of β-amyloid plaques and neurofibrillary tangles (-: no, a: minor, b: moderate, c: strong staining). Immunohistochemistry for VMS1 using human paraffin sections (#) and a human Vibratome section (*). VMS1 staining of tangle-like structures was observed in 6 out of 11 non-demented controls (55%) but in 15 out of 20 AD patients (75%). 5 out of 6 non-demented controls with VMS1 staining of tangle-like structures were 72 years and older and these show both neurofibrillary tangles and UBB^{+1} accumulation. 13 out of 15 AD patients with VMS1 staining of tangle-like structures do show both neurofibrillary tangles and UBB^{+1} accumulation. [1]Information provided by the Netherlands Brain Bank.

Patient	Age (years)[1]	Sex (F/M)[1]	Plaques[1]	Tangles[1]	UBB^{+1} accumulation[1] ($Ubi2^{+1}$)	VMS1 staining of tangle-like structures
Non-demented controls						
01#	34	M	-	-	-	-
01#	43	M	-	-	-	-
03#	51	M	-	-	-	+++
04#	58	M	-	+[a]	+	-
05#	65	F	-	-	-	-
06#	72	M	+[b]	+[c]	+	+
07#	80	F	+[b]	+[c]	+	++
08#	82	F	-	+[c]	+	+
09#	85	M	+[b]	+[b]	+	+
10#	90	F	+[b]	+[b]	+	+
11#	90	F	-	+[a]	+	-
AD patients						
12#	40	M	+[a]	+[c]	+	+++
13#	49	M	+[b]	+[c]	+	+
14#	54	F	+[b]	+[c]	+	++
15#	56	F	+[b]	+[a]	-	++
16#	61	M	+[b]	+[c]	+	++
17#	66	M	+[c]	+[c]	+	-
18#	70	F	+[c]	+[a]	+	+
19#	70	M	+[c]	+[c]	-	-
20#	73	F	+[b]	+[c]	+	-
21#	77	M	+[b]	+[c]	+	+++
22#	77	M	+[b]	+[c]	-	+++
23#	81	M	+[b]	+[c]	+	+++
24#	83	F	+[b]	+[c]	+	++
25#	85	F	+[b]	+[c]	+	+
26#	86	M	+[b]	+[c]	+	++
27#	88	M	+[b]	+[c]	+	-
28#	90	F	+[c]	+[c]	+	-
29#	92	F	+[c]	+[c]	+	+++
30#	83	F	+[c]	+[c]	+	+++
31*	92	F	+[c]	+[c]	+	+

Table S6 (related to Figures 7+S7 and Table S5):

Clinico-pathological information of non-demented controls and AD patients

Information provided by the Netherlands Brain Bank.

Patient	Braak stage	Age (years)	Sex (F/M)	Dementia duration (years)	Postmortem delay (h)	Fixation duration (days)	Brain weight (g)	Cause of death
Non-demented controls								
01	0	34	M	-	<17	1124	1348	Empyema of pleura, fibrous pleuritis and fibrous pericarditis, AIDS
02	0	43	M	-	23	53	1260	Non-Hodgkin lymphoma
03	0	51	M	-	6	47	1518	Liposarcoma, ileus
04	0	58	M	-	24	1088	1797	Lung carcinoma, massive hemorrhage
05	0	65	F	-	24	403	1234	Pulmonary embolism
06	2	72	M	-	4	126	1330	Myocardial infarction, cardiogenic shock
07	2	80	F	-	36	65	1205	Cardiogenic shock
08	1	82	F	-	48	38	1100	Myocardial infarction, ventricular fibrillation
09	3	85	M	-	5	126	1050	Cardiac failure, myocardial infarction, coronary sclerosis, lung emphysema
10	3	90	F	-	2	48	1110	Postoperative infections
11	1	90	F	-	5	143	1040	Metabolic acidosis
AD patients								
12	5	40	M	5-6	3	28	1410	AD, cachexia
13	6	49	M	6	4	33	1426	AD, epilepsy
14	5	54	F	5	3	78	1055	AD, cachexia
15	4	56	F	4-5	22	48	1180	AD, bronchopneumonia, dehydration
16	6	61	M	3	6	30	1180	AD, fever
17	6	66	M	15	3	30	1270	AD, ischemic cerebral stroke, cachexia, sepsis
18	6	70	F	12	13	34	780	AD, status epilepticus
19	6	70	M	12	4	125	1325	AD, ileus, urinary tract infection
20	5	73	F	11	4	66	1106	AD, dehydration, circulation failure
21	5	77	M	7	4	75	1168	AD, pneumonia
22	2	77	M	>5	4	127	1095	AD, bronchial pneumonia
23	5	81	M	6	4	66	1088	AD, bacterial infection
24	5	83	F	14	6	127	1005	AD, cachexia, urinary tract infection
25	4	85	F	4	2	39	1020	AD, heart disease, anaemia
26	5	86	M	10	4	77	1303	AD, uraemia
27	3	88	M	4	5	75	1058	AD, decompensatio cordis
28	5	90	F	>8	3	38	1060	AD, dehydration
29	4	92	F	3	4	124	896	AD, cachexia, uraemia
30	4	83	F	5	5	32.	1288	AD, vascular encephalopathy
31	5	92	F	6	3	335	964	AD, dehydration, cachexia

Supplemental Discussion

Here, we established a yeast model for dissecting cell death mechanisms triggered by UBB^{+1}. UBB^{+1} accumulation resulted in a progressive loss of clonogenic cell survival, accompanied with increased levels of oxidative stress, culminating in apoptosis and necrosis. In neuronal cultures, UBB^{+1} expression has been linked to apoptosis (de Vrij et al., 2001; Tan et al., 2007). However, either high expression levels or the presence of other neurotoxic proteins, such as huntingtin, were needed for efficient cell killing (de Pril et al., 2004; de Pril et al., 2007; de Pril et al., 2010; de Vrij et al., 2001; Tan et al., 2007). Consistently, transgenic expression of UBB^{+1} in mice failed to cause overt neurodegeneration although it did affect spatial reference memory and caused a central dysfunction of respiratory regulation (Fischer et al., 2009; Irmler et al., 2012; van Tijn et al., 2011). Therefore, our data support the hypothesis that prolonged high levels of UBB^{+1} are required for cell killing.

Several lines of evidence suggest for a pivotal role of mitochondria. Yeast cells expressing UBB^{+1} demonstrated (i) increased levels of oxidative stress, (ii) impaired recovery of the mitochondrial network, when shifting stationary yeast cultures to fresh media, (iii) increased cellular oxygen consumption, (iv) increased mitochondrial membrane potential, accompanied by (v) depletion of cellular ATP levels, and (vi) decrease in the mitochondrial respiratory chain components Rip1 and cytochrome *c*, and (vii) significantly attenuated cytotoxicity in a yeast strain lacking the second isoform of cytochrome *c*. Previously, it was shown that UBB^{+1} could trigger neuronal apoptosis accompanied by reduced mitochondrial movement (Tan et al., 2007). Mitochondrial impairment is an AD hallmark and likely contributes to neurodegeneration (Rodolfo et al., 2010). Therefore, the data obtained with UBB^{+1}-expressing yeast cells corroborate essential features of cell death-relevant mitochondrion dysfunctions found in AD neurons.

It appears intriguing that UBB^{+1} interferes with the UPS (Fischer et al., 2009; Lindsten et al., 2002; Tank and True, 2009; van Tijn et al., 2007; van Tijn et al., 2010) paralleling the

observation that the UPS is also compromised during aging and age-related neurodegeneration (Dennissen et al., 2010). In contrast, increased UPS capacities antagonize aging and increase life span in yeast and flies (Chondrogianni et al., 2014; Kruegel et al., 2011). Our data suggest that the cumulated impact of UBB^{+1} and the age-intrinsic derangement of the UPS contribute to the pathogenesis of AD and other UBB^{+1}-related disorders, implying that stimulation of the UPS might have neuroprotective effects.

Supplemental Experimental Procedures

Yeast expression plasmids

Construct name	Copy no.	Promoter	Plasmid selection	References
pESC-HIS-nFLAG	2µ	*GAL10*	HIS3	U. Janschek, University of Graz, Graz, Austria
pESC-HIS-nFLAG-UBB	2µ	*GAL10*	HIS3	This study
pESC-HIS-nFLAG-UBB^{+1}	2µ	*GAL10*	HIS3	This study
pESC-HIS-nFLAG-UBB^{+1}-K29,48R	2µ	*GAL10*	HIS3	This study
pESC-HIS	2µ	*GAL10*	HIS3	Agilent Technologies
pESC-HIS-TDP-43	2µ	*GAL10*	HIS3	(Braun et al., 2011)
pESC-HIS-Vms1	2µ	*GAL10*	HIS3	This study
pESC-LEU	2µ	*GAL10*	LEU2	Agilent Technologies
pESC-LEU-nFLAG-UBB^{+1}	2µ	*GAL10*	LEU2	This study
pYES2-mtyeRFP	2µ	*GAL1*	URA3	D. Scholz, University of Bayreuth, Bayreuth, Germany
pYES2-Ub-G76V-GFP	2µ	*GAL1*	URA3	(Heessen et al., 2003)
pBY011	ARS/CEN4	*GAL1*	URA3	PlasmID, DF/HCC DNA Resource Core, Boston, MA, USA
pBY011-RPN4	ARS/CEN4	*GAL1*	URA3	PlasmID
pRS426	2µ	*None*	URA3	Agilent Technologies
pRS426-Vms1	2µ	*Endogenous*	URA3	(Heo et al., 2010)

Using a PCR-based method, human ubiquitin B (UBB), frameshift UBB^{+1}, and UBB^{+1}-K29,48R were subcloned from pcDNA3.1 (van Tijn et al., 2007) via *Not*I and *Cla*I restriction sites into the multiple cloning site 1 of a modified pESC-HIS vector (Agilent Technologies, Waldbronn, Germany) encoding a human Kozak sequence and a N-terminal FLAG-tag. For this purpose, the following primers were designed (forward: 5'- AAT AGC GGC CGC CAT GCA GAT CTT CGT GAA AAC CCT TAC C-3' for UBB, UBB^{+1}, and UBB^{+1}-K29,48R) and (reverse: 5'-TTA TAT CGA TTC ACT GGG CTC CAC TTC CAG GG-3' for UBB^{+1}, and UBB^{+1}-K29,48R; reverse: 5'-TAT TAT CGA TTC AAC CAC CTC TCA GAC GCA GGA CCA GGT G-3' for UBB).

Yeast strains and growth conditions

Yeast strain	Strain type	Genetic background	References
BYa wt	BY4741	MATa, *his3*Δ1; *leu2*Δ0; *met15*Δ0; *ura3*Δ0; ρ^+	EUROSCARF
BYa wt ρ^0	BY4741	MATa, *his3*Δ1; *leu2*Δ0; *met15*Δ0; *ura3*Δ0; ρ^0	(Büttner et al., 2008)
BYa Δ*aif1*	BY4741	MATa, *his3*Δ1; *leu2*Δ0; *met15*Δ0; *ura3*Δ0; *YNR074C*::kanMX4	EUROSCARF
BYa Δ*arg1*	BY4741	MATa, *his3*Δ1; *leu2*Δ0; *met15*Δ0; *ura3*Δ0; *YOL058W*::kanMX4	EUROSCARF
BYa Δ*arg2*	BY4741	MATa, *his3*Δ1; *leu2*Δ0; *met15*Δ0; *ura3*Δ0; *YJL071W*::kanMX4	EUROSCARF
BYa Δ*arg3*	BY4741	MATa, *his3*Δ1; *leu2*Δ0; *met15*Δ0; *ura3*Δ0; *YJL088W*::kanMX4	EUROSCARF
BYa Δ*arg4*	BY4741	MATa, *his3*Δ1; *leu2*Δ0; *met15*Δ0; *ura3*Δ0; *YHR018C*::kanMX4	EUROSCARF
BYa Δ*arg4* Δ*lys2* (for SILAC and targeted metabolomics)	BY4741	MATa, *his3*Δ1; *leu2*Δ0; *met15*Δ0; *ura3*Δ0; *YHR018C*::kanMX4; *YBR115C*::*URA3*	(Büttner et al., 2013)
BYa Δ*arg5,6*	BY4741	MATa, *his3*Δ1; *leu2*Δ0; *met15*Δ0; *ura3*Δ0; *YER069W*::kanMX4	EUROSCARF
BYa Δ*arg7*	BY4741	MATa, *his3*Δ1; *leu2*Δ0; *met15*Δ0; *ura3*Δ0; *YMR062C*::kanMX4	EUROSCARF
BYa Δ*arg8*	BY4741	MATa, *his3*Δ1; *leu2*Δ0; *met15*Δ0; *ura3*Δ0; *YOL140W*::kanMX4	Open Biosystems
BYa Δ*cyc1*	BY4741	MATa, *his3*Δ1; *leu2*Δ0; *met15*Δ0; *ura3*Δ0; *YJR048W*::kanMX4	EUROSCARF
BYa Δ*cyc7*	BY4741	MATa, *his3*Δ1; *leu2*Δ0; *met15*Δ0; *ura3*Δ0; *YEL039C*::kanMX4	EUROSCARF
BYa Δ*gpd1*	BY4741	MATa, *his3*Δ1; *leu2*Δ0; *met15*Δ0; *ura3*Δ0; *YDL022W*::kanMX4	Open Biosystems
BYa Δ*hac1*	BY4741	MATa, *his3*Δ1; *leu2*Δ0; *met15*Δ0; *ura3*Δ0; *YFL031W*::kanMX4	EUROSCARF
BYa Δ*ire1*	BY4741	MATa, *his3*Δ1; *leu2*Δ0; *met15*Δ0; *ura3*Δ0; *YHR079C*::kanMX4	EUROSCARF
BYa Δ*kex1*	BY4741	MATa, *his3*Δ1; *leu2*Δ0; *met15*Δ0; *ura3*Δ0; *YGL203C*::kanMX4	EUROSCARF
BYa Δ*lys1*	BY4741	MATa, *his3*Δ1; *leu2*Δ0; *met15*Δ0; *ura3*Δ0; *YIR034C*::kanMX4	EUROSCARF
BYa Δ*myo3*	BY4741	MATa, *his3*Δ1; *leu2*Δ0; *met15*Δ0; *ura3*Δ0; *YKL129C*::kanMX4	Open Biosystems
BYa Δ*npl4*	BY4741	MATa, *his3*Δ1; *leu2*Δ0; *met15*Δ0; *ura3*Δ0; *YBR170C*::kanMX4	EUROSCARF
BYa Δ*nuc1*	BY4741	MATa, *his3*Δ1; *leu2*Δ0; *met15*Δ0; *ura3*Δ0; *YJL208C*::kanMX4	EUROSCARF
BYa Δ*ort1*	BY4741	MATa, *his3*Δ1; *leu2*Δ0; *met15*Δ0; *ura3*Δ0; *YOR130C*::kanMX4	EUROSCARF
BYa Δ*put1*	BY4741	MATa, *his3*Δ1; *leu2*Δ0; *met15*Δ0; *ura3*Δ0; *YLR142W*::kanMX4	Open Biosystems
BYa Δ*rpn4*	BY4741	MATa, *his3*Δ1; *leu2*Δ0; *met15*Δ0; *ura3*Δ0; *YDL020C*::kanMX4	EUROSCARF
BYa Δ*str3*	BY4741	MATa, *his3*Δ1; *leu2*Δ0; *met15*Δ0; *ura3*Δ0; *YGL184C*::kanMX4	Open Biosystems
BYa Δ*ubi4*	BY4741	MATa, *his3*Δ1; *leu2*Δ0; *met15*Δ0; *ura3*Δ0; *YLL039C*::kanMX4	EUROSCARF
BYa Δ*ubp6*	BY4741	(yMS485) MATa *his3*Δ1; *leu2*Δ0; *met15*Δ0; *ura3*Δ0; *ubp6*Δ::*URA3*	(Kruegel et al., 2011)
BYa Δ*ubr2*	BY4741	(BR2194) MATα *his3*Δ1; *leu2*Δ0; *met15*Δ0; *ura3*Δ0; *ubr2*Δ::*URA3*	(Kruegel et al., 2011)

BYa Δ*vms1*	BY4741	MATa, *his3*Δ1; *leu2*Δ0; *met15*Δ0; *ura3*Δ0; *YDR049W*::kanMX4	(Heo et al., 2010)
BYa Δ*ybh3*	BY4741	MATa, *his3*Δ1; *leu2*Δ0; *met15*Δ0; *ura3*Δ0; *YNL305C*::kanMX4	EUROSCARF
BYa Δ*yuh1*	BY4741	MATa, *his3*Δ1; *leu2*Δ0; *met15*Δ0; *ura3*Δ0; *YJR099W*::kanMX4	Open Biosystems
WCG4a wt	WCG4a	MATa; *ura3*; *leu2-3,112*; *his3-11,15*; Can^S Gal^+	(Heinemeyer et al., 1993)
WCG4a *pre1-1*	WCG4a	MATa; *pre1-1*; *ura3*; *leu2-3,112*; *his3-11,15*; Can^S Gal^+	(Heinemeyer et al., 1993)
WCG4a *pre2-1*	WCG4a	MATa; *pre2-1*; *ura3*; *leu2-3,112*; *his3-11,15*; Can^S Gal^+	(Heinemeyer et al., 1993)
WCG4a *pre2-2*	WCG4a	MATa; *pre2-2*; *ura3*; *leu2-3,112*; *his3-11,15*; Can^S Gal^+	(Heinemeyer et al., 1993)
WCG4a *pre1-1 pre2-1*	WCG4a	MATa; *pre1-1*; *pre2-1*; *ura3*; *leu2-3,112*; *his3-11,15*; Can^S Gal^+	(Heinemeyer et al., 1993)
WCG4a *pre1-1 pre2-2*	WCG4a	MATa; *pre1-1*; *pre2-2*; *ura3*; *leu2-3,112*; *his3-11,15*; Can^S Gal^+	(Heinemeyer et al., 1993)
WCG4a *CDC48*-wt	WCG4a	MATa; *ura3*; *leu2-3,112*; *his3-11,15*; *cdc48::URA3*; YEp52(*LEU2*)-*CDC48*	(Jarosch et al., 2002)
WCG4a *cdc48*-S565G	WCG4a	MATa; *ura3*; *leu2-3,112*; *his3-11,15*; *cdc48::URA3*; YEp52(*LEU2*)-*cdc48*-S565G	(Jarosch et al., 2002)
CEN.PK-113-7D (for generation of internal standards for targeted metabolomics)			M. Klimacek, TU Graz, Graz, Austria

Strains were grown in YPD according to (Sherman, 2002), or in synthetic complete (SC) media either according to (Sherman, 2002) or containing 0.17% yeast nitrogen base (Difco, Otto Nordwald, Hamburg, Germany), 0.5% $(NH_4)_2SO_4$ and 30 mg/L of all amino acids (except 80 mg/L histidine and 200 mg/L leucine), 30 mg/L adenine, and 320 mg/L uracil. SC media contained either 2% glucose (SCD) or 2% galactose (SCGal) as carbon sources. Plasmid transformation and maintenance were done by growth in selective SC media, using the auxotrophic markers of the yeast strains. Gene expression was under the control of galactose-regulated promoters. Transformed yeast strains were pre-grown in selective SC media repressing expression (SCD) for 6 h at 28°C in either flasks with 145 rpm or in 96 deep-wells with 250 rpm until an OD_{600} of 0.4. Expression was induced either in quadruple-indented flasks or in 96 deep-wells by shifting to selective SC media inducing expression (SCGal).

For stable isotope labeling (SILAC) and targeted metabolomics, a yeast strain of BY4741 background lacking *ARG4* and *LYS2* genes was co-transformed with either two vector controls (pESC-LEU-nFLAG and pESC-HIS), or with UBB^{+1} expression construct and

vector control (pESC-LEU-nFLAG-UBB^{+1} and pESC-HIS), or with both UBB^{+1} and Vms1 expression constructs (pESC-LEU-nFLAG-UBB^{+1} and pESC-HIS-Vms1). Yeast cells were grown in SC media according to (Sherman, 2002) with the following modifications: 30 mg/L proline, 50 mg/L arginine, 80 mg/L lysine. For SILAC, yeast cells were grown in media supplemented either with Lys0 and Arg0 (normal isotopes), or with Lys4 and Arg6, or with Lys8 and Arg10 (heavy isotopes, Silantes, Munich, Germany). In a biological replicate the assignment of the isotope labels was changed. Pre-growth in SCD media and expression in SCGal media was done as described above. For targeted metabolomics, yeast cells were grown in media supplemented with Lys0 and Arg0 (normal isotopes).

Determination of respiratory deficiency

Wild-type and knock-out strains were streaked out on YPD (4% glucose, 1% yeast extract, 2% bacto peptone, 2% Agar; Difco) and YPGly (3% glycerol, 1% yeast extract, 2% bacto peptone, 2% Agar Agar). Plates were incubated at 30°C for three days. Respiratory deficiency of the respective yeast strains was indicated by a growth deficiency on YPGly, which can only be used to support growth by respiration.

Measuring cytotoxicity based on growth

Yeast clones transformed with UBB^{+1} and TDP-43 constructs or vector controls were grown overnight in SCD-HIS medium. For spot dilution assays (growth on solid media), cultures were normalized to an optical density (OD_{600}) of 0.5 in ddH_2O, serially diluted (1:10) in ddH_2O, and spotted onto solid nutrient-containing media inducing (SCGal-HIS) or repressing (SCD-HIS) expression of UBB^{+1} or TDP-43. Plates were incubated for two days at 30°C before analysis. For growth assays (growth in liquid media), cultures were diluted in SCD-HIS media and grown to an OD_{600} of 0.4, shifted to expression medium (SCGal-HIS), and grown overnight. After dilution in expression medium to an OD_{600} of 0.1 growth was

followed at 30°C in quadruple-indented flasks. Three samples (*i.e.* three distinct yeast clones per transformed construct) were measured in parallel. The mean values and the standard deviations were calculated from the OD_{600} values of the samples and illustrated graphically (see Figures 2B).

Measuring cytotoxicity based on clonogenicity/survival

Clonogenic assays determine the survivability of yeast cultures by determining the number of yeast cells that remain capable to form new colonies on agar plates upon ideal nutrient conditions. Cell densities (cells/mL) of yeast cultures expressing proteins or carrying vector controls were measured with an automated cell counter (CASY1, Roche Innovatis, Bielefeld, Germany, or Z2 Coulter Particle Count and Size Analyzer, Beckman Coulter, Krefeld, Germany). For this, (stationary) cultures were diluted in PBS (1:1,000), and the number of cells (particles with the size of 2 to 6.7 µm) was determined by measuring voltage variations during vacuuming of 100 µL aliquots through a 50 µM aperture. Each sample measurement was performed in duplicate. For plating, cultures were diluted in ddH_2O, and aliquots containing 500 cells were plated either on YPD or on selective SC agar plates containing glucose, on which expression of proteins of interest was repressed. The colony forming units (CFUs), *i.e.*, colonies grown after two days of incubation at 30°C were counted manually, or automatically using a colony counter (LemnaTech, Würselen, Germany).

In every experiment and for every time point or condition (*e.g.* stressed *vs.* unstressed), the CFU of a culture inoculated by an individual yeast clone was determined in duplicate. At least three distinct yeast clones per yeast strain and transformed construct were analyzed in parallel. In other words, in every experiment and for every time point or condition, the CFU of a distinct yeast strain transformed with a distinct construct was based on at least six CFU measurements. Further, each experiment was repeated independently for at least three times.

The mean values and the standard errors were calculated from the CFUs of all experiments and illustrated graphically (see Figures 2C, S2A+B). For statistical analysis, the absolute clonogenicities (CFU[500]) of the different strains were compared.

When comparing the cytotoxic effects of UBB^{+1} in different yeast strains, the CFUs obtained using yeast cells carrying vector controls were set to 100% in every experiment and strain. The mean values and the standard errors were calculated from the relative clonogenicities of all experiments and illustrated graphically as percent change values (Survival [%]) (see Figures 3B+D, 4H+I, 5B, 6A-C, Figures S3A+B, S4D+E, S5A, S6A-C). For statistical analysis the relative clonogenicities upon UBB^{+1} expression among the different strains (usually wild-type *vs.* mutant strains) were compared.

When comparing the protective effects of Rpn4 or Vms1 in cells expressing UBB^{+1}, the CFUs obtained using yeast cells without UBB^{+1} expression were set to 100% in every experiment and strain. The mean values and the standard errors were calculated from the relative clonogenicities of all experiments and illustrated graphically as percent change values (Survival upon UBB^{+1} expression [%]) (see Figures 3F, 6D, Figures S3C, S6D). For statistical analysis the relative clonogenicities upon UBB^{+1} expression between strains with endogenous levels of Rpn4 or Vms1, or elevated levels of Rpn4 or Vms1 were compared.

Measurement of oxidative stress and cell death

Oxidative stress was determined by measuring the conversion of dihydroethidium (DHE, Sigma-Aldrich, Vienna, Austria) to the red fluorescent ethidium (Madeo et al., 1999) applying a fluorescence plate reader. $5x10^6$ cells per sample were pelleted in 96-well plates. Cell pellets in each well were resuspended in 250 µL DHE-staining solution (2.5 µg/mL in PBS for DHE; 2.5 mg/mL DHE stock solution in DMSO). After 10 min of incubation at RT, fluorescence was measured as relative fluorescence units (RFU) in the GENiosPro 96-well fluorescence plate reader (Tecan, Grödig, Austria) with the following settings: fluorescence

top, excitation 515 nm, emission 595 nm, gain 45, number of reads 6, integration time 40 µs. Staining solution was used for blank measurements. Samples were measured in duplicate, and at least three samples (*i.e.* distinct yeast clones) were determined per strain, construct, and condition. Experiments were repeated independently at least five times. The mean values and the standard errors were calculated from the RFUs of all experiments and illustrated graphically (see Figures 2D, S2A+B). For statistical analysis, the RFUs of the different strains were compared.

For validating data on an individual cell basis, DHE- or PI-stained samples (propidium iodide [PI] is a 'vital dye', which stains cells with disintegrated plasma membranes) were measured by flow cytometry (BD FACSAria, BD Biosciences, Heidelberg, Germany) with the following settings: filter sets: PE for DHE (excitation 488/532 nm, emission 578 nm) and PerCP-Cy5.5 for PI (excitation, 488/532 nm, emission, 695 nm); flow rate: 4. Results were analyzed with the BD FACSDiva software V 5.0. 30,000 cells were evaluated per sample, and at least three samples (*i.e.* distinct yeast clones) were determined per strain, construct, and condition. Unstained samples were used as controls. Experiments were repeated independently at least four times. The mean values and the standard errors were calculated from the proportions of stained cells (%) of all experiments and illustrated graphically (see Figures 4A, 6E+F). For statistical analysis, the proportions of stained cells (%) of the different strains were compared.

For measuring oxidative stress levels (DHE) and incidences of cell death (PI) upon UBB^{+1} expression in strains with disrupted arginine/ornithine or lysine biosynthesis the subsequent analysis was performed by flow cytometry (BD LSRFortessa, BD Biosciences) as described above. 30,000 cells per sample were evaluated by using BD FACSDiva software (BD Biosciences). Six samples (*i.e.* distinct yeast clones) were determined per strain, construct, and condition. Experiments were repeated independently at least three times. When comparing the cytotoxic effects of UBB^{+1} in different yeast strains, the proportions of DHE-

or PI-stained cells obtained using yeast cells carrying vector controls were set to 100% in every experiment, strain, and condition. The mean values and the standard errors were calculated from the relative DHE- or PI-staining of all experiments and illustrated graphically as percent change values (DHE -> Ethidium [%] or PI staining [%]) (see Figures 5E-G, Figures S5B). For statistical analysis the relative DHE- or PI-staining upon UBB^{+1} expression among the different strains (usually wild-type *vs.* mutant strains) were compared.

Determination of morphological markers of apoptosis and necrosis

Annexin V/PI co-staining (with Annexin V-FLUOS Staining Kit, Roche Applied Sciences, Mannheim, Germany, and PI, Sigma-Aldrich) and terminal deoxynucleotidyl transferase dUTP nick end labeling (TUNEL) (*In Situ* Cell Death Detection Kit, Roche Applied Sciences) were performed to discriminate among early apoptotic, late apoptotic/secondary necrotic and necrotic cells, or between apoptotic and non-apoptotic cells, respectively (Büttner et al., 2007). To determine the frequency of morphological phenotypes, cells were evaluated by flow cytometry (BD FACSAria) and BD FACSDiva software V 5.0 with the following settings: for Annexin V/PI: filter sets FITC (excitation 488 nm, emission 519 nm) and PerCP-Cy 5.5 (excitation 488/532 nm, emission 695 nm), flow rate: 1; for TUNEL: filter set FITC (excitation 488 nm, emission 519 nm); spectral overlap PerCP-Cy 5.5/FITC: 4.0; flow rate: 1. 30,000 cells were evaluated per sample, and at least three samples (*i.e.* distinct yeast clones) were determined per strain, construct, and condition. Unstained samples and PI-only and Annexin V-only stained samples were used as controls. Experiments were performed independently eight times. The mean values and the standard errors were calculated from the proportions of stained cells (%) of all experiments and illustrated graphically (see Figures 2E+F). For statistical analysis, the proportions of stained cells (%) of the different strains were compared.

Measurement of mitochondrial fragmentation

UBB^{+1} or vector control and a red fluorescent protein (yeRFP) fused with a mitochondrial targeting sequence (pYES2-mtyeRFP) were expressed (SCGal-URA/-HIS) for two days. Under these late stationary-phase conditions, the mitochondria were predominantly fragmented. In contrast to logarithmically growing cells, in which mitochondria are highly fused (Westermann, 2010). The two days old stationary phase cultures were then shifted to fresh media repressing expression of UBB^{+1} (SCD-URA/-HIS) and inducing regrowth of yeast cells. After 3 h the proportion of cells whose mitochondria remain fragmented was quantified. At least 500 cells were evaluated per experiment and condition. Experiments were repeated independently twelve times. Representative cells which expressed UBB^{+1} and mitochondrially-targeted yeRFP showing mitochondrial network and fragmented mitochondria, respectively, are shown in Figure S4A.

Measurement of cellular oxygen consumption

Oxygen consumption of stationary yeast cultures was analyzed using the FireSting optical oxygen sensor system (Pyro Science, Aachen, Germany). Prior to measurements the electrodes were calibrated with deionized H_2O representing the 100% reference value and 1% $NaSO_3$ representing 0% reference value. Oxygen depletion in 2 mL yeast culture samples was determined under continuous stirring at 28°C in 2 mL bottles, sealed with parafilm in order to avoid re-oxygenation of the medium. The decrease of the oxygen concentration over time was calculated and normalized to the number of living cells within the sample. The number of living cells was determined by measuring both the exact cell densities (cells/mL) using an automated cell counter (*e.g.* CASY1) and the proportion of these cells with intact plasma membrane (cells that are not stained with PI) using flow cytometry. At least four different samples (*i.e.* distinct yeast clones) were determined per strain, construct, and condition. Experiments were performed independently at least three times.

When analyzing the effects of UBB^{+1} expression on cellular oxygen consumption, the oxygen consumption of yeast cells carrying vector controls was set to 100% in every experiment. The mean values and the standard errors were calculated from the relative oxygen consumption of all experiments and illustrated graphically as percent change values (Cellular oxygen consumption [%]) (see Figure 4C). For statistical analysis the relative oxygen consumption upon UBB^{+1} expression was compared with the relative oxygen consumption of cells carrying vector controls.

When analyzing the effects of high Vms1 levels on cellular oxygen consumption of UBB^{+1}-expressing cells, the oxygen consumption of yeast cells with endogenous Vms1 levels was set to 100% in every experiment. The mean values and the standard errors were calculated from the relative oxygen consumption of all experiments and illustrated graphically as percent change values (Cellular oxygen consumption upon UBB^{+1} expression [%]) (see Figure 6G). For statistical analysis the relative oxygen consumption upon high levels of Vms1 (Vms1) expression was compared with the relative oxygen consumption of cells with endogenous levels of Vms1 (vector control).

Determination of mitochondrial membrane potential

Mitochondrial membrane potential was assessed cytofluorometrically by staining cells with tetramethylrhodamine methyl ester (TMRM, Molecular Probes, Life Technologies), a fluorescent dye that accumulates within mitochondria dependent on their membrane potential. Staining and analyses were performed as described in (Büttner et al., 2011) with slight modifications. Briefly, aliquots of $5x10^6$ cells were harvested at the indicated time points, washed and incubated with 5 µM TMRM at 28°C in the dark for 30 min. Cells were washed to remove excess dye and subjected to flow cytometric analyses using the BD LSRFortessa (BD Biosciences) with the following settings: filter sets: PE (excitation 488/532 nm, emission 578 nm); flow rate: 4. The mean fluorescence intensity of 30,000 cells per sample was

determined by subtracting the background signal of unstained samples. Data were normalized to the number of living cells within a sample as described in the 'measurement of cellular oxygen consumption'. At least four samples (*i.e.* distinct yeast clones) were measured per strain, construct, and condition. Experiments were performed independently at least four times.

When analyzing the effects of UBB^{+1} expression on mitochondrial membrane potential, the mitochondrial membrane potential of yeast cells carrying vector controls was set to 100% in every experiment. The mean values and the standard errors were calculated from the relative mitochondrial membrane potential of all experiments and illustrated graphically as percent change values (Mitochondrial membrane potential [%]) (see Figure 4D). For statistical analysis the relative mitochondrial membrane potential upon UBB^{+1} expression was compared with the relative mitochondrial membrane potential of cells carrying vector controls.

When analyzing the effects of Vms1 expression on mitochondrial membrane potential of UBB^{+1}-expressing cells, the mitochondrial membrane potential of yeast cells without Vms1 expression was set to 100% in every experiment. The mean values and the standard errors were calculated from the relative mitochondrial membrane potential of all experiments and illustrated graphically as percent change values (Mitochondrial membrane potential upon UBB^{+1} expression [%]) (see Figure 6H). For statistical analysis the relative mitochondrial membrane potential upon high levels of Vms1 (Vms1) was compared with the relative mitochondrial membrane potential of cells with endogenous levels of Vms1 (vector control).

Determination of cellular ATP level

To determine the ATP level of yeast cells, intracellular metabolites were obtained using hot ethanol extraction. Briefly, $1x10^8$ cells were harvested and quick-frozen in liquid nitrogen, resuspended in 0.5 mL of boiling ethanol (75% ethanol, 10 mM $(NH_4)_2SO_4$) and

incubated at 90°C for 3 min. Residual cell debris was removed by centrifugation (-4°C, 14,000 rpm, 20 min) and 10 µL of the supernatant was taken for the subsequent determination of ATP levels using the ATP Determination Kit (Molecular Probes, Life Technologies). This assay is based on an ATP-dependent reaction of recombinant firefly luciferase, which induces bioluminescence of its substrate D-luciferin and is directly correlated with the ATP content. Luminescence induced by the sample was assessed with a Luminoskan Ascent microplate reader (Labsystems, Thermo Scientific). Data were normalized to the number of living cells within a sample as described in the 'measurement of cellular oxygen consumption'. At least three samples (*i.e.* distinct yeast clones) were measured per strain, construct, and condition. Experiments were performed independently at least four times.

When analyzing the effects of UBB^{+1} expression on cellular ATP levels, the cellular ATP levels of yeast cells carrying vector controls was set to 100% in every experiment. The mean values and the standard errors were calculated from the relative cellular ATP levels of all experiments and illustrated graphically as percent change values (Cellular ATP level [%]) (see Figure 4E). For statistical analysis the relative cellular ATP levels upon UBB^{+1} expression was compared with the relative cellular ATP levels of cells carrying vector controls.

When analyzing the effects of Vms1 expression on cellular ATP levels of UBB^{+1}-expressing cells, the cellular ATP levels of yeast cells without Vms1 expression was set to 100% in every experiment. The mean values and the standard errors were calculated from the relative cellular ATP levels of all experiments and illustrated graphically as percent change values (Cellular ATP levels upon UBB^{+1} expression [%]) (see Figure 6I). For statistical analysis the relative cellular ATP levels upon high levels of Vms1 (Vms1) was compared with the relative cellular ATP levels of cells with endogenous levels of Vms1 (vector control).

Measurement of UPS activities

For determining the level of polyubiquitylated proteins in cellular extracts, immunoblots of cellular extracts were incubated with an ubiquitin-specific antibody (1:8000, mouse monoclonal, BD Biosciences). Immunosignals of the peak chain in the range of 15 to 200 kDa were quantified with ImageJ 1.47m as described in 'SDS-PAGE and immunoblot analyses'. The ubiquitin-specific immunosignals of the peak chain in the immunoblot lane which was loaded with extracts from cells transformed with vector controls were set to 100% in every experiment. The experiments were repeated independently for five times.

The ubiquitin-fusion protein ubiquitin-G76V-GFP was co-expressed with UBB^{+1} or vector controls in SCGal-HIS/-URA. GFP fluorescence (relative fluorescence units, RFU) and optical densities (OD_{600}) were determined in 96-well format using the FLUOstar Omega plate reader with the following settings for (i) OD_{600} measurements: number of flashes per scan point 5, path length correction 200 µL, well scanning 5x5, diameter 2 mm; for (ii) measurements of fluorescence intensities: endpoint, number of flashes per well 10, top optic, excitation 485 nm, emission 520 nm, gain 2000, orbital averaging 'on', diameter 2 mm. RFU was normalized to OD_{600} in every single well, in order to determine the level of ubiquitin-GFP fusion proteins per culture. Each sample was measured once. Five samples (*i.e.*, distinct yeast clones) were tested per construct, and condition. Experiments were performed independently at least five times. The mean values and the standard errors were calculated from the RFU/OD_{600} values of all experiments and illustrated graphically (see Figures 1D). For statistical analysis, the RFU/OD_{600} values of the different strains were compared.

Measurement of chymotrypsin-like proteasomal activities were performed using the Proteasome-Glo™ Cell-Based Assay (Promega, Heidelberg, Germany) (Ruenwai et al., 2011). Yeast strains with mutated genes encoding proteasomal subunits were grown in YPD until logarithmic phase, whereas cells expressing UBB^{+1} or *RPN4* were grown in SCGal-HIS or SCGal-URA for different periods. Cells were then diluted in YPD, and SCGal-HIS or

SCGal-URA, respectively, to an OD_{600} of 0.04 (equivalent to approximately 40'000 cells). 25 µL of diluted yeast cultures were then mixed with 25 µL of cell-based reagent. This reagent causes permeabilization of yeast cells, and enables the incorporation of the substrate succinyl-leucine-leucine-valine-tyrosine-aminoluciferin, which is specific for chymotrypsin-like proteasomal activities. The increase in luminescence activity (relative luminescence unit, RLU) by proteolytic cleavage of aminoluciferin was measured until steady state in 384-well format using the FLUOstar Omega plate reader (BMG Labtech, Ortenberg, Germany) with the following settings: measurement type luminescence, measurement interval time 5 sec, emission lens, gain 3600. Each sample was measured in triplicate. For UBB^{+1}, and *RPN4*-expressing cultures, at least three samples (*i.e.*, yeast clones transformed with expression constructs and vector controls, respectively) were tested per strain, construct, and condition. Experiments were performed independently at least three times. The RLUs obtained using yeast cells carrying vector controls (for Figures 3E and S1C) or wild-type yeast cells (for Figure 3A+C) were set to 100% in every experiment. The mean values and the standard errors were calculated from the relative proteasomal activities of all experiments and illustrated graphically as percent change values (Proteasomal activity [%]) (see Figure 3A+C+E, Figure S1C). For statistical analysis the relative proteasomal activities (%) among the different expression constructs or strains were compared.

Generation of cell extracts and cell fractionation

$5x10^7$ cells were pelleted by centrifugation. Cell pellets were resuspended in 100 µL of ddH_2O, and cell suspensions were mixed with 100 µL of 0.2 M NaOH (Kushnirov, 2000). After incubation on ice for 15 min, cells were pelleted by centrifugation and resuspended in 100 µL Laemmli sample buffer (2% (w/v) SDS, 10% (v/v) glycerol, 2% (v/v) β-mercapto ethanol, 60 mM Tris-HCl pH 6.8, bromophenol blue). After thorough mixing, cell suspensions were heated for 7 min at 97°C, cooled down on ice, and frozen at -80°C until use.

Isolation of crude mitochondria was performed by differential centrifugation according to (Braun et al., 2009) with minor modifications. Protein concentrations were determined applying Bradford assay. Samples were either directly incubated in Laemmli sample buffer, or precipitated according to (Wessel and Flügge, 1984) and then resuspended in Laemmli sample buffer prior SDS-PAGE.

SDS-PAGE and immunoblot analyses

Tricine-SDS-PAGE and immunoblot analyses were used for protein analyses (Schägger, 2006; Towbin et al., 1979). Cell extracts were thawed at RT and centrifuged for 1 min at 16.000 *g*. 12 µL of supernatant (equivalent to $6x10^6$ cells) were used for separation on 12% Tricine-SDS polyacrylamide gels using a SDS-PAGE separation apparatus (Mini Protean Tetra System, Bio-Rad, Munich, Germany). Protein transfer on PVDF membranes (pore size 0.2 µm, Immuno-Blot PVDF Membrane For Protein Blotting, Bio-Rad) was performed in a wet blotting chamber (Mini Protean Tetra System, Bio-Rad). Membranes were incubated in blocking buffer (5% (w/v) ECL Advance blocking agent [GE Healthcare] for anti-UBB^{+1} or non-fat milk [Carl Roth, Karlsruhe, Germany] for all other antibodies in TBS-T (1% (v/v) Tween-20) for 1 h at RT or overnight at 4°C. The first antibody was diluted in blocking buffer (for the mouse monoclonal antibodies anti-FLAG M2 [1:1,000] [Sigma-Aldrich], anti-ubiquitin [1:8,000] [BD Biosciences, Heidelberg, Germany], and for the rabbit polyclonal antibodies anti-Cdc48 (serum 70) [1:1000 to 1:2500] (Fröhlich et al., 1991), anti-cytochrome *c* [1:1,000] [N. Pfanner], anti-hexokinase [1:15,000], anti-Por1 [1:1,000] [W. Neupert, Munich, Germany], anti-Rip1 [1:2,000] [N. Pfanner], and anti-SSC1 [1:2,000] [N. Pfanner]) and anti-UBB^{+1} [Ubi3, bleeding 050897; 1:1,000] (de Vrij et al., 2001)). Incubation was performed for 1 h at RT or overnight at 4°C. Membranes were washed with TBS-T three times for 10 min, and were then incubated for 1 h at RT with the respective secondary antibody coupled with horseradish peroxidase (goat anti-rabbit IgG or goat anti-mouse IgG

[Promega and Sigma-Aldrich, respectively], diluted 1:10,000 in blocking buffer). Membranes were washed with TBS-T three times for 10 min. Immunodetection was done using either self-made luminol or self-made luminol supplemented with Lumigen TMA-6 (Lumigen, Beckman Coulter, MI, USA). Membranes were incubated for 2 min with luminol solution and were exposed to and digitized in an ImageQuant LAS 4000 (GE Healthcare, Munich, Germany) with the following settings (method: chemiluminescence, exposure time: increment, sensitivity/resolution: standard, high, or super depending on signal strength). Images were processed with Adobe Photoshop CS6 (Adobe).

Immunoblot quantification was done with the gel analysis method in ImageJ 1.47m. Briefly, the peak area (or peak chain area) of the immunosignal of interest (*e.g.* fl-UBB^{+1} detected with anti-UBB^{+1}) was quantified and normalized to the immunosignal of a loading control (*e.g.* hexokinase detected with α-Hxk). Saturated immunosignals or peaks (or peak chains) which could not be discriminated from background signals were discarded. Experiments were repeated at least three times.

Sample preparation for mass spectrometry

Crude mitochondrial extracts were taken up in SDS lysis buffer, thawed, reduced with 1 mM DTT (Sigma-Aldrich) for 5 min at 95°C and alkylated using 5.5 mM iodoacetamide (Sigma-Aldrich) for 30 min at 25°C. Protein mixtures were separated by SDS-PAGE using 4-12% Bis-Tris mini gradient gels (NuPAGE, Invitrogen). The gel lanes were cut into 10 equal slices, which were in-gel digested with trypsin (Promega) (Shevchenko et al., 2006), and the resulting peptide mixtures were processed on STAGE tips as described (Rappsilber et al., 2007).

Mass spectrometry measurements and data analysis

Generation of mass spectrometric raw data and their analyses was performed as described in (Sprenger et al., 2013). Samples analyzed by MS were measured on a LTQ Orbitrap XL mass spectrometer (Thermo Fisher Scientific, Bremen, Germany) coupled to an Eksigent NanoLC-ultra. HPLC-column tips (fused silica) with 75 µm inner diameter were self-packed (Gruhler et al., 2005) with Reprosil-Pur 120 ODS-3 to a length of 20 cm. No pre-column was used. Peptides were injected at a flow of 500 nL/min in 92% buffer A (0.5% acetic acid in HPLC gradient grade water) and 2% buffer B (0.5% acetic acid in 80% acetonitrile, 20% water). Separation was achieved by a linear gradient from 10% to 30% of buffer B at a flow rate of 250 nL/min. The mass spectrometer was operated in the data-dependent mode and switched automatically between MS (max. of 1 $x10^6$ ions) and MS/MS. Each MS scan was followed by a maximum of five MS/MS scans in the linear ion trap using normalized collision energy of 35% and a target value of 5,000. Parent ions with a charge state of z = 1 and unassigned charge states were excluded from fragmentation. The mass range for MS was m/z = 370 to 2,000. The resolution was set to 60,000. MS parameters were as follows: spray voltage 2.3 kV; no sheath and auxiliary gas flow; ion transfer tube temperature 200°C.

The MS raw data files were uploaded into the MaxQuant software version 1.4.0.8. (Cox and Mann, 2008) which performs peak and SILAC-pair detection, generates peak lists of mass error corrected peptides and data base searches (Andromeda search engine). A full length yeast database (UniProt, May 2013, 6,651 entries) containing common contaminants was employed, carbamidomethyl cysteine was set as fixed modification and methionine oxidation and protein amino-terminal acetylation were set as variable modifications. Triple SILAC was chosen as quantitation mode. Three miss cleavages were allowed, enzyme specificity was trypsin/P, and the MS/MS tolerance was set to 0.5 Da. The average mass precision of identified peptides was in general less than 1 ppm after recalibration. Peptide lists

were further used by MaxQuant to identify and relatively quantify proteins using the following parameters: peptide, and protein false discovery rates (FDR) were set to 0.01, maximum peptide posterior error probability (PEP) was set to 0.1, minimum peptide length was set to 6, minimum number peptides for identification and quantitation of proteins was set to two of which one must be unique, minimum peptide ratio count was set to 2, and identified proteins have been re-quantified. The "match-between-run" option (1 min) was used. Perseus version 1.2.0.16. (Cox and Mann, 2008) was used to identify significantly changed proteins ($p < 0.05$) under different treatments.

Extraction of metabolites for targeted metabolomics

Culture aliquots of OD_{600} ~ 20 (from four different yeast clones of each genotype) were harvested by filtration using 0.22 µm sterile filters, washed once (on filter) with 5 mL ddH_2O and immediately quenched by deep-freezing the filters in liquid nitrogen. Filtration and washing step was performed in less than 30 sec until freezing step. Metabolites were extracted by two different methods with extracts obtained from uniformly ^{13}C-labeled (U13C) yeast cells (see below) serving as an internal standard (Istd). U13C-Istd was applied directly on frozen filters prior to extraction. For acid extraction of metabolites, cells (washed directly from frozen filters) were resuspended in 1 mL ice-cold 5% trichloroacetic acid (TCA) and incubated for 1 h on ice with occasionally vortexing. Supernatants (10 min; 10,000 *g*) were lyophilized and resuspended in 200 µL ddH_2O. For extraction with hot ethanol, cells were incubated in 2.5 mL boiling ethanol solution (75% ethanol, 10 mM ammonium acetate) and incubated for 2 min at 96°C. Supernatants were collected, N_2 evaporated to ~ ¼ of initial volume at RT and finally lyophilized and reconstituted in 200 µL ddH_2O. Extracts were stored at -80°C until metabolite measurements were performed with LC/MS.

Total number of cells of each sample was determined after extraction from cell pellets resuspended and appropriately diluted in water using CASY cell counter technology (Roche) in order to normalize the results from the LC/MS measurement.

To generate U13C-Istd, the prototrophic yeast (*S. cerevisiae* strain CEN.PK113-7D) was grown for 24 h or 72 h (an equal mix of the two cultures were used) on uniformly-labeled ^{13}C-glucose as sole carbon source using medium as described above but lacking any amino acids or bases. Acid or ethanol extracts of labeled yeast cells were performed as for unlabeled cells (see above) using 30% methanol as a final solvent and stored at -80°C upon use. 15 µL of this extract served as U13C-Istd for each sample.

Targeted metabolomics

Metabolites were determined using ion pair reversed-phase liquid chromatography coupled to negative electro spray high resolution mass spectrometry (IP-RP-LC/HRMS). The method was adapted with parts from (Bennett et al., 2008; Buescher et al., 2010). All analyses were carried out on an Ultimate 3000 System coupled to an Exactive XL Mass spectrometer (Orbitrap-system, Thermo Fisher Scientific) using an electrospray ion source. The system was controlled by Xcalibur Software 2.2. The HPLC column was an Atlantis T3 3 µm, 150 x 2.1 mm (Waters). Eluent A consisted of 5% MeOH (v/v) in water containing 10 mM tributylamine and 15 mM acetic acid. Eluent B was isopropanol. Table A shows a detailed gradient description.

Metabolites were detected in negative ESI mode using high resolution (R = 50,000). Peak area ratios to uniformly ^{13}C-labeled internal standards (U13C-Istd, see section on *Extraction of Metabolites*) were calculated for relative quantification of the metabolites listed in Table B using Tracefinder Software (Thermo Fisher Scientific).

Table A: HPLC gradient for targeted metabolomics.

Eluent A: 5% MeOH (v/v) in water, 10 mM tributylamine, 15 mM acetic. Eluent B: isopropanol

time [min]	%A	flow rate [µml/min]
0	0	350
7	0	350
11	2	350
12	9	300
16	9	300
18	25	250
19	50	200
32	70	200
34	0	200
36	0	300
37	0	350
39	0	350

Table B: Compounds for relative quantification

Retention time	Compound	unlabeled	^{13}C-labeled
		m/z	m/z
0.67	Ornithine	131.0826	136.0994
0.79	Lysine	145.0983	151.1184
0.85	Arginine	173.1044	179.1245

Immunohistochemistry

Postmortem tissues of hippocampi from AD patients and non-demented controls were obtained from the Netherlands Brain Bank (Amsterdam, The Netherlands) (Table S6) as 6 µm thick paraffin sections. Immunohistochemistry was performed as previously described (Zouambia et al., 2008). Sections were deparaffinated by subsequent treatment with xylene (2x 15 min), ethanol (2x 10 min 100%, 2x 10 min 96%, 10 min 80%, 10 min 70%, and 10 min 60%), and formic acid (30 min). After rinsing in ddH_2O (30 min), and in TBS (3x 10 min), sections were incubated overnight at 4°C with antibodies against misfolded tau (MC1, Peter Davies, NY, USA, mouse monoclonal, 1:100), UBB^{+1} (Ubi2A, rabbit polyclonal,

1:500) (Fischer et al., 2003), VMS1 (ANKZF1, ab94790, Abcam, rabbit polyclonal, 1:500), and VDAC1 (ab14734, Abcam, mouse monoclonal, 1:500). All dilutions were in SUMI buffer [50 mM Tris buffered saline with 0.25 % (w/v) gelatine and 0.5 % (v/v) Triton X-100, pH 7.6]. After rinsing in TBS (3x 10 min), sections were incubated for 1 h at RT with biotinylated secondary donkey anti-mouse or donkey anti-rabbit antibodies (Jackson Laboratories, Bar Habor, Main, U.S.A; 1:400 in SUMI buffer), followed by washing in TBS-T/TBS/TBS-T (10 min each), and by incubation for 1 h at RT with avidin-biotin-peroxidase complex (ABC, Vector Labs, Brunschwig Chemie, Amsterdam, The Netherlands, 1:400 in TBS-T). After washing in TBS (2x 10 min), and incubation with Tris buffer (50 mM Tris-HCl, pH 7.6, 10 min), sections were stained with Tris-buffered 3,3'-diaminobenzidine (DAB) intensified by 0.04 % (w/v) nickel chloride (pH 7.6) for 5 to 20 min, dependent on antibody and background staining. Staining was stopped by incubation in ddH_2O (3x 10 min), and sections were mounted on glass slides. After drying overnight, sections were dehydrated by subsequent treatment with ethanol (3 min 50%, 3 min 60%, 3 min 70%, 3 min 80%, 2x 3 min 96%, 2x 10 min 100%), Ultraclear (3x 10 min, Mallinokrodt Baker B.V., Deventer, The Netherlands), and coverslipped with Pertex mounting media (Leica Biosystems).

Statistics

For statistics SigmaPlot V13 (Systat Software, Erkrath, Germany) was used. For comparing two groups, either unpaired two-tailed Student's t-test with ad hoc normality and equal variance tests, or paired two-tailed Student's t-tests with ad hoc normality tests were applied. Rank Sum Tests were used for comparing two groups if ad hoc tests failed. For comparing many groups One Way ANOVA or One Way Repeated Measures ANOVA with ad hoc normality and equal variance tests, and post hoc tests (Dunn's, Holm-Sidak, Bonferroni methods) were applied. If ad hoc tests failed, ANOVA on Ranks or Repeated Measures ANOVA on Ranks were used with post hoc tests (Dunn's, Tuckey methods).

Differences were considered to be marked with p-values < 0.1 and significant with p-values ≤ 0.05. If not other stated, error bars indicate the standard errors of the mean or percent change values obtained from the independent experiments. For details see Figure legends and Table S1.

Supplemental References

Bennett, B.D., Yuan, J., Kimball, E.H., and Rabinowitz, J.D. (2008). Absolute quantitation of intracellular metabolite concentrations by an isotope ratio-based approach. Nat Protoc *3*, 1299-1311.

Braun, R.J., Kinkl, N., Zischka, H., and Ueffing, M. (2009). 16-BAC/SDS-PAGE analysis of membrane proteins of yeast mitochondria purified by free flow electrophoresis. Methods Mol Biol *528*, 83-107.

Braun, R.J., Sommer, C., Carmona-Gutierrez, D., Khoury, C.M., Ring, J., Büttner, S., and Madeo, F. (2011). Neurotoxic 43-kDa TAR DNA-binding Protein (TDP-43) Triggers Mitochondrion-dependent Programmed Cell Death in Yeast. J Biol Chem *286*, 19958-19972.

Buescher, J.M., Moco, S., Sauer, U., and Zamboni, N. (2010). Ultrahigh performance liquid chromatography-tandem mass spectrometry method for fast and robust quantification of anionic and aromatic metabolites. Anal Chem *82*, 4403-4412.

Büttner, S., Bitto, A., Ring, J., Augsten, M., Zabrocki, P., Eisenberg, T., Jungwirth, H., Hutter, S., Carmona-Gutierrez, D., Kroemer, G., *et al.* (2008). Functional mitochondria are required for alpha-synuclein toxicity in aging yeast. J Biol Chem *283*, 7554-7560.

Büttner, S., Eisenberg, T., Carmona-Gutierrez, D., Ruli, D., Knauer, H., Ruckenstuhl, C., Sigrist, C., Wissing, S., Kollroser, M., Fröhlich, K.U., *et al.* (2007). Endonuclease G regulates budding yeast life and death. Mol Cell *25*, 233-246.

Büttner, S., Ruli, D., Vogtle, F.N., Galluzzi, L., Moitzi, B., Eisenberg, T., Kepp, O., Habernig, L., Carmona-Gutierrez, D., Rockenfeller, P., *et al.* (2011). A yeast BH3-only protein mediates the mitochondrial pathway of apoptosis. EMBO J *30*, 2779-2792.

Chondrogianni, N., Georgila, K., Kourtis, N., Tavernarakis, N., and Gonos, E.S. (2014). 20S proteasome activation promotes life span extension and resistance to proteotoxicity in *Caenorhabditis elegans*. FASEB J *71*, 303-320.

Cox, J., and Mann, M. (2008). MaxQuant enables high peptide identification rates, individualized p.p.b.-range mass accuracies and proteome-wide protein quantification. Nat Biotechnol *26*, 1367-1372.

de Pril, R., Fischer, D.F., Maat-Schieman, M.L., Hobo, B., de Vos, R.A., Brunt, E.R., Hol, E.M., Roos, R.A., and van Leeuwen, F.W. (2004). Accumulation of aberrant ubiquitin induces aggregate formation and cell death in polyglutamine diseases. Hum Mol Genet *13*, 1803-1813.

de Pril, R., Fischer, D.F., Roos, R.A., and van Leeuwen, F.W. (2007). Ubiquitin-conjugating enzyme E2-25K increases aggregate formation and cell death in polyglutamine diseases. Mol Cell Neurosci *34*, 10-19.

de Pril, R., Hobo, B., van Tijn, P., Roos, R.A., van Leeuwen, F.W., and Fischer, D.F. (2010). Modest proteasomal inhibition by aberrant ubiquitin exacerbates aggregate formation in a Huntington disease mouse model. Mol Cell Neurosci *43*, 281-286.

Fischer, D.F., De Vos, R.A., Van Dijk, R., De Vrij, F.M., Proper, E.A., Sonnemans, M.A., Verhage, M.C., Sluijs, J.A., Hobo, B., Zouambia, M., *et al.* (2003). Disease-specific accumulation of mutant ubiquitin as a marker for proteasomal dysfunction in the brain. FASEB J *17*, 2014-2024.

Fröhlich, K.U., Fries, H.W., Rüdiger, M., Erdmann, R., Botstein, D., and Mecke, D. (1991). Yeast cell cycle protein CDC48p shows full-length homology to the mammalian protein VCP and is a member of a protein family involved in secretion, peroxisome formation, and gene expression. J Cell Biol *114*, 443-453.

Gruhler, A., Olsen, J.V., Mohammed, S., Mortensen, P., Faergeman, N.J., Mann, M., and Jensen, O.N. (2005). Quantitative phosphoproteomics applied to the yeast pheromone signaling pathway. Mol Cell Proteomics *4*, 310-327.

Heessen, S., Dantuma, N.P., Tessarz, P., Jellne, M., and Masucci, M.G. (2003). Inhibition of ubiquitin/proteasome-dependent proteolysis in *Saccharomyces cerevisiae* by a Gly-Ala repeat. FEBS Lett *555*, 397-404.

Irmler, M., Gentier, R.J., Dennissen, F.J., Schulz, H., Bolle, I., Holter, S.M., Kallnik, M., Cheng, J.J., Klingenspor, M., Rozman, J., *et al.* (2012). Long-term proteasomal inhibition in transgenic mice by UBB(+1) expression results in dysfunction of central respiration control reminiscent of brainstem neuropathology in Alzheimer patients. Acta Neuropathol *124*, 187-197.

Jarosch, E., Taxis, C., Volkwein, C., Bordallo, J., Finley, D., Wolf, D.H., and Sommer, T. (2002). Protein dislocation from the ER requires polyubiquitination and the AAA-ATPase Cdc48. Nat Cell Biol *4*, 134-139.

Kushnirov, V.V. (2000). Rapid and reliable protein extraction from yeast. Yeast *16*, 857-860.

Madeo, F., Fröhlich, E., Ligr, M., Grey, M., Sigrist, S.J., Wolf, D.H., and Fröhlich, K.U. (1999). Oxygen stress: a regulator of apoptosis in yeast. J Cell Biol *145*, 757-767.

Ohlmeier, S., Kastaniotis, A.J., Hiltunen, J.K., and Bergmann, U. (2004). The yeast mitochondrial proteome, a study of fermentative and respiratory growth. J Biol Chem *279*, 3956-3979.

Prokisch, H., Scharfe, C., Camp, D.G., 2nd, Xiao, W., David, L., Andreoli, C., Monroe, M.E., Moore, R.J., Gritsenko, M.A., Kozany, C., *et al.* (2004). Integrative analysis of the mitochondrial proteome in yeast. PLoS Biol *2*, e160.

Rappsilber, J., Mann, M., and Ishihama, Y. (2007). Protocol for micro-purification, enrichment, pre-fractionation and storage of peptides for proteomics using StageTips. Nat Protoc *2*, 1896-1906.

Reinders, J., Zahedi, R.P., Pfanner, N., Meisinger, C., and Sickmann, A. (2006). Toward the complete yeast mitochondrial proteome: multidimensional separation techniques for mitochondrial proteomics. J Proteome Res *5*, 1543-1554.

Ruenwai, R., Neiss, A., Laoteng, K., Vongsangnak, W., Dalfard, A.B., Cheevadhanarak, S., Petranovic, D., and Nielsen, J. (2011). Heterologous production of polyunsaturated fatty acids in *Saccharomyces cerevisiae* causes a global transcriptional response resulting in reduced proteasomal activity and increased oxidative stress. Biotechnol J *6*, 343-356.

Schägger, H. (2006). Tricine-SDS-PAGE. Nat Protoc *1*, 16-22.

Sherman, F. (2002). Getting started with yeast. Methods Enzymol *350*, 3-41.

Shevchenko, A., Tomas, H., Havlis, J., Olsen, J.V., and Mann, M. (2006). In-gel digestion for mass spectrometric characterization of proteins and proteomes. Nat Protoc *1*, 2856-2860.

Sickmann, A., Reinders, J., Wagner, Y., Joppich, C., Zahedi, R., Meyer, H.E., Schonfisch, B., Perschil, I., Chacinska, A., Guiard, B.*, et al.* (2003). The proteome of *Saccharomyces cerevisiae* mitochondria. Proc Natl Acad Sci U S A *100*, 13207-13212.

Sprenger, A., Weber, S., Zarai, M., Engelke, R., Nascimento, J.M., Gretzmeier, C., Hilpert, M., Boerries, M., Has, C., Busch, H.*, et al.* (2013). Consistency of the proteome in primary human keratinocytes with respect to gender, age, and skin localization. Mol Cell Proteomics *12*, 2509-2521.

Towbin, H., Staehelin, T., and Gordon, J. (1979). Electrophoretic transfer of proteins from polyacrylamide gels to nitrocellulose sheets: procedure and some applications. Proc Natl Acad Sci U S A *76*, 4350-4354.

van Tijn, P., Hobo, B., Verhage, M.C., Oitzl, M.S., van Leeuwen, F.W., and Fischer, D.F. (2011). Alzheimer-associated mutant ubiquitin impairs spatial reference memory. Physiol Behav *102*, 193-200.

Wessel, D., and Flügge, U.I. (1984). A method for the quantitative recovery of protein in dilute solution in the presence of detergents and lipids. Anal Biochem *138*, 141-143.

Westermann, B. (2010). Mitochondrial fusion and fission in cell life and death. Nat Rev Mol Cell Biol *11*, 872-884.

Zouambia, M., Fischer, D.F., Hobo, B., De Vos, R.A., Hol, E.M., Varndell, I.M., Sheppard, P.W., and Van Leeuwen, F.W. (2008). Proteasome subunit proteins and neuropathology in tauopathies and synucleinopathies: Consequences for proteomic analyses. Proteomics *8*, 1221-1236.

Detailed Author Contributions

Figure/Table	Designed the experiment	Performed the experiment	Analyzed the data	Prepared the figure/ table
Figure 1A-C	R.J.B.	K.P.	R.J.B., K.P.	R.J.B., C.S.
Figure 1D	R.J.B.	R.J.B.	R.J.B.	R.J.B., C.S.
Figure 2A-F	R.J.B.	R.J.B.	R.J.B.	R.J.B., C.S.
Figure 3A+C+E	R.J.B.	R.J.B.	R.J.B.	R.J.B., C.S.
Figure 3B+F	R.J.B.	C.S., R.J.B.	C.S., R.J.B.	R.J.B., C.S.
Figure 3D	R.J.B.	C.L., R.J.B.	C.L., R.J.B.	R.J.B., C.S.
Figure 4A	R.J.B., C.S.	R.J.B., C.S.	R.J.B., C.S.	R.J.B., C.S.
Figure 4B	R.J.B.	R.J.B.	R.J.B.	R.J.B., C.S.
Figure 4C-E	C.S., R.J.B.	C.S.	C.S., R.J.B.	R.J.B., C.S.
Figure 4F+G	R.J.B.	K.P.	R.J.B., K.P., C.L.	R.J.B., C.S.
Figure 4H	R.J.B., C.S.	C.S., R.J.B.	C.S., R.J.B.	R.J.B., C.S.
Figure 4I	R.J.B.	R.J.B.	R.J.B.	R.J.B., C.S.
Figure 5A	F.M., J.D., R.J.B.	V.I.D., K.P.	V.I.D., R.J.B.	R.J.B., C.S.
Figure 5B	R.J.B.	C.L.	C.L., R.J.B.	R.J.B., C.S.
Figure 5C	F.M., T.E., C.M., C.S., R.J.B.	C.S., T.E., G.T.	T.E., C.S., G.T.	R.J.B., C.S.
Figure 5D	-	-	-	R.J.B., C.S.
Figure 5E	F.M., C.S., R.J.B.	C.S.	C.S., R.J.B.	R.J.B., C.S.
Figure 5F+G	F.M., C.S., R.J.B.	L.H.	L.H., R.J.B.	R.J.B., C.S.
Figure 6A-C	R.J.B.	R.J.B., C.L.	R.J.B., C.L.	R.J.B., C.S.
Figure 6D-F	F.M., C.S.	C.S.	C.S., R.J.B.	R.J.B., C.S.
Figure 6G-I	C.S., R.J.B.	C.S.	C.S., R.J.B.	R.J.B., C.S.
Figure 6J	F.M., J.D., R.J.B.	V.I.D., K.P.	V.I.D., R.J.B.	R.J.B., C.S.
Figure 6K	F.M., T.E., C.M., C.S., R.J.B.	C.S., T.E., G.T.	T.E., C.S., G.T.	R.J.B., C.S.
Figure 7A-D	F.W.v.L., R.J.B.	R.J.B., R.J.G.G.	R.J.G.G., F.W.v.L., R.J.B.	F.M., C.S., R.J.B.
Figure S1A+B	R.J.B.	K.P.	R.J.B., K.P.	R.J.B., C.S.
Figure S1C	R.J.B.	R.J.B.	R.J.B.	R.J.B., C.S.
Figure S2A-E	R.J.B.	R.J.B.	R.J.B.	R.J.B., C.S.
Figure S3A	R.J.B.	C.S., R.J.B.	C.S., R.J.B.	R.J.B., C.S.
Figure S3B	R.J.B.	C.L., R.J.B.	C.L., R.J.B.	R.J.B., C.S.
Figure S3C	R.J.B.	C.L., R.J.B.	C.L., R.J.B.	R.J.B., C.S.
Figure S3D-K	R.J.B.	C.L.	C.L.	R.J.B., C.S.
Figure S4A	R.J.B.	R.J.B.	R.J.B.	R.J.B., C.S.
Figure S4B+C	R.J.B.	K.P.	R.J.B., K.P.	R.J.B., C.S.
Figure S4D	R.J.B., C.S.	C.S., R.J.B.	C.S., R.J.B.	R.J.B., C.S.
Figure S4E	R.J.B.	R.J.B.	R.J.B.	R.J.B., C.S.
Figure S4F-H	R.J.B.	K.P.	R.J.B., K.P.	R.J.B., C.S.
Figure S4I	R.J.B.	R.J.B.	R.J.B.	R.J.B., C.S.
Figure S5A	R.J.B.	C.L.	C.L., R.J.B.	R.J.B., C.S.
Figure S5B	F.M., C.S., R.J.B.	C.S.	C.S., R.J.B.	R.J.B., C.S.
Figure S6A-C	R.J.B.	R.J.B., C.L.	R.J.B., C.L.	R.J.B., C.S.
Figure S6D	F.M., C.S.	C.S.	C.S., R.J.B.	R.J.B., C.S.
Figure S6E-H	R.J.B.	C.L.	C.L.	R.J.B., C.S.
Figure S6I+J	R.J.B.	K.P.	C.L.	R.J.B., C.S.
Figure S7	F.W.v.L., R.J.B.	R.J.B., R.J.G.G.	R.J.G.G., F.W.v.L., R.J.B.	R.J.B., F.M., C.S.
Table S1	-	-	-	R.J.B.
Tables S2-S4	F.M., J.D., R.J.B.	V.I.D., K.P.	V.I.D., R.J.B.	R.J.B.
Tables S5+S6	F.W.v.L., R.J.B.	R.J.B., R.J.G.G.	R.J.G.G., F.W.v.L., R.J.B.	R.J.B., F.W.v.L.